

**EXTRACTION OF DRILLING-ANGULAR VELOCITIES  
USING A NODAL-SPATIAL ARRAY  
OF IN-PLANE TRANSLATIONAL VELOCITIES**

by

**George Stergios Galaitis**

Thesis submitted to the Faculty of the  
Virginia Polytechnic Institute and State University  
in partial fulfillment of the requirements for the degree of  
**MASTERS OF SCIENCE**

in

**MECHANICAL ENGINEERING**

APPROVED:

  
L. D. Mitchell, Chairman

  
A. L. Wicks

  
R. L. West

May 1993

Blacksburg, Virginia

C.2

L17  
S655  
V855  
1993  
G353  
C.2

**EXTRACTION OF DRILLING-ANGULAR VELOCITIES  
USING A NODAL-SPATIAL ARRAY  
OF IN-PLANE TRANSLATIONAL VELOCITIES**

by

George Stergios Galaitis

Committee Chairman: L. D. Mitchell  
Mechanical Engineering

(ABSTRACT)

A theoretical technique to extract drilling-angular velocities from a nodal-spatial array of in-plane translational velocities is developed. The technique utilizes numerical methods for simulation of solutions. A finite element method using I-DEAS 4.1 is used for calculation of in-plane translational velocities and a MATLAB code is written for extraction of the drilling-angular velocities. The case of data with noise content is also considered. All numerical results are compared to a closed-form theoretical solution which is used as a reference for accuracy. Recommendations are made for future testing and experimental applications of this technique.

# Acknowledgements

I would like to thank Professor Larry D. Mitchell for his continuous guidance and endless patience during the last nine months. I was very fortunate to study under a well known and respected advisor and I thank him dearly for his effort and time.

I would also like to thank Professor A. L. Wicks, Professor R. L. West, and Professor C. E. Knight for their support and contribution toward my work and research. Their high expectation was extremely motivating to me and brings out the best of all graduate students in the Mechanical Engineering of Virginia Polytechnic Institute and State University.

Finally, I would like to thank Zonic Corporation for the financial support which made this research possible.

# Table of Contents

<b>Introduction.....</b>	<b>1</b>
1.1 Purpose of Research.....	1
1.1.1 Three-Dimensional Vibration.....	2
1.1.2 Laser Vibrometry.....	3
1.2 Background.....	6
<b>Literature Review.....</b>	<b>9</b>
2.1 In-Plane Mode Shapes of Rectangular Plates.....	9
2.2 In-Plane Mode Geometry.....	12
2.3 Lamé Theory.....	20
2.4 Drilling Degrees of Freedom and Drilling Mode Shapes.....	22
<b>Theory.....</b>	<b>23</b>
3.1 The Curl.....	23
3.2 The Curl of a Translational Velocity Field.....	28
<b>Analytical Simulations.....</b>	<b>33</b>
4.1 Lamé-Mode Shape of a Square Plate.....	34
4.2 Lamé-Mode Shape of a Rectangular Plate.....	41

<b>Numerical Simulations.....</b>	<b>48</b>
5.1 I-DEAS Finite Element Dynamic Code.....	48
5.2 MATLAB Drilling-Velocity Extraction Code.....	53
5.3 Validation of Numerical Methods.....	56
5.3.1 Theory vs. Finite Element Code.....	56
5.3.2 Theory vs. MATLAB Code.....	59
5.3.3 Theory vs. Finite Element+MATLAB Code.....	62
5.3.4 Theory vs. MATLAB Code with Noise Content.....	68
<b>Applications.....</b>	<b>78</b>
6.1 Numerical Applications.....	78
6.2 Experimental Applications.....	84
<b>Conclusions and Recommendations.....</b>	<b>85</b>
7.1 Conclusions.....	85
7.2 Recommendations.....	88
<b>References.....</b>	<b>89</b>
<b>The First Three In-Plane Modes of a Square Plate.....</b>	<b>94</b>
<b>The First Three In-Plane Modes of a Rectangular Plate.....</b>	<b>96</b>
<b>MATLAB Code for Extraction of Drilling-Mode Shapes.....</b>	<b>98</b>
<b>Vita.....</b>	<b>101</b>

## List of Illustrations

Figure 1.	VPI Sensor made by Ometron Inc., London, England.....	5
Figure 2.	In-plane vibration patterns of displacement, mode AS-1.....	15
Figure 3.	In-plane vibration patterns of displacement, mode AS-2.....	15
Figure 4.	In-plane vibration patterns of displacement, mode SS-1.....	16
Figure 5.	In-plane vibration patterns of displacement, mode SS-2.....	16
Figure 6.	In-plane vibration patterns of displacement, mode AA-1.....	17
Figure 7.	In-plane vibration patterns of displacement, mode AA-2.....	17
Figure 8.	In-plane vibration patterns of displacement, mode SA-1.....	19
Figure 9.	In-plane vibration patterns of displacement, mode SA-2.....	19
Figure 10.	Convention for calculation of curl.....	24
Figure 11.	Measurement of rotation in flexure of bodies.....	30
Figure 12.	Total angular velocity for in-plane flexure of plates.....	30
Figure 13.	Lamé mode of a square plate, displacement field.....	35
Figure 14.	Lamé mode of a square plate, in-plane velocity $V_x$ .....	37
Figure 15.	Lamé mode of a square plate, in-plane velocity $V_y$ .....	37
Figure 16.	Lamé mode of a square plate, $\partial V_y/\partial x$ .....	39
Figure 17.	Lamé mode of a square plate, $\partial V_x/\partial y$ .....	39
Figure 18.	Drilling-Lamé mode of a square plate, $\dot{\theta}_z$ .....	40
Figure 19.	Lamé mode of a rectangular plate, displacement field.....	42
Figure 20.	Lamé mode of a rectangular plate, in-plane velocity $V_x$ .....	43
Figure 21.	Lamé mode of a rectangular plate, in-plane velocity $V_y$ .....	43
Figure 22.	Lamé mode of a rectangular plate, $\partial V_y/\partial x$ .....	45
Figure 23.	Lamé mode of a rectangular plate, $\partial V_x/\partial y$ .....	45

Figure 24. Drilling-Lamé mode of a rectangular plate, $\dot{\theta}_z$ .....	47
Figure 25. Lamé mode of a square plate by using I-DEAS 4.1.....	57
Figure 26. MATLAB code, $\partial V_y/\partial x$ .....	60
Figure 27. MATLAB code, $\partial V_x/\partial y$ .....	60
Figure 28. MATLAB code, drilling-mode shape.....	61
Figure 29. Finite element code, in-plane translational velocity $V_x$ .....	64
Figure 30. Finite element code, in-plane translational velocity $V_y$ .....	64
Figure 31. Finite element+MATLAB code, $\partial V_y/\partial x$ .....	65
Figure 32. Finite element+MATLAB code, $\partial V_x/\partial y$ .....	65
Figure 33. Finite element+MATLAB code, drilling-mode shape.....	66
Figure 34. Gaussean noise ( $\sigma = 1\%$ of $V_{\max}$ ), in-plane velocity $V_x$ .....	70
Figure 35. Gaussean noise ( $\sigma = 1\%$ of $V_{\max}$ ), in-plane velocity $V_y$ .....	70
Figure 36. Gaussean noise ( $\sigma = 1\%$ of $V_{\max}$ ), drilling mode.....	71
Figure 37. First in-plane mode of a square plate using I-DEAS 4.1.....	80
Figure 38. First in-plane mode of a square plate, $V_x$ .....	81
Figure 39. First in-plane mode of a square plate, $V_y$ .....	81
Figure 40. First in-plane mode of a square plate, $\partial V_y/\partial x$ .....	82
Figure 41. First in-plane mode of a square plate, $\partial V_x/\partial y$ .....	82
Figure 42. First in-plane mode of a square plate, $\dot{\theta}_z$ .....	83
Figure A1. Square plate, first in-plane eigenvector.....	94
Figure A2. Square plate, second in-plane eigenvector.....	95
Figure A3. Square plate, third in-plane eigenvector.....	95
Figure B1. Rectangular plate, first in-plane eigenvector.....	96
Figure B2. Rectangular plate, second in-plane eigenvector.....	97
Figure B3. Rectangular plate, third in-plane eigenvector.....	97

## List of Tables

Table 1. Validation of finite element code, %error of $V_x$ .....	58
Table 2. Finite element+MATLAB code, %error in $\dot{\theta}_z$ .....	67
Table 3. Sample mean value of drilling-mode shape, $N = 100$ .....	72
Table 4. Sample standard deviation of drilling-mode shape, $N = 100$ .....	73
Table 5. Upper bound of 95% confidence interval, $N = 100$ .....	75
Table 6. Lower bound of 95% confidence interval, $N = 100$ .....	76
Table 7. Actual values of drilling-mode shape.....	77

# Nomenclature

## Mathematical Symbols

$| |$  An array of points

$\nabla$  Del operator

## Roman

$C, C_1, C_2$  Constants

$D_x, D_y, D_z$  Displacements along  $x, y,$  and  $z$  axes

$E$  Modulus of Elasticity

$f_n$  Natural Frequency

$\mathbf{F}()$  Vector function

$\mathbf{i}$  Unit vector along  $x$ -axis

$I$  Integral

$I_x, I_y, I_z$  Integrals evaluated for paths around  $x, y,$  and  $z$  axes

$\mathbf{j}$  Unit vector along  $y$ -axis

$\mathbf{k}$  Unit vector along  $z$ -axis

$L, L_1, L_2$  Length of side

$m$  Number of columns of array

$n$  Number of rows of array

$\mathbf{n}$  Unit normal vector

$ns_x, ns_y$  Number of spectral lines in  $x$  and  $y$  axes

$N$	Number of samples
$\mathbf{r}$	Unit vector in radial direction
$S_{pq}$	Elastic compliance
$S$	Arc length measured along a curve
$S_{\hat{\theta}_z}$	Standard deviation of a sample of drilling velocities
$t$	Thickness
$\mathbf{t}$	Unit vector tangent
$T_1, T_2$	Stress
$V_x, V_y, V_z$	In-plane translational velocities in $x$ , $y$ , and $z$ axes
$V_x^{theory}$	Theoretical in-plane translational velocity along $x$ -axis
$V_x^{fe}$	Finite element in-plane translational velocity along $x$ -axis
$V_{max}$	Maximum in-plane translational velocity
$x$	Translation along $x$ -axis
$y$	Translation along $y$ -axis
$z$	Translation along $z$ -axis
$\mathbf{z}$	Unit vector in $z$ -direction

### Greek

$\Delta S$	Enclosed area of a path
$\boldsymbol{\theta}$	Unit vector in $\theta$ -direction
$\theta_x, \theta_y, \theta_z$	Rotations around $x$ , $y$ , and $z$ axes
$\dot{\theta}_x, \dot{\theta}_y, \dot{\theta}_z$	Rotational velocities around $x$ , $y$ , and $z$ axes
$\dot{\theta}_z^{theory}$	Theoretical drilling-angular velocity
$\dot{\theta}_z^{fe+MATLAB}$	Numerical drilling-angular velocity
$\bar{\theta}_z$	Sample mean value of drilling-angular velocity

$\mu_{\dot{\theta}_z}$	True mean value of population for drilling velocities
$\nu$	Poisson's ratio
$\rho$	Mass density
$\sigma$	Standard deviation of the population for drilling velocities
$v$	displacement function
$\phi$	Unit vector in $\phi$ -direction
$\omega$	Angular frequency

# Dedication

This study is dedicated to my parents, Stergios and Elpiniki Galaitsis. My father Stergios Galaitsis, a native Greek, was a multitalented well educated bank employee whose dream was to acquire higher education in the United States of America. He deceased in 1975. His spirit will be always with me. My mother Elpiniki Galaitsis is an endless source of energy and strength. She made my father's dream true through me. I thank you both.

# Chapter 1

## Introduction

This research is a theoretical study in extraction of rotational degrees of freedom from a spatial array of translational degrees of freedom. The geometric characteristics of in-plane mode shapes for rectangular plates are carefully examined. Utilizing numerical techniques, angular velocity extraction is performed, and mode shapes associated with in-plane rotation are determined. The technical usefulness of this work is explored in some detail. The boundaries and limitations of this effort are identified and taken under consideration. The ultimate goal is to set up a foundation for experiments, using one-dimensional laser vibrometers for measuring all six degrees of freedom (three translations and three rotations).

### *1.1 Purpose of Research*

The importance of this investigation is explained here while the specific objectives are stated. The concepts of three-dimensional vibration and laser vibrometry are also introduced.

### 1.1.1 Three-Dimensional Vibration

In theory of vibrations most studies consider one or two dimensions of motion. This is done in order to simplify the problem. It gives emphasis in the method of solving by avoiding the complicated mathematical derivations of a three-dimensional case.

Real-life vibrations of structures are always three dimensional. A complete description of motion for a three-dimensional body in space, is made possible with the use of quantities called "degrees of freedom". In the context of a Cartesian or rectangular coordinate system, a vibrating object can have up to six degrees of freedom per point. Naturally, a body in space has infinite degrees of freedom because it is composed by a continuum of points. However, for most calculations a finite number of points and, thus, a finite number of degrees of freedom are used. The number of degrees of freedom depends on the application. Some applications need few hundreds, others require thousands.

A degree of freedom is an independent quantity used to describe motion [1]<sup>1</sup>. A complete description of motion has three translations ( $x$ ,  $y$ , and  $z$ ), and three rotations ( $\theta_x$ ,  $\theta_y$ , and  $\theta_z$ ). The translational degrees of freedom are defined as linear motion along the  $x$ ,  $y$ , and  $z$  axes.

---

<sup>1</sup> Numbers in brackets refer to references listed at the end of this thesis.

Similarly, the rotational degrees of freedom are defined as angular motion about each of the respective axes. Depending on the boundary conditions, if no constraints and restraints are applied, all six degrees of freedom will be present for a point. Nowadays, laser vibrometry is envisioned as a powerful tool for three-dimensional experimental measurements when properly applied.

### **1.1.2 Laser Vibrometry**

One of the objectives of this work is to enhance and broaden the horizons of laser vibrometry. The use of laser vibrometry is a technological advancement in experimental modal analysis [2,3,4,5,6,7]. Vibration measurement is accomplished without any contact, transducer attachments, cabling and connectors [8]. The setup is convenient for use in high temperature, polluted, radio-active, and hazardous areas. Laser vibrometers have automated, fast scanning capabilities with high spatial resolution [9].

In laser vibrometry, combining translational and rotational degrees of freedom could reduce the uncertainty in experimental measurements. It also adds another dimension in spatial description of mode shapes [10,11]. A laser vibrometer able to measure all six degrees of freedom will fully describe the three-dimensional vibration of structures.

In the past few years, a device called VPI Sensor is been frequently used in the Structural Imaging and Modal Analysis Laboratory of Mechanical Engineering Department at Virginia Polytechnic Institute and State University (see Fig. 1). The VPI Sensor is a Michelson interferometer developed and manufactured by Ometron Inc., London, England. It is a non-contact velocity transducer capable of measuring velocities of a vibrating solid surface.

The Doppler effect is utilized as a concept, in which waves reflected from a vibrating object, undergo a frequency change. A velocity toward the laser results in a upward shift in the laser-light frequency, and a velocity away from the laser results in a downward frequency shift. The laser beam is separated into reference and signal beams. The diffusely reflected signal beam coming from the vibrating surface is recombined with the original reference beam. The recombined beam now pulses on and off at a frequency equal to the Doppler shift induced by the instantaneous velocity of the structure. Then, the VPI Sensor operates like an FM receiver. The vibration Doppler signals are fed to a dual-channel balanced modulator where electronic frequency shifting takes place. This is done to allow the detection of positive and negative Doppler shifts. Finally, this frequency-coded velocity is FM demodulated in order to get the unfiltered or filtered velocity output [12].

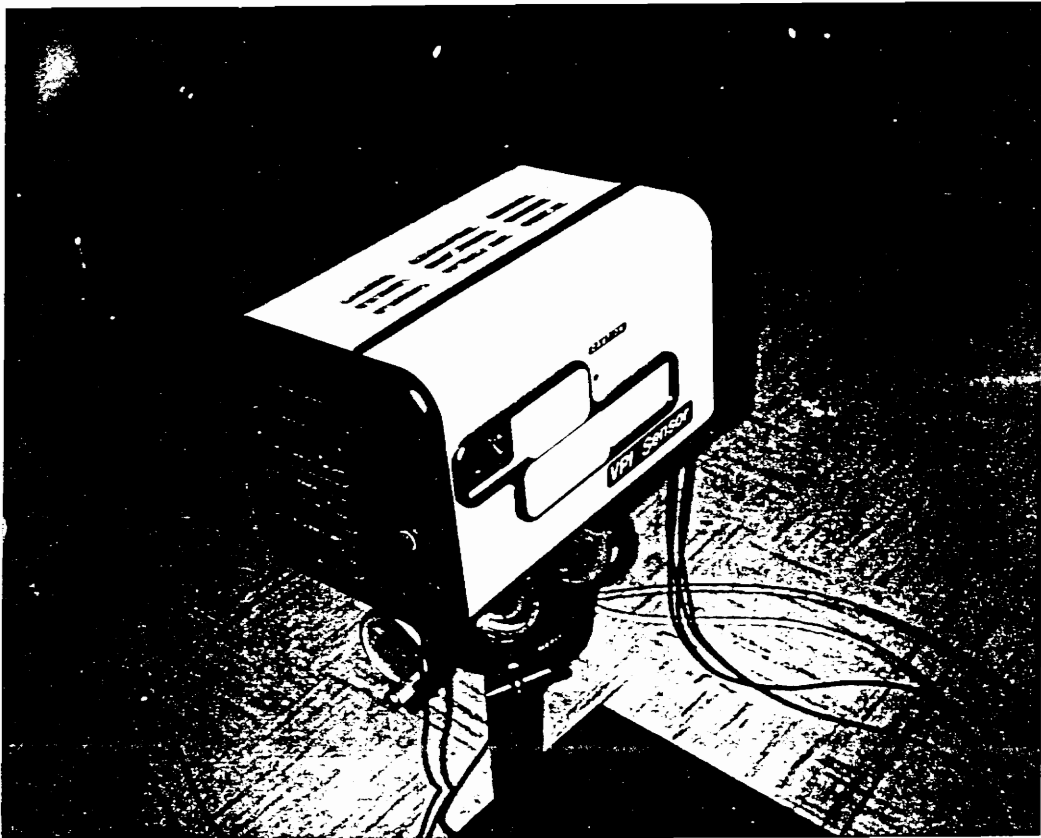


**Figure 1. VPI Sensor made by Ometron Inc., London, England.**

## *1.2 Background*

VPI Sensor is a one-dimensional, laser-Doppler vibrometer [13]. The procedure described above, is used for velocity data acquisition of the line-of-sight structural motion. Such measurements involve only one degree of freedom per point for a vibrating surface [14], the line of sight motion.

Various researchers worked on improving the dynamic imaging of VPI Sensor. Kochersberger [15] and Sun [16] developed a method for angular velocity extraction using a DFT-IDFT technique (Discrete Fourier Transform-Inverse Discrete Fourier Transform). Differentiation was performed in the spatial frequency domain, and the data were smoothed by filtering out the measurement noise using digital filtering of the spatial data. Their efforts resulted on measurement of two more degrees of freedom; rotations about  $x$  and  $y$  axes ( $\theta_x$  and  $\theta_y$ ).

Arruda [17], presents another surface smoothing method. The coefficients of a two-dimensional Discrete Fourier Series with arbitrary period and frequency, are estimated by least-squares. This method minimizes the leakage and could be used with non-equally-spaced and non-rectangular spatial domain data. It also has a lower computational cost than in [16]; however, the implementation of this method is not as practical as the Discrete Fourier Transform method.

Donovan [18], and Abel [19] worked in measurement of in-plane velocities (translations along  $x$  and  $y$  axes), using the VPI Sensor. Their technique

utilizes measurements taken in three independent positions (shots of a single point from different view angles). During this procedure, the VPI Sensor is physically moved from one position to the next. Data collection happens in different time intervals. The simultaneous use of three lasers is still under consideration. This means that five degrees of freedom are available based on these collective works;  $x$ ,  $y$ ,  $z$ ,  $\theta_x$ , and  $\theta_y$  [15,16,17,18,19].

The remaining degree of freedom is the rotation about the  $z$ -axis,  $\theta_z$ . The purpose of this research is to develop a method of measurement or extraction of  $\theta_z$ . In order to reach this goal, a combination of analytical and numerical methods was used. Linking the work of the above researchers is of great importance, because the full-field velocity data of a vibrating surface, can now be determined using laser vibrometry.

Dealing with three-dimensional vibration of structures directly, could complicate calculations. In order to simplify this case scenario, this research is focused on vibrations of rectangular or square isotropic-thin plates. There is not any load applied, and the boundary conditions are free-free-free-free. Plate thickness for most calculations is negligible. The material used is structural steel.

Before any calculations, a basic knowledge of in-plane vibrations is needed. The next chapter, is a review of the theory behind in-plane vibrations and modal geometric characteristics.

It is assumed that the reader has some understanding of vibrations and modal analysis. If not, elementary textbooks such as Thomson [20], and Bendat [21] can be used as references.

## Chapter 2

### Literature Review

This chapter is a review of literature already existing on contour mode shapes of thin rectangular plates. The history of these relatively recent developments will be explored, in order to justify their significance. The in-plane mode shapes are grouped according to their geometric characteristics. Finally, the terms "drilling-mode shape" and "drilling degree of freedom" will be briefly explained and reviewed.

#### *2.1 In-Plane Mode Shapes of Rectangular Plates*

The elastic vibrations of solid bodies with rectangular shape have been the object of many scientific investigations in the last two centuries. Nevertheless, few solutions are available in the literature and they are governed by many restrictions and limitations [22,23]. The vibration of plates with different geometry including rectangular, is covered by Leissa [24]; however, solutions of in-plane vibration are not present there.

Some work has been done on in-plane vibration of rotating blades using shallow shell theory and the Ritz method to determine the frequencies and mode shapes of turbomachinery blades [25,26,27,28,29].

Analytical solutions of in-plane vibration for rectangular plates are very few, and usually are not closed-form in nature. Most of them utilize Rayleigh-Ritz approximation techniques; moreover, the derivations are tedious and complicated. The equations of in-plane motion are coupled to the equations of out-of-plane motion, and uncoupling them is a very complex procedure. It is difficult to obtain exact solutions because of restrictions imposed by boundary conditions to the differential equations of motion. The boundary conditions of a plate can complicate or simplify the desired solution. A free-free-free-free condition is commonly used. Partial-differential equation solutions using separated variables, do not easily satisfy the conditions on all the plate surfaces at the same time.

Wauer [30], describes a method of calculating in-plane mode shapes and natural frequencies for free-free-free-free rectangular plates. In [30], missing symbols and inconsistent use of equations creates chaotic mathematical manipulations. Corrections to this paper are available from its author but they too have problems. Kobayashi [31], uses the Ritz method to determine in-plane mode shapes for point-supported rectangular plates. In [31], not enough information is presented for the reader to reproduce the results.

From a theoretical point of view, the above solutions can be of great importance. Nevertheless, performing an experiment to measure in-plane vibrations by mechanical means could be very challenging. There is a large number of out-of-plane modes that appear before the first in-plane mode, not to mention the fact that out-of-plane and in-plane mode shapes could be very closely coupled with each other. Also, the in-plane mode shapes are difficult to excite without having a way to predict the out-of-plane motion in the neighborhood of the desired natural frequency. For all these reasons, literature based on experiments measuring in-plane vibrations of rectangular plates is almost non-existent.

Lloyd [32], makes use of a finite-difference method to calculate in-plane mode shapes of rectangular and square plates of piezoelectric ceramic. Utilizing the electric properties of thin, rectangular piezoelectric resonators, he experimentally excites several in-plane mode shapes. The mode shapes are grouped according to their geometrical configuration and electrical properties like the piezoelectric strength. Then, the numerical solutions are compared to experimental results and closed-form theoretical solutions, if available. Closed-form theoretical solutions are given only for specific mode shapes. These are present for square plates or rectangular plates of 3:1 aspect ratio. They are called "Lamé mode shapes" after the French mathematician Lamé [33,34,35] who first described their characteristics.

The exact theory of Lamé could be used as a foundation for theoretical simulations. As a result, it is employed in this research as a reference in order to validate numerical results.

## ***2.2 In-Plane Mode Geometry***

Lloyd [32], groups in-plane mode shapes of rectangular thin plates according to their geometry. Different aspect ratios of rectangular plates are considered for each mode shape, in order to clarify the characteristics of that particular natural frequency. Two types of contour mode shapes are discussed: the flexural and the extensional type. The flexural contains modes of "bending", and "shear" type. The extensional contains modes of "length", "edge", and "radial" type. This notation fails to convey to the reader a clear understanding for in-plane mode shapes. Using finite elements, Kawai [36] specifies some additional flexural and extensional modes that were not included in Lloyd's work.

Based on [37,30,31], a new notation is used for later publications. For a free-free-free-free, thin, rectangular plate the boundary conditions are symmetric. The in-plane modes will be symmetric or antisymmetric with respect to the  $x$ -axis and  $y$ -axis. Symmetry about an axis is defined as exact correspondence of geometrical configuration on opposite sides of the specific dividing axis (mirror-image concept). When there is no symmetry about an axis, then the structure is antisymmetric about this axis.

Four possible cases need to be studied, and the first eight in-plane mode shapes will be introduced (two of each case).

### ***1. Antisymmetric-Symmetric Case (AS-#)***

The first case includes all in-plane mode shapes that are antisymmetric with respect to  $x$ -axis and symmetric with respect to  $y$ -axis (mirror image about the  $y$ -axis).

#### **AS-1**

This is the in-plane "bending" mode. The long side is a half cycle of a sine wave. The flexural characteristics become more evident as the aspect ratio becomes greater (see Fig. 2).

#### **AS-2**

This is another "bending" mode. It is the first overtone or second spatial harmonic of AS-1 (see Fig. 3).

### ***2. Symmetric-Symmetric Case (SS-#)***

The second case includes all in-plane mode shapes that are symmetric with respect to  $x$ -axis and symmetric with respect to  $y$ -axis (mirror image about both the  $x$ -axis and  $y$ -axis).

#### **SS-1**

It is the fundamental "length" mode of vibration (see Fig. 4), an extension along the length of the structure.

As one side becomes larger compared to the other, the transverse vibration of the long side is small compared to the longitudinal vibration of the short side. Approaching square dimensions (not shown here), the characteristics of this mode decline. This is a Lamé result described in detail in chapter 4.

## **SS-2**

The "edge" mode, shown in Fig. 5, acquired its name from displacement patterns which suggest that motion is confined to the corners of the plate. For a 3:1 aspect-ratio plate (not shown here), the corners do not translate but simply rotate. This is another Lamé result described in detail in chapter 4.

### ***3. Antisymmetric-Antisymmetric Case (AA-#)***

The third case is valid for in-plane mode shapes that are antisymmetric with respect to  $x$ -axis and antisymmetric with respect to  $y$ -axis. Neither the  $x$  or  $y$  axes are axes of symmetry for the plate.

## **AA-1**

The first "shear" in-plane mode is shown in Fig. 6. The shear characteristics of this mode, are more evident for a square plate.

## **AA-2**

The second "shear" mode is shown in Fig. 7. This is the second spatial harmonic of the AA-1 along the short side.

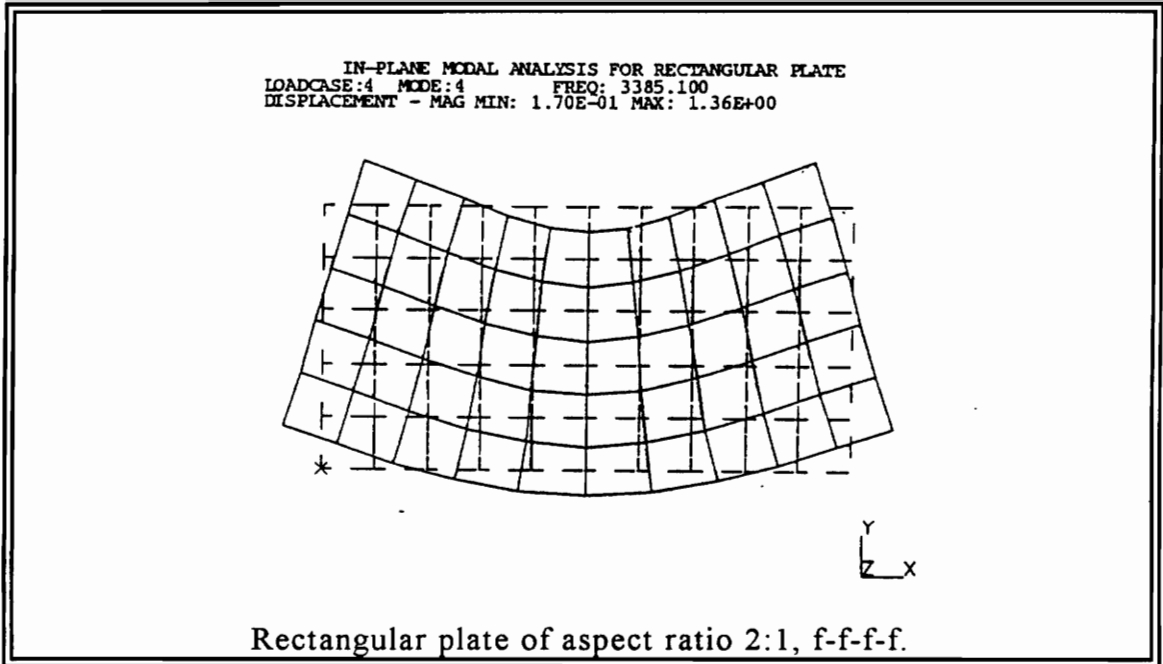


**Figure 2. In-plane vibration patterns of displacement, mode AS-1.**

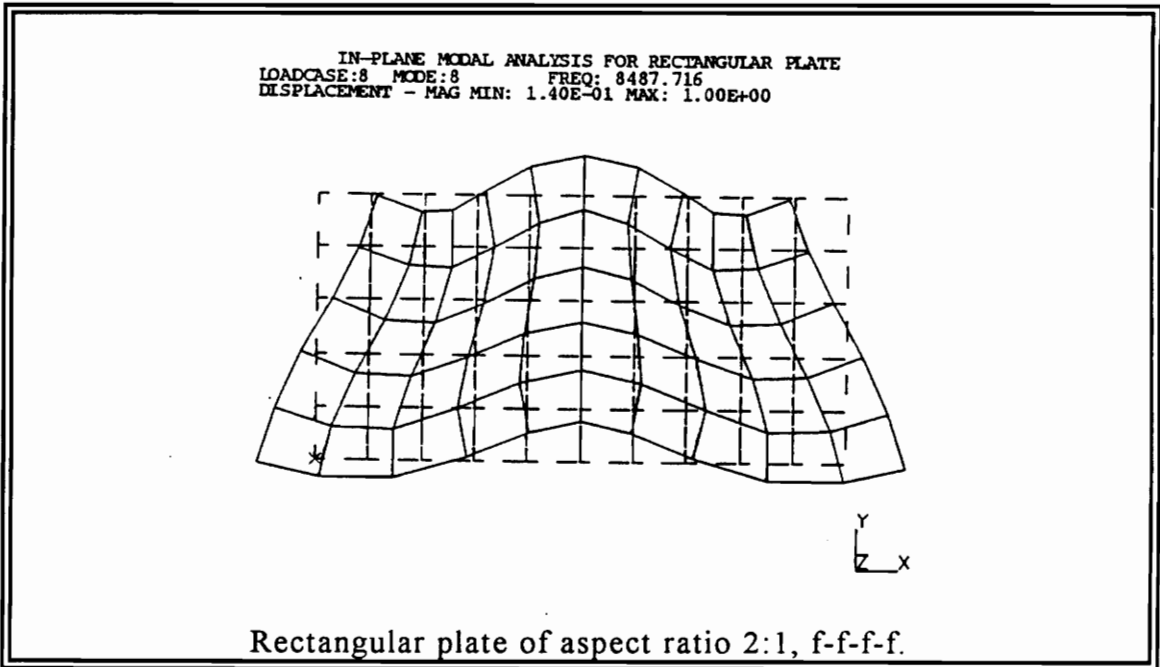


**Figure 3. In-plane vibration patterns of displacement, mode AS-2.**

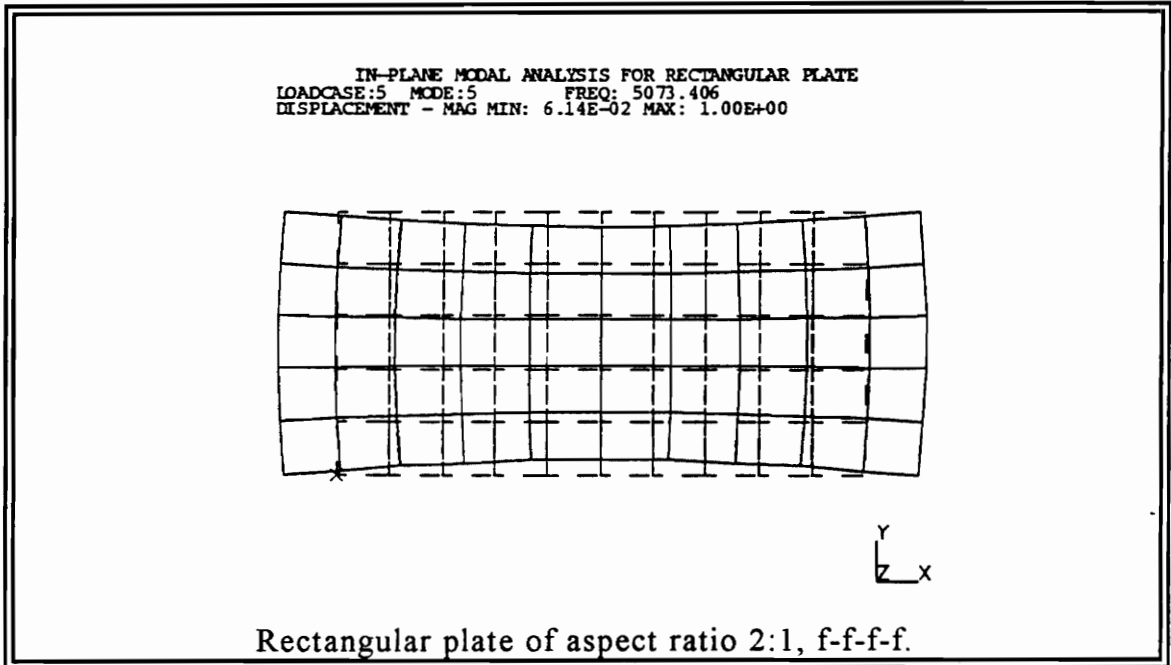


**Figure 4. In-plane vibration patterns of displacement, mode SS-1.**

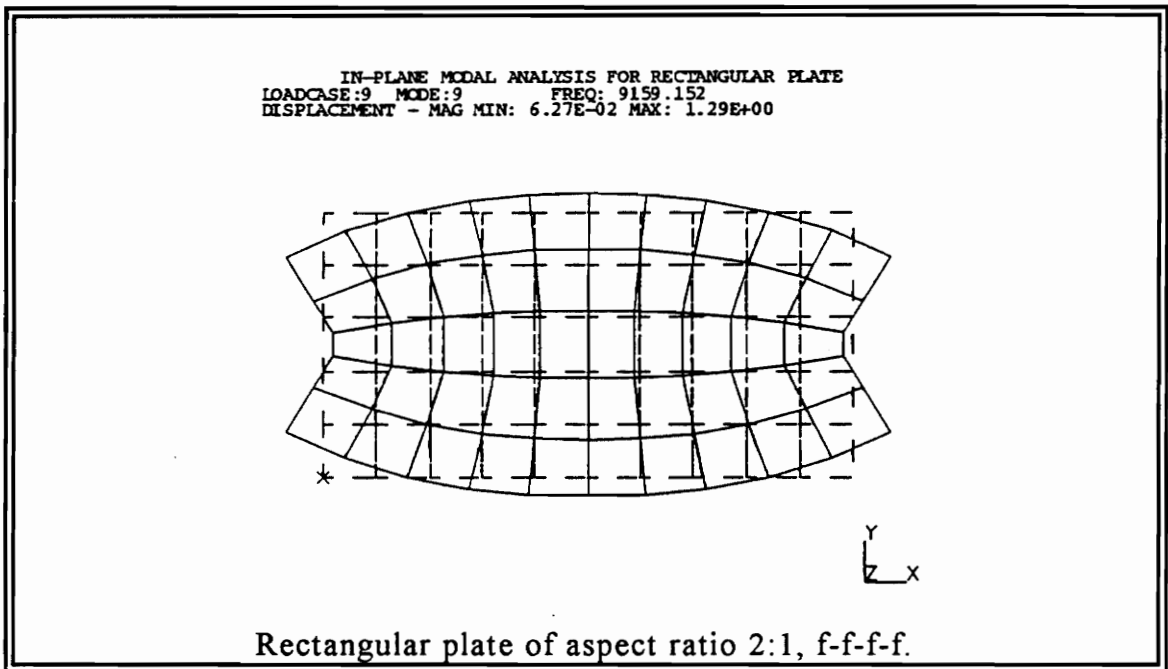


**Figure 5. In-plane vibration patterns of displacement, mode SS-2.**

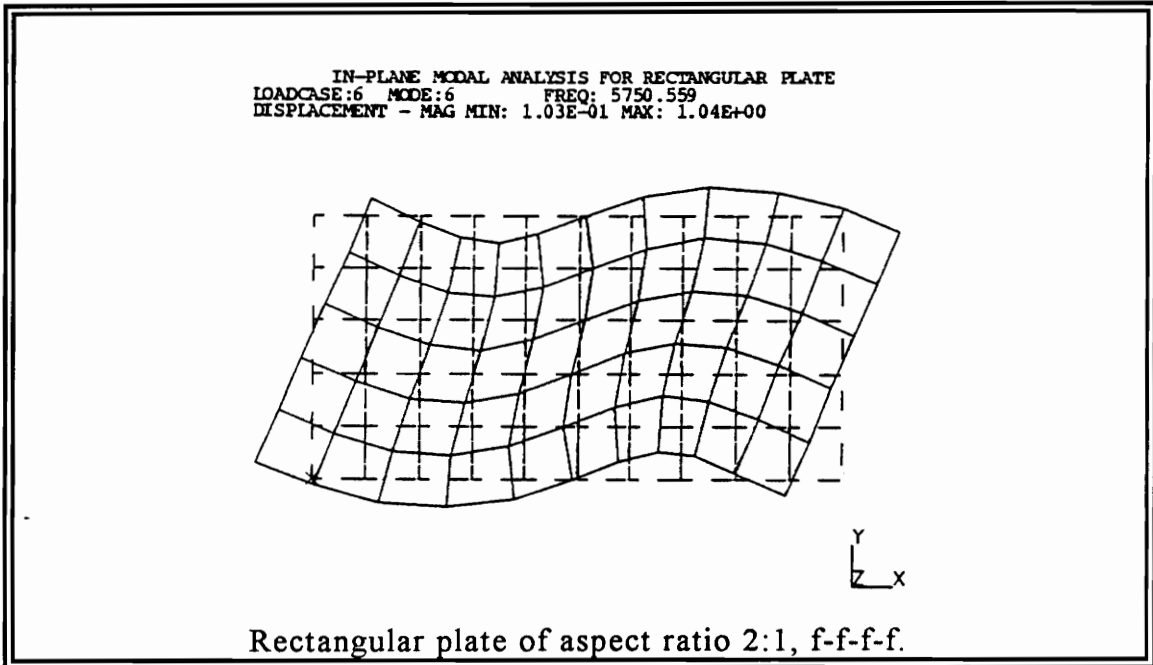


**Figure 6. In-plane vibration patterns of displacement, mode AA-1.**

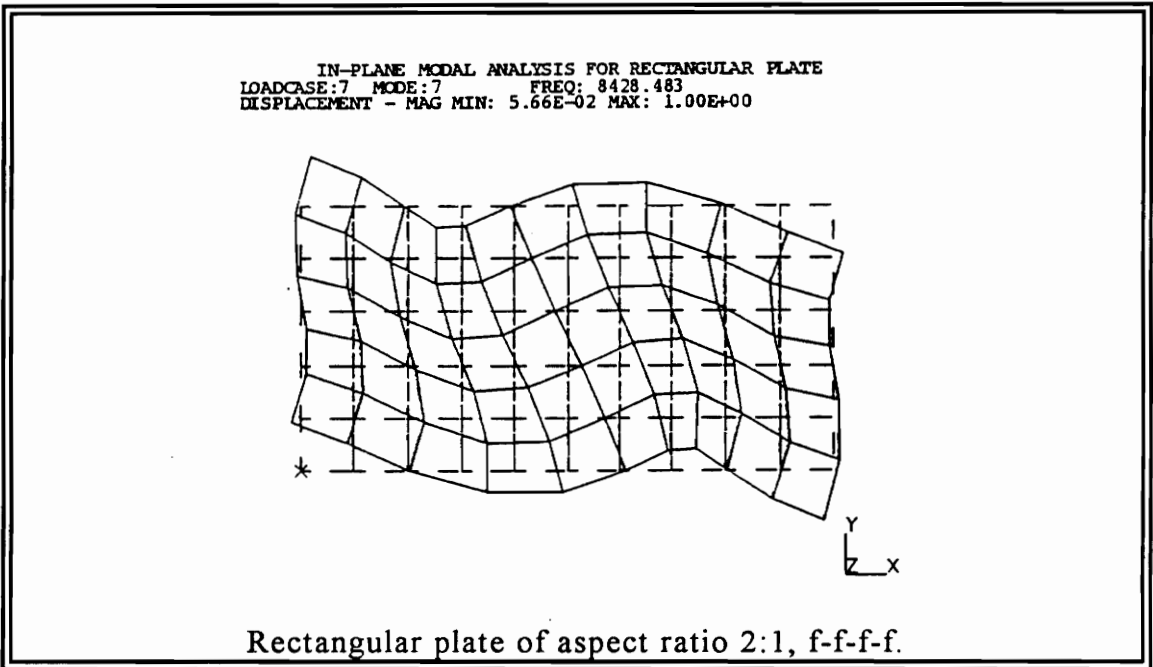


**Figure 7. In-plane vibration patterns of displacement, mode AA-2.**

#### **4. Symmetric-Antisymmetric Case (SA-#)**

The final and fourth case is for in-plane mode shapes that are symmetric with respect to  $x$ -axis and antisymmetric with respect to  $y$ -axis (mirror image about the  $x$ -axis).

##### **SA-1**

This is a mode combining "extensional" and "flexural" characteristics as shown in Fig. 8.

##### **SA-2**

It is the second  $x$ -axis spatial harmonic of the SA-1 in-plane mode (see Fig. 9).

Figures 2 to 9, were developed using finite element analysis in I-DEAS version 4.1.<sup>2</sup> A thin, rectangular plate of aspect ratio 2:1 was used. Boundary conditions are free for all sides. The finite elements are thin shell, linear quadrilaterals. The material is steel of:  $E = 204\text{GPa}$   $\nu = 0.29$ , and  $\rho = 7820\text{kg/m}^3$ .

---

<sup>2</sup> After the third or fourth mode shape the accuracy is reduced significantly.

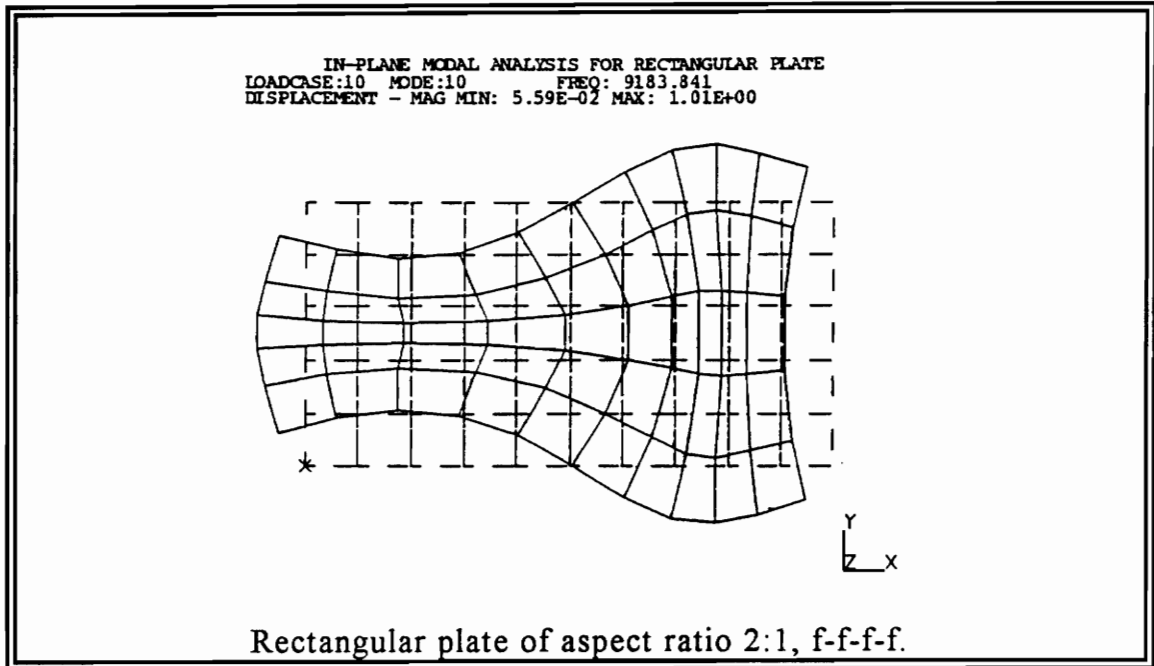


**Figure 8. In-plane vibration patterns of displacement, mode SA-1.**

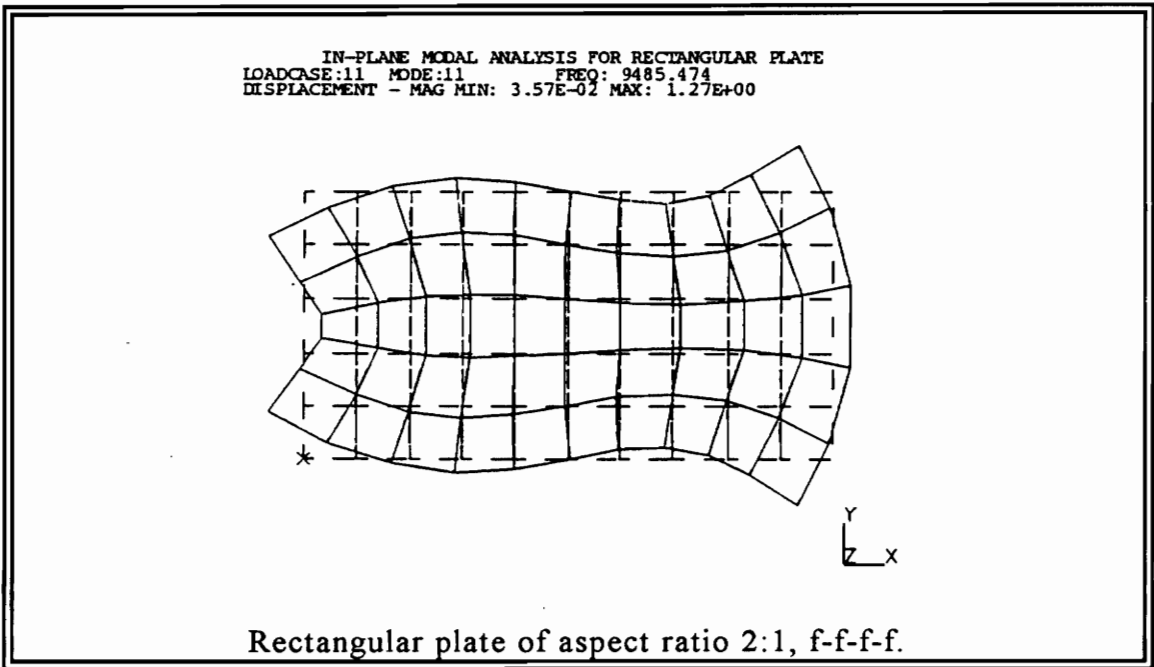


**Figure 9. In-plane vibration patterns of displacement, mode SA-2.**

## 2.3 Lamé Theory

Lamé [33] was the first to describe three-dimensional vibration of isotropic, rectangular parallelepipeds with all six faces traction-free. These solutions are closed-form and exact. Mindlin [35] used the Lamé theory for the calculation of two-dimensional simple modes of crystals. Considering the stress-strain relation and using the theory of elasticity he determined the equations of motion for simple crystals (displacement of the form  $u(x,y,t)$  and  $v(x,y,t)$ ). The stress-equations of motion are:

$$\frac{\partial T_1}{\partial x} = \rho \frac{\partial^2 u}{\partial t^2}, \quad \frac{\partial T_2}{\partial y} = \rho \frac{\partial^2 v}{\partial t^2} \quad \text{where } T_1, T_2 \text{ are stresses.} \quad (2.1)$$

The stresses  $T_1$  and  $T_2$  are functions of the  $\partial u/\partial x$ ,  $\partial v/\partial y$  and terms of elastic compliances  $s_{pq}$  (where  $p, q = 1, 2$  for plane stress). Evaluating a set of equations in [35] for  $T_1$  and  $T_2$  equal to zero at the corner points of the rectangular crystal, the equations of motion are:

$$u = A \cos(\xi x) \sin(\eta y) e^{i\omega t}, \quad v = B \sin(\xi x) \cos(\eta y) e^{i\omega t}. \quad (2.2)$$

The angular frequency of the vibration is given in Eq. (2.3). Note that there is a  $\pi$  in the equation which is very unusual.

$$\omega = (\pi / L) \sqrt{E / \rho} \quad (2.3)$$

Dividing the angular frequency with  $2\pi$  results in a frequency measured in Hz given by Eq. (2.4).

$$f = \frac{1}{2L} \sqrt{E/\rho} \quad (2.4)$$

Lloyd [32] used the Lamé theory [33] and Mindlin's work for crystals [35] as a reference for his experimental results. The equations listed below are based on Eqs. (2.2 and 2.4).

$$\begin{aligned} D_x &= C \sin\left(\frac{\pi x}{L}\right) \cos\left(\frac{\pi y}{L}\right) \\ D_y &= -C \cos\left(\frac{\pi x}{L}\right) \sin\left(\frac{\pi y}{L}\right) \\ f_n &= \frac{0.5 \sqrt{E/\rho}}{L\sqrt{1+\nu}} \end{aligned} \quad (2.5)$$

The above equations are valid for a square-isotropic thin plate. In chapter 4 these formulas are used for analytical simulations. The next section is used in order to clarify the terminology of this thesis.

## ***2.4 Drilling Degrees of Freedom and Drilling Mode Shapes***

The term "drilling degrees of freedom" is used for motion associated to in-plane rotation. It is widely used for literature related to the finite element methods. Most finite element codes do not possess drilling degrees of freedom. According to Knight [38], the drilling degrees of freedom are often present in a code but they give inaccurate results. They have the form of a spring constant, and their presence makes other calculations within the algorithm possible.

Attempts to develop finite elements that utilize all six degrees of freedom have mostly failed. Some researchers were more successful than others; however, the accuracy of their results is very debatable. For a detailed description of such work refer to Hughes [39], Sze [40], and Handa [41].

A "drilling-mode shape" is a state of vibration with a displacement configuration corresponding to in-plane angular motion. It is called "drilling" because of the resulting activity that takes place when a drill is used on a wall or a plane. Transducer technology limitations made research on drilling mode shapes almost impossible. Late advancements like the development of rotational accelerometers and laser vibrometry, allow in-plane vibrations and drilling mode vibrations to receive the experimental attention that they deserve [11,15].

# Chapter 3

## Theory

As explained in the previous chapters, the extraction of rotational degrees of freedom from a spatial array of translational degrees of freedom is desired. For such computation, a mathematical formulation relating the rotational degrees of freedom to the translational degrees of freedom must be known. In this chapter the above formulation is accomplished with the use of vector calculus.

### *3.1 The Curl*

The word "curl" itself suggests that it has to do with things rotating, swirling, or curling around. The curl is defined with the aid of a line integral around a closed path [42]. In Fig. 10, curve  $C$  is traced so that the enclosed area  $\Delta S$  is always to the left. Using the right-hand rule the normal points "up" as shown. Every closed path defines a plane. There is an infinite number of paths (planes of different normal) to enclose a point of a given vector function  $F(x, y, z)$ .

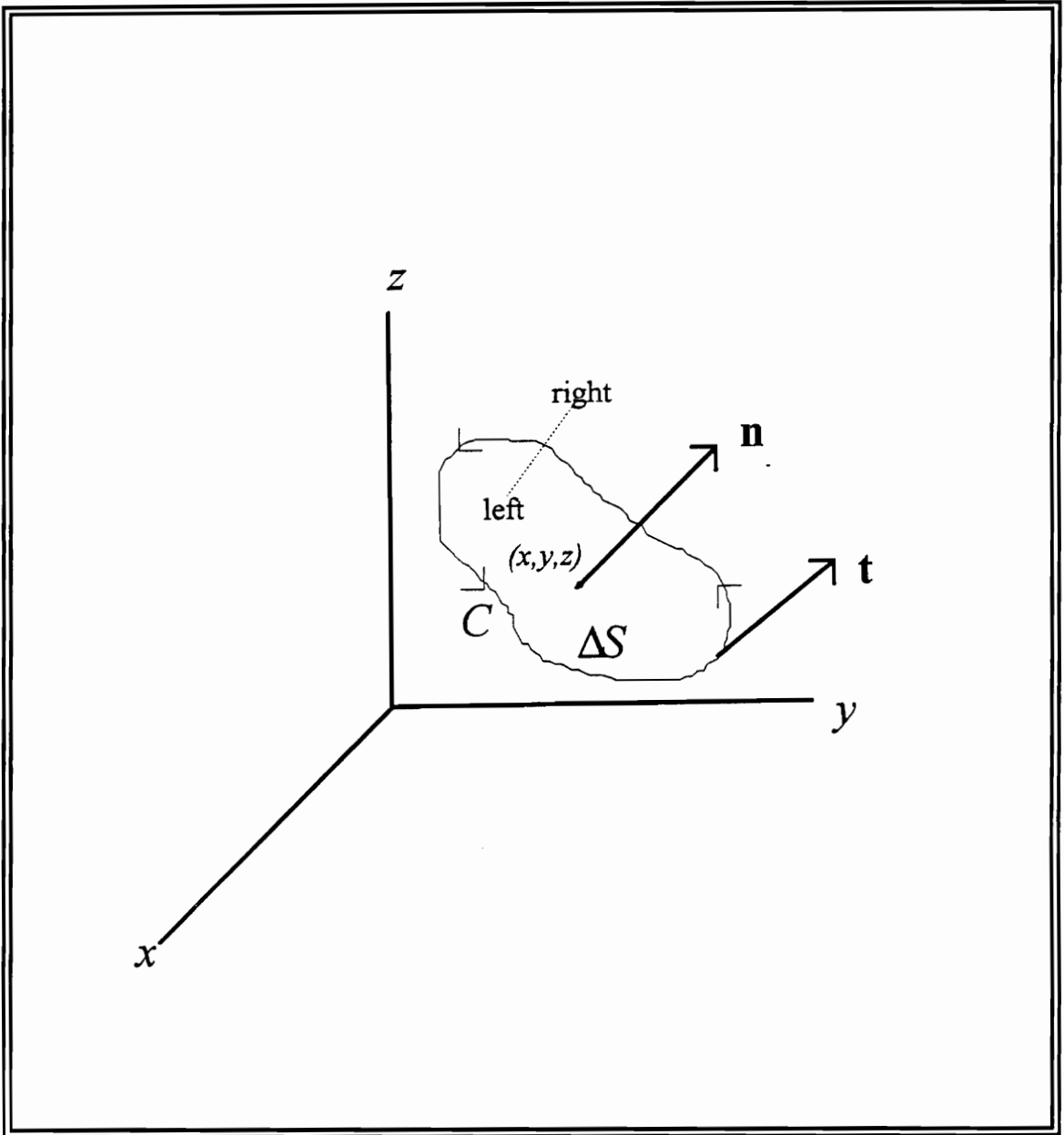


Figure 10. Convention for calculation of curl.

For one specific path of a closed curve  $C$  with a unit normal  $\mathbf{n}$ , let  $s$  be the arc length measured along the curve  $C$ . Let also  $\mathbf{t}$  denote a unit vector tangent to the curve  $C$  of the closed path. If  $\Delta S$  is the enclosed area of the path, using the right-hand rule convention the integral  $I$  given in Eq. (3.1) is calculated (see Fig. 10).

$$I = \lim_{\Delta S \rightarrow 0} \frac{1}{\Delta S} \oint \mathbf{F} \cdot \mathbf{t} \, ds \quad (3.1)$$

When the integral of Eq. (3.1) is evaluated for a path whose normal is  $\mathbf{i}$ , the result is Eq. (3.2).

$$I_x = \frac{\partial F_z}{\partial y} - \frac{\partial F_y}{\partial z} \quad (3.2)$$

Similarly, when the integral of Eq. (3.1) is evaluated for a closed path of normal  $\mathbf{j}$  and for a closed path of normal  $\mathbf{k}$  the results are Eqs. (3.3 and 3.4).

$$I_y = \frac{\partial F_x}{\partial z} - \frac{\partial F_z}{\partial x} \quad (3.3)$$

$$I_z = \frac{\partial F_y}{\partial x} - \frac{\partial F_x}{\partial y} \quad (3.4)$$

The quantities given in Eqs. (3.2, 3.3, and 3.4) are the Cartesian components of a vector called "curl of  $\mathbf{F}$ ". This vector is given in Eq. (3.5).

$$\text{curl } \mathbf{F} = I_x \mathbf{i} + I_y \mathbf{j} + I_z \mathbf{k} \quad (3.5)$$

Schey [42] defines the curl as the limit of the ratio of circulation to area as the area tends to zero. The curl of  $\mathbf{F}$  is also considered as a vector function of position because the limit of Eq. (3.1) has different values for different points  $(x, y, z)$ . In the early calculus textbooks the word *rotation* (abbreviated "rot") was used for what is called now the *curl*. In general, the curl of three-dimensional vector field measures the tendency for angular motion (rotation) around every point of the field.

In order to simplify these derivations, the Cartesian coordinate system has been used. When the Cartesian coordinate system is not the most convenient way for calculations the cylindrical or the spherical systems can be used. For a cylindrical coordinate system the curl is given in Eq. (3.6).

$$\text{curl } \mathbf{F} = \left( \frac{1}{r} \frac{\partial F_z}{\partial \theta} - \frac{\partial F_\theta}{\partial z} \right) \mathbf{r} + \left( \frac{\partial F_r}{\partial z} - \frac{\partial F_z}{\partial r} \right) \boldsymbol{\theta} + \left( \frac{1}{r} \frac{\partial(rF_\theta)}{\partial r} - \frac{1}{r} \frac{\partial F_r}{\partial \theta} \right) \mathbf{z} \quad (3.6)$$

Likewise, for a spherical coordinate system the curl is given in Eq. (3.7).

$$\begin{aligned} \text{curl } \mathbf{F} = & \left( \frac{1}{r \sin \theta} \frac{\partial(\sin \theta F_\phi)}{\partial \theta} - \frac{1}{r \sin \theta} \frac{\partial F_\theta}{\partial \phi} \right) \mathbf{r} + \left( \frac{1}{r \sin \theta} \frac{\partial F_r}{\partial \phi} - \frac{1}{r} \frac{\partial(rF_\phi)}{\partial r} \right) \boldsymbol{\theta} \\ & + \left( \frac{1}{r} \frac{\partial(rF_\theta)}{\partial r} - \frac{1}{r} \frac{\partial F_r}{\partial \theta} \right) \boldsymbol{\phi} \end{aligned} \quad (3.7)$$

In many math books the curl of a function is given as a "del cross  $\mathbf{F}$ ".

$$\text{curl } \mathbf{F} = \nabla \times \mathbf{F} \quad (3.8)$$

For this research the Cartesian coordinate system is used because it provides an easy and convenient way to express the equations; however, Eq. (3.5) is still difficult to memorize. A mnemonic device to remember the curl in a Cartesian coordinate system is given in Eq. (3.9).

$$\text{curl } \mathbf{F} = \begin{vmatrix} \mathbf{i} & \mathbf{j} & \mathbf{k} \\ \frac{\partial}{\partial x} & \frac{\partial}{\partial y} & \frac{\partial}{\partial z} \\ F_x & F_y & F_z \end{vmatrix} \quad (3.9)$$

When the three by three determinant of Eq. (3.9) is expanded the result is identical to Eq. (3.5). (Provided that for example  $\left(\frac{\partial}{\partial x}\right)F_y = \frac{\partial F_y}{\partial x}$  is a valid assumption.)

### 3.2 The Curl of a Translational Velocity Field

In section 3.1 the curl is defined and its basic meaning is explained. A more careful examination leads to results of great significance for this research. Going back to the original model of chapters 1 and 2, assume a three-dimensional vibration of a thin-rectangular plate with free-free-free-free boundary conditions. Utilizing a Cartesian coordinate system where  $x$  and  $y$  are the in-plane directions; and  $z$ , the out-of-plane direction, assume a linear velocity vector field given in Eq. (3.10).

$$\mathbf{V}(x, y, z) = V_x \mathbf{i} + V_y \mathbf{j} + V_z \mathbf{k} \quad (3.10)$$

Based on derivations of section 3.1, the "curl" of the *linear* velocity field is given in Eq. (3.11).

$$\text{curl} (\mathbf{V}(x, y, z)) = \left( \frac{\partial V_z}{\partial y} - \frac{\partial V_y}{\partial z} \right) \mathbf{i} + \left( \frac{\partial V_x}{\partial z} - \frac{\partial V_z}{\partial x} \right) \mathbf{j} + \left( \frac{\partial V_y}{\partial x} - \frac{\partial V_x}{\partial y} \right) \mathbf{k} \quad (3.11)$$

For a thin rectangular plate of thickness  $t$ , the gradient with respect to  $z$  is negligible; in other words, when  $t \rightarrow 0$  then  $\frac{\partial V_y}{\partial z} \rightarrow 0$  and  $\frac{\partial V_x}{\partial z} \rightarrow 0$ . The remaining terms are given in Eq. (3.12).

$$\text{curl} (\mathbf{V}(x,y,z)) = \left( \frac{\partial V_z}{\partial y} \right) \mathbf{i} + \left( -\frac{\partial V_z}{\partial x} \right) \mathbf{j} + \left( \frac{\partial V_y}{\partial x} - \frac{\partial V_x}{\partial y} \right) \mathbf{k} \quad (3.12)$$

Each term of Eq. (3.12) has a physical meaning. Using fundamental principles from mechanics of materials and beam bending, the slope  $dz/dy$  measures the angle of flexure as shown in Fig. 11 (for small angles  $dz/dy = \tan\theta = \theta$ ). The derivative of the angle with respect to time results in  $\dot{\theta}_x$ , which is the angular velocity vector with direction normal to the plane coming out of the page when looking at Fig. 11. Using the above definition of rotation for flexure of solid bodies, the first two terms of Eq. (3.12) can be interpreted as follows:

$$\dot{\theta}_x = \frac{\partial V_z}{\partial y} \quad (\text{angular velocity about x-axis}) \quad (3.13)$$

$$\dot{\theta}_y = -\frac{\partial V_z}{\partial x} \quad (\text{angular velocity about y-axis}). \quad (3.14)$$

Using a similar approach shown in Fig. 12 the third term of Eq. (3.12) is interpreted as the total angular velocity about z-axis measured by the two partial derivatives given in Eq. (3.15).

$$\dot{\theta}_z = \frac{\partial V_y}{\partial x} - \frac{\partial V_x}{\partial y} \quad (\text{angular velocity about z-axis}) \quad (3.15)$$

Eq. (3.15) is the fundamental equation of this research. It relates the rotational degrees of freedom to the translational degrees of freedom. The angular velocity about the out-of-plane z-axis ( $\dot{\theta}_z$ ) is a function of the linear in-plane velocities ( $V_x$  and  $V_y$ ).

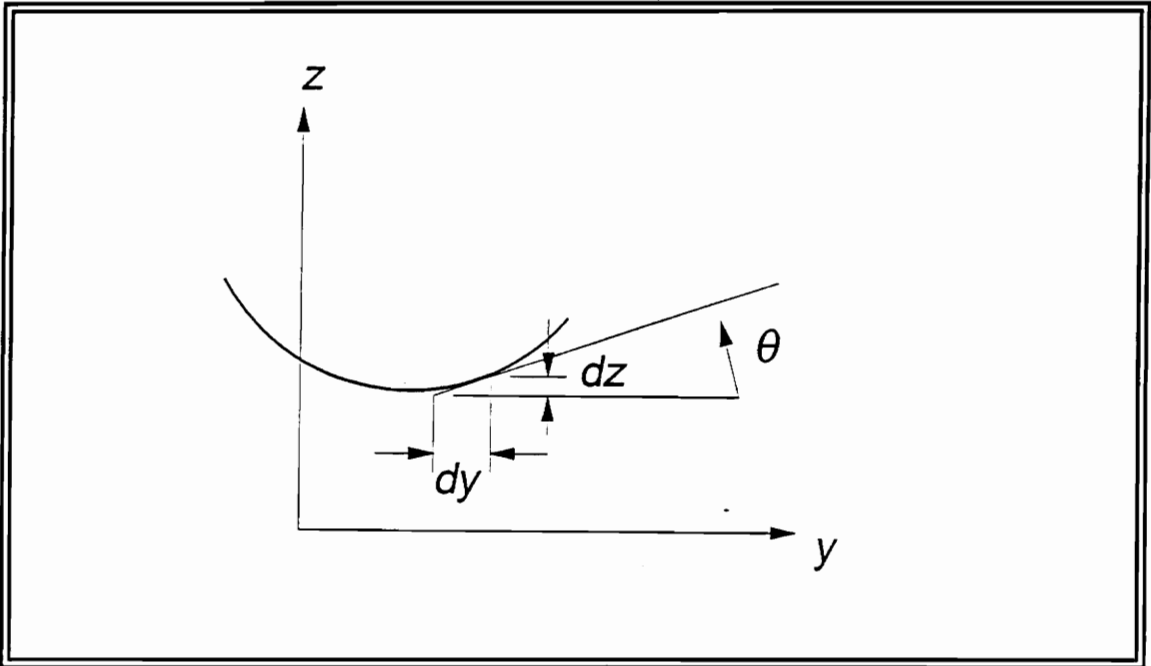


Figure 11. Measurement of rotation in flexure of bodies.

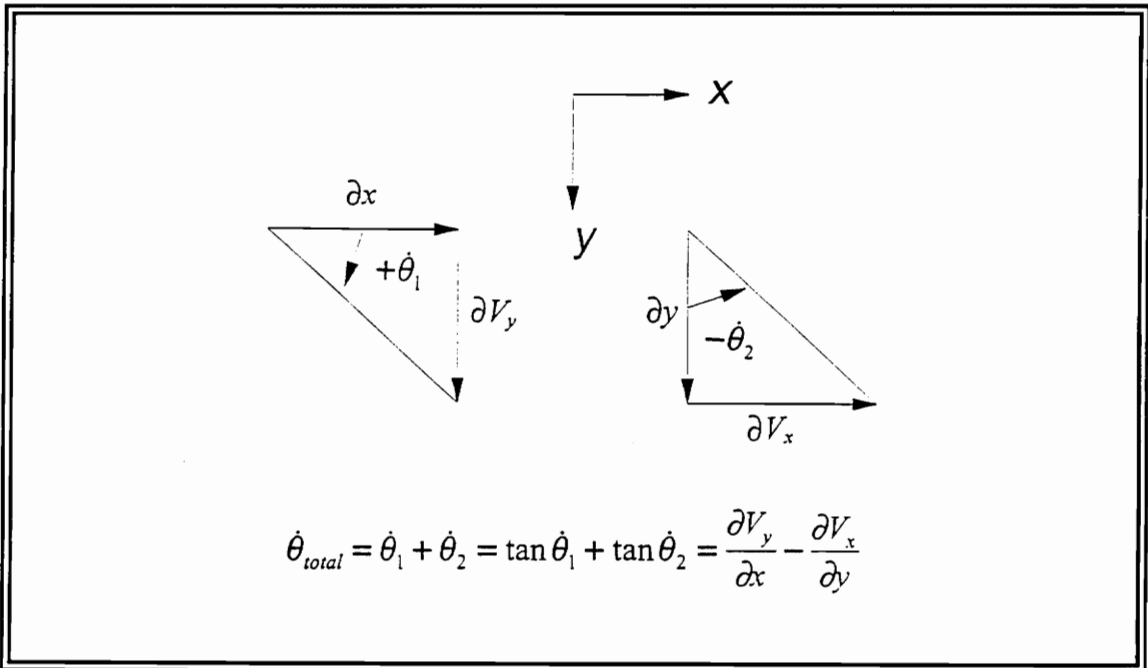


Figure 12. Total angular velocity for in-plane flexure of plates.

For a spatial array of translational degrees of freedom, the rotational degrees of freedom are extracted for each point by performing two steps. First, take the partial derivatives of the in-plane velocities according to Eq. (3.15). Then, subtract the two terms. As a result the value of the angular velocity for the every point of the array is determined.

Proper use of Eq. (3.15) makes possible the calculation of drilling-mode shapes provided the in-plane translations are known. In the chapters to follow, the reader is introduced to numerical and analytical techniques that were used for the extraction of drilling-mode shapes.

It is important to notice that Eqs. (3.13, 3.14, and 3.15) are valid for thin surfaces; in other words, for surfaces where the gradient with respect to thickness is small enough to be considered negligible. When a solid cube is vibrating in a three-dimensional manner, all terms of Eq. (3.11) have to be considered. In this case there are no dominating dimensions in the structure because all length, width, and height are equal; moreover, all gradients with respect to  $x$ ,  $y$ , and  $z$  directions are equally important and significant. The extraction of angular degrees of freedom of such a vibrating structure is a more complicated procedure.

The three-dimensional vibration of thin-rectangular plates is a simpler case where the length and the width of the plate are the dominating dimensions.

The thickness is small, and the extraction of angular degrees of freedom is performed easier because all gradients with respect to  $z$  direction are negligible  $\left(\frac{\partial}{\partial z} \rightarrow 0\right)$ .

Finally, it is important to notice that this thesis deals with flexure of solid plates. Rotation of rigid bodies around an axis of constant angular velocity gives a different meaning to the curl but it is also a different case [43]. In fluid mechanics the curl of the linear velocity field is called vorticity and it is equal to twice the angular velocity vector [44]. This should not confuse the reader. In this thesis, based on the definition of rotation for flexure of solid bodies, the curl of the *linear* velocity field is equal to the *angular* velocity field [45].

## Chapter 4

### Analytical Simulations

In the previous chapter the relation between the translational and rotational degrees of freedom is successfully derived by utilizing the "curl". Before the developing of an algorithm that handles real-life experimental data, there is a need for a reference solution. In other words, taking the curl of a three-dimensional translational-velocity field is not enough for the extraction of the rotational-velocity field. In order to validate the results, it is important to know how accurate they are.

In this chapter a closed-form analytical solution is developed which is used as a reference for the numerical calculations of the next chapters. Acquiring a complete solution consists of two steps. First simulate the in-plane translational velocities and second calculate the rotational velocities by using the curl. As explained earlier, for simplification the vibrating structure is a thin-rectangular plate with free-free-free-free boundary conditions. To avoid unnecessary-tedious calculations of complicated-mode shapes, the exact theory of Lamé is used as a foundation for theoretical simulations [32,33,35].

A Lamé mode of a thin-rectangular plate has corners that do not translate in either  $x$  or  $y$  axes. The equations of motion for in-plane displacements are simple harmonic functions. The Lamé theory is valid only for two in-plane mode shapes. The SS-1 (Symmetric-Symmetric-1) mode shape of a square plate, and the SS-2 (Symmetric-Symmetric-2) mode shape of a 3:1 aspect-ratio rectangular plate. As explained in chapter 2, these two in-plane mode shapes are symmetric with respect to both  $x$  and  $y$  axes. For the same plate, the SS-1 as expected has a lower natural frequency than SS-2; however, the characteristics of a Lamé mode will not be present if the aspect ratio of the rectangular plate is other than 1:1 or 3:1.

#### ***4.1 Lamé-Mode Shape of a Square Plate***

In [32] a closed-form theoretical solution is available for the Lamé mode (SS-1 mode) of a square-isotropic thin plate with boundary conditions free-free-free-free. The equations of motion for in-plane displacements and natural frequency are given. The displacement field is described in Eqs. (4.1 and 4.2) and shown in Fig. 13.

$$D_x = C \sin\left(\frac{\pi x}{L}\right) \cos\left(\frac{\pi y}{L}\right) \quad (4.1)$$

$$D_y = -C \cos\left(\frac{\pi x}{L}\right) \sin\left(\frac{\pi y}{L}\right) \quad (4.2)$$

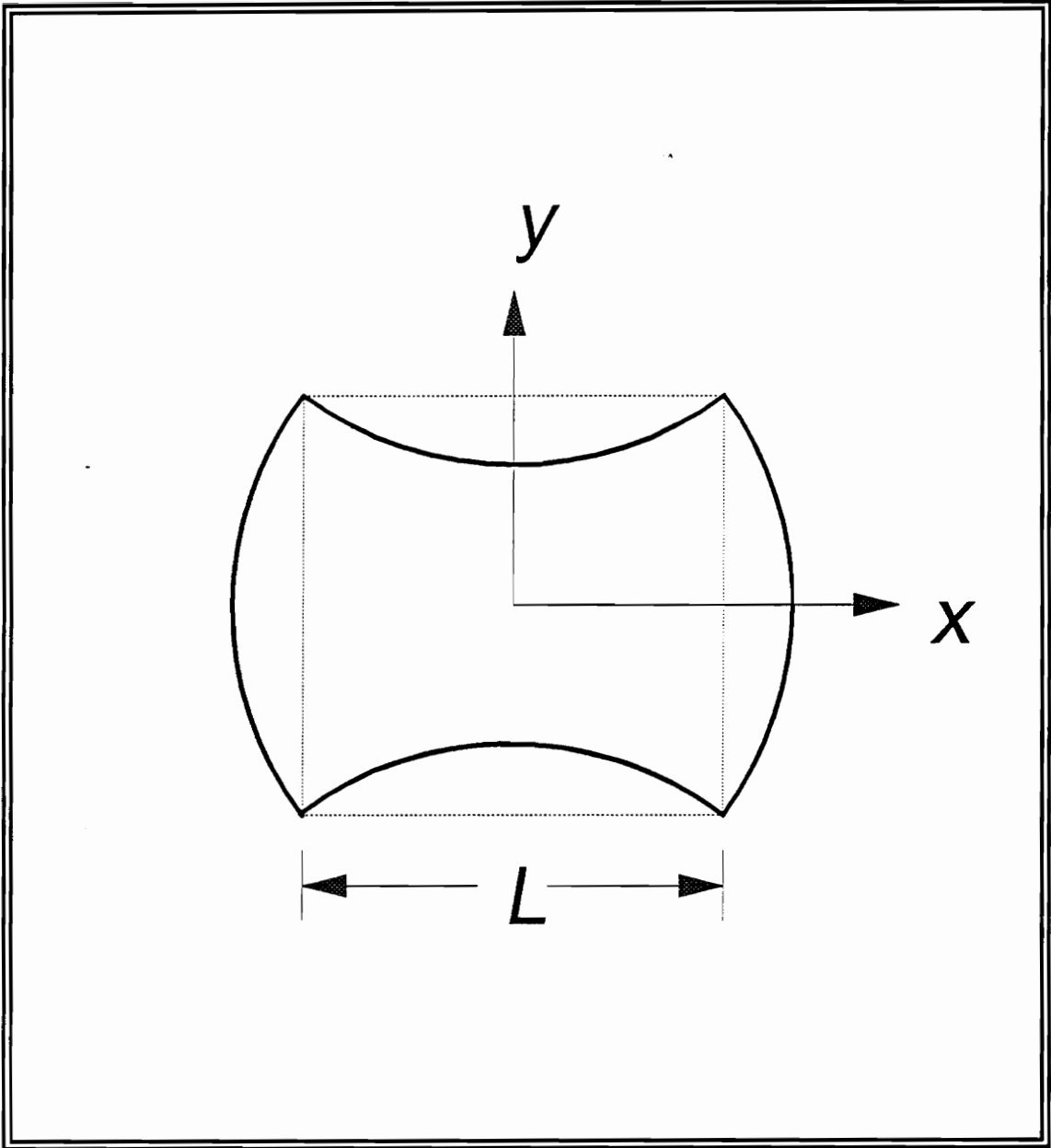


**Figure 13. Lamé mode of a square plate, displacement field.**

In order to get the velocity field multiply each displacement equation with  $j\omega$  (where  $\omega = 2\pi f_n$  and  $f_n$  is the natural frequency). Assuming  $C_I = j\omega C$ , the velocity field is described in Eqs. (4.3 and 4.4). The in-plane velocities can be simulated (using Axum 2.0) for a  $11 \times 11$  spatial array as shown in Figs. 14 and 15.

$$V_x = C_1 \sin\left(\frac{\pi x}{L}\right) \cos\left(\frac{\pi y}{L}\right) \quad (4.3)$$

$$V_y = -C_1 \cos\left(\frac{\pi x}{L}\right) \sin\left(\frac{\pi y}{L}\right) \quad (4.4)$$

For a square-isotropic thin plate of known properties, the natural frequency of the Lamé mode is easily calculated by Eq. (4.5).

$$f_n = \frac{0.5\sqrt{E/\rho}}{L\sqrt{1+\nu}} \quad (4.5)$$

For a structural-steel square plate:  $E = 206.8\text{GPa}$ ,  $\rho = 7820\text{kg/m}^3$ ,  $\nu = 0.29$ , and  $L = 1.0\text{m}$ . Using Eq. (4.5) results in  $f_n = 2263.7\text{Hz}$ . This result will be verified in later chapters by the use of numerical methods. In order to extract the angular velocity field from Eqs. (4.3 and 4.4) the  $\partial V_x/\partial y$  and  $\partial V_y/\partial x$  need to be calculated. Performing partial differentiation in this manner gives Eqs. (4.6 and 4.7).

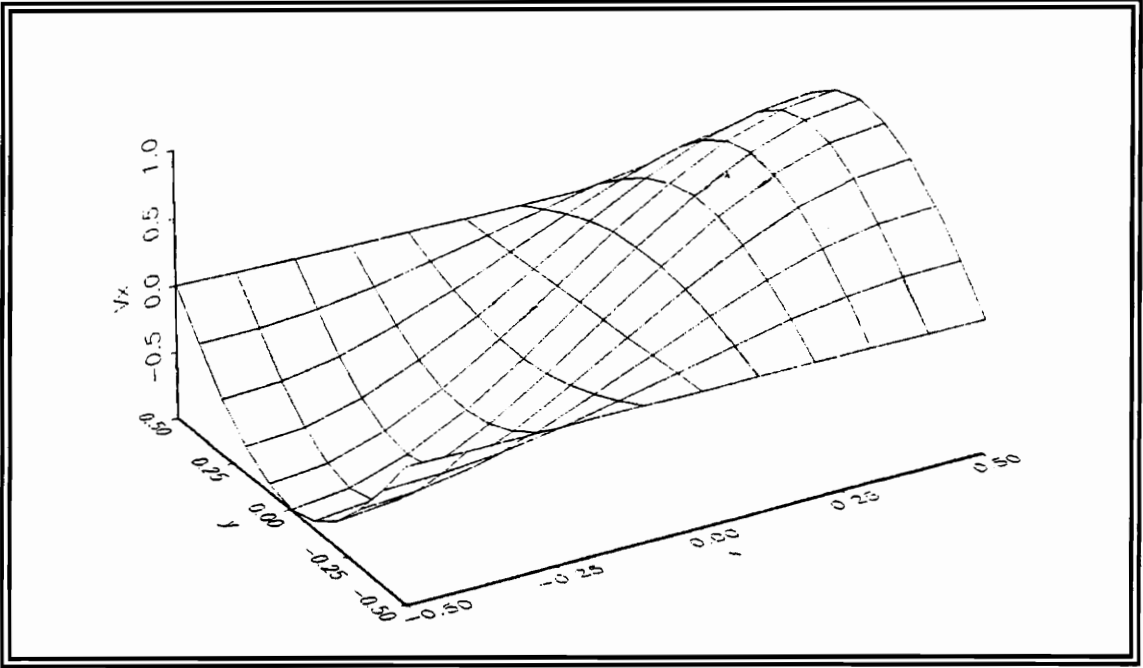


**Figure 14. Lamé mode of a square plate, in-plane velocity  $V_x$ .**

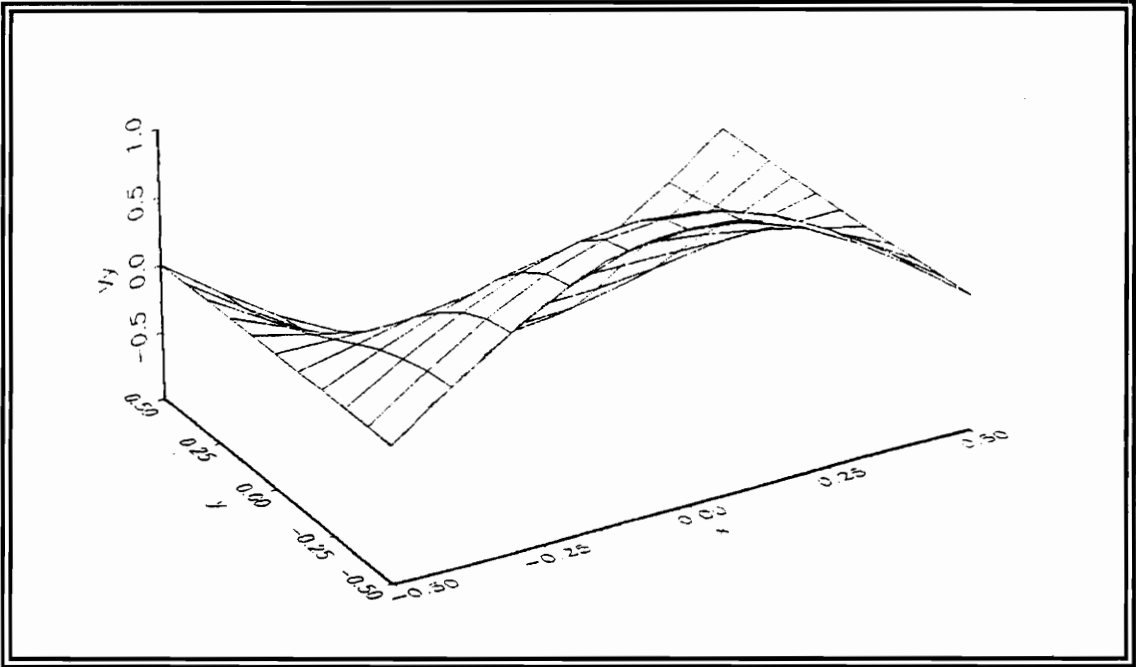


**Figure 15. Lamé mode of a square plate, in-plane velocity  $V_y$ .**

$$\frac{\partial V_x}{\partial y} = -C_1 \frac{\pi}{L} \sin\left(\frac{\pi x}{L}\right) \sin\left(\frac{\pi y}{L}\right) \quad (4.6)$$

$$\frac{\partial V_y}{\partial x} = C_1 \frac{\pi}{L} \sin\left(\frac{\pi x}{L}\right) \sin\left(\frac{\pi y}{L}\right) \quad (4.7)$$

Subtracting Eq. (4.6) from Eq. (4.7) results in Eq. (4.8) which is an explicit closed-form solution for a Lamé-drilling velocity mode shape ( for square thin plate).

$$\dot{\theta}_z = \frac{\partial V_y}{\partial x} - \frac{\partial V_x}{\partial y} = C_2 \sin\left(\frac{\pi x}{L}\right) \sin\left(\frac{\pi y}{L}\right) \quad (4.8)$$

where  $C_2 = 2\pi C_1/L$ ; and  $x, y$  are the Cartesian coordinates. The two partial derivatives have been simulated for the  $11 \times 11$  spatial array of points as shown in Figs. 16 and 17. Likewise, Fig. 18 is a simulation of the Lamé-drilling mode shape for a thin-square plate.

Please notice that the maxima and minima of rotational motion are located at the corners of the plate as expected.

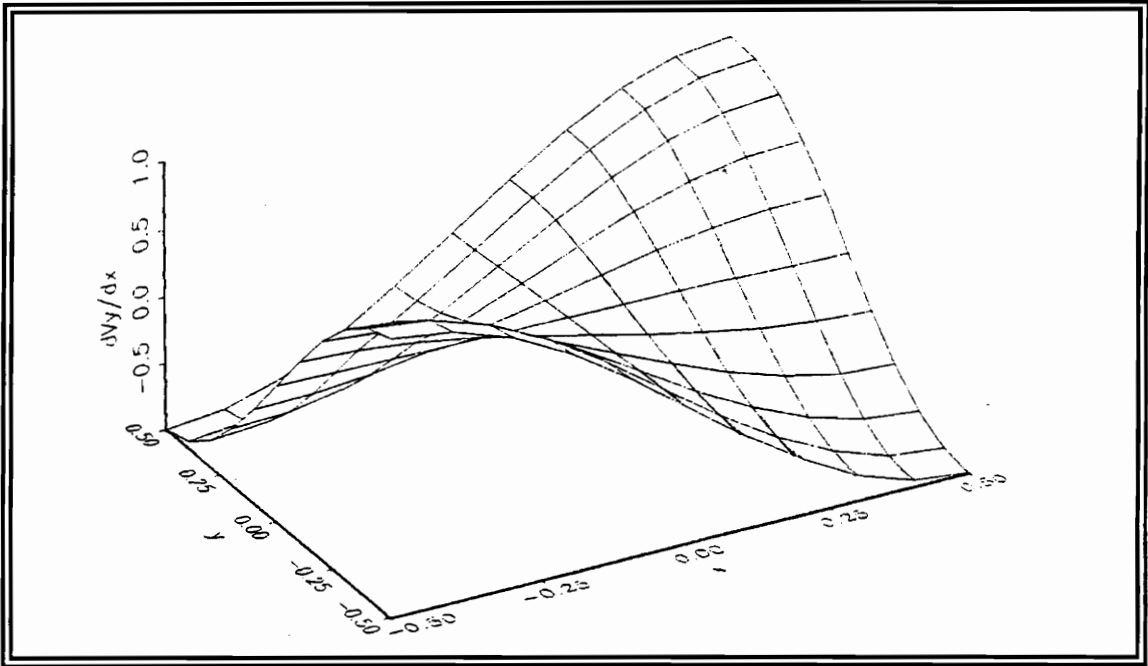


Figure 16. Lamé mode of a square plate,  $\partial V_y/\partial x$ .

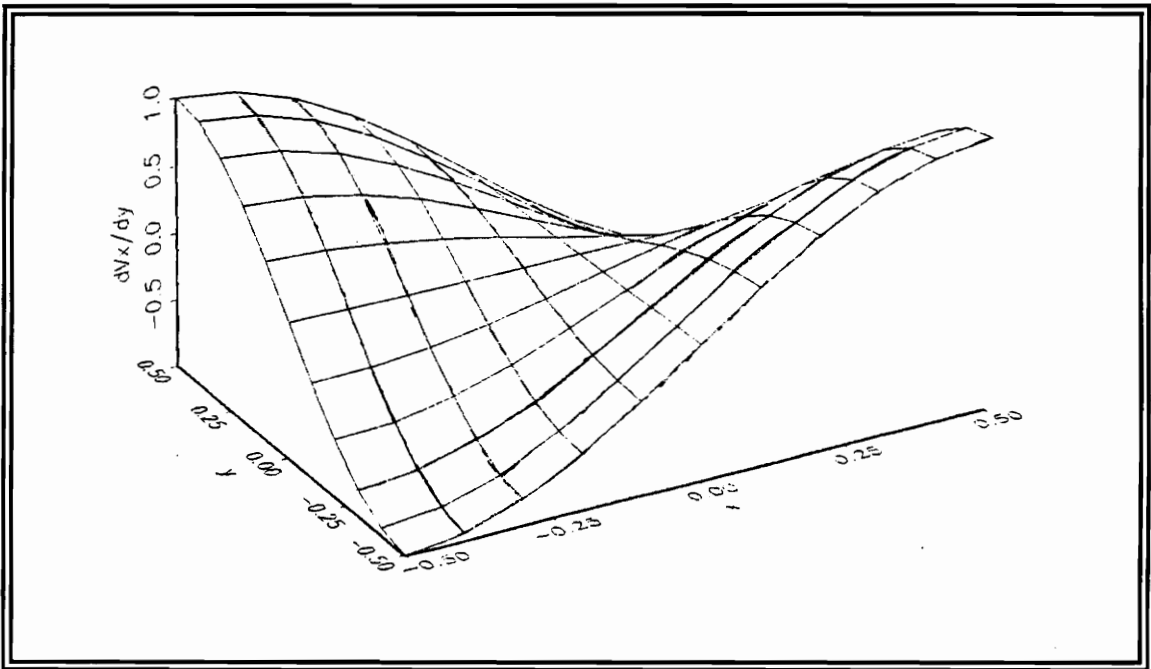


Figure 17. Lamé mode of a square plate,  $\partial V_x/\partial y$ .

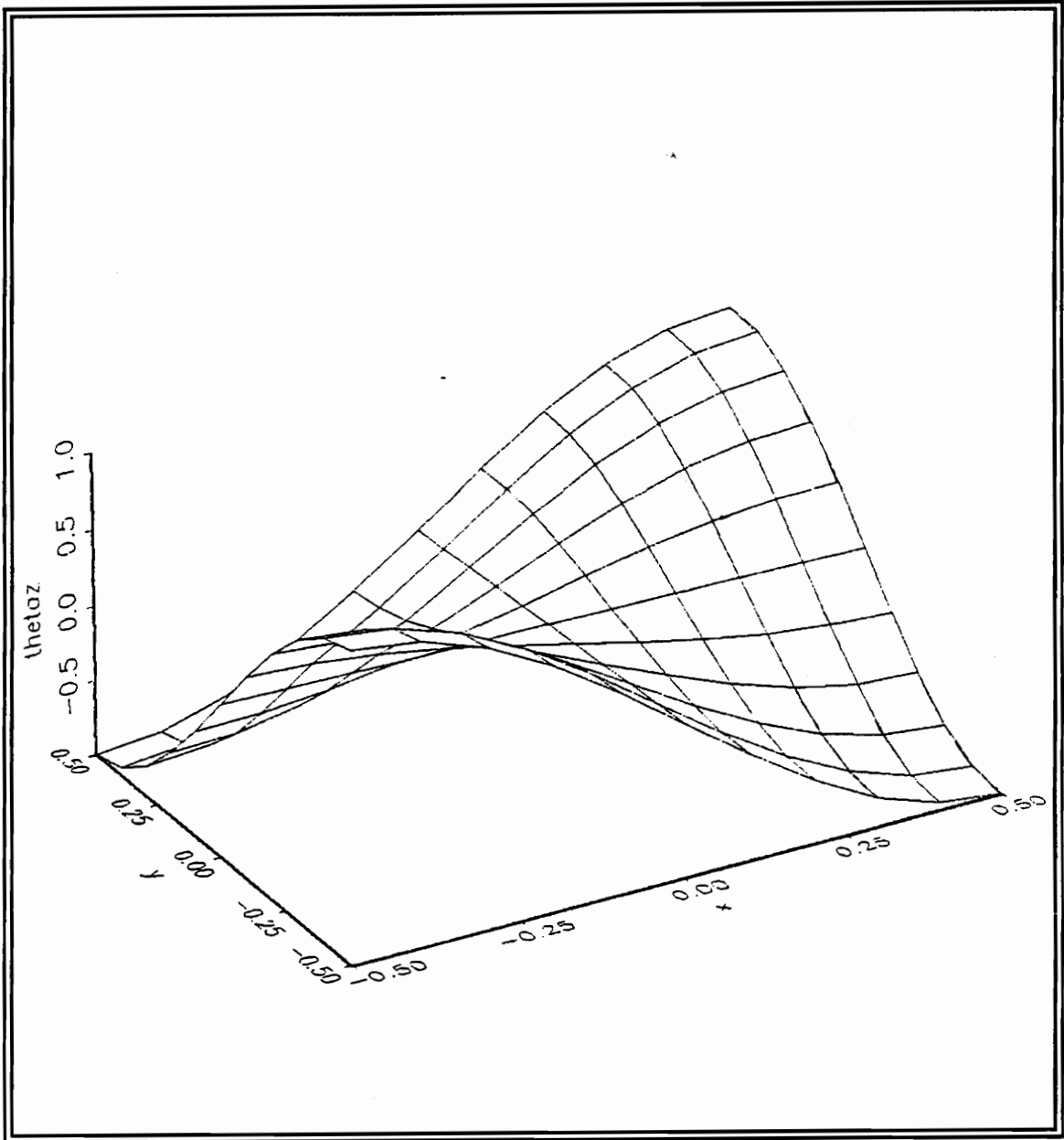


Figure 18. Drilling-Lamé mode of a square plate,  $\theta_{z2}$ .

## 4.2 Lamé-Mode Shape of a Rectangular Plate

In [32] a closed-form theoretical solution is also available for the Lamé mode (SS-2 mode) of a rectangular-isotropic thin plate (3:1 aspect ratio) with boundary conditions free-free-free-free. The equations of motion for in-plane displacements and natural frequency are given. The displacement field is described in Eqs. (4.9 and 4.10) and shown in Fig. 19.

$$D_x = C \sin\left(\frac{3\pi x}{L_1}\right) \cos\left(\frac{\pi y}{L_2}\right) \quad (4.9)$$

$$D_y = -C \cos\left(\frac{3\pi x}{L_1}\right) \sin\left(\frac{\pi y}{L_2}\right) \quad (4.10)$$

In order to get the velocity field multiply each displacement equation with  $j\omega$  (where  $\omega = 2\pi f_n$  and  $f_n$  is the natural frequency). Assuming  $C_1 = j\omega C$ , the velocity field is described in Eqs. (4.11 and 4.12). The in-plane velocities can be simulated (using Axum 2.0) for a 6×16 spatial array as shown in Figs. 20 and 21.

$$V_x = C_1 \sin\left(\frac{3\pi x}{L_1}\right) \cos\left(\frac{\pi y}{L_2}\right) \quad (4.11)$$

$$V_y = -C_1 \cos\left(\frac{3\pi x}{L_1}\right) \sin\left(\frac{\pi y}{L_2}\right) \quad (4.12)$$

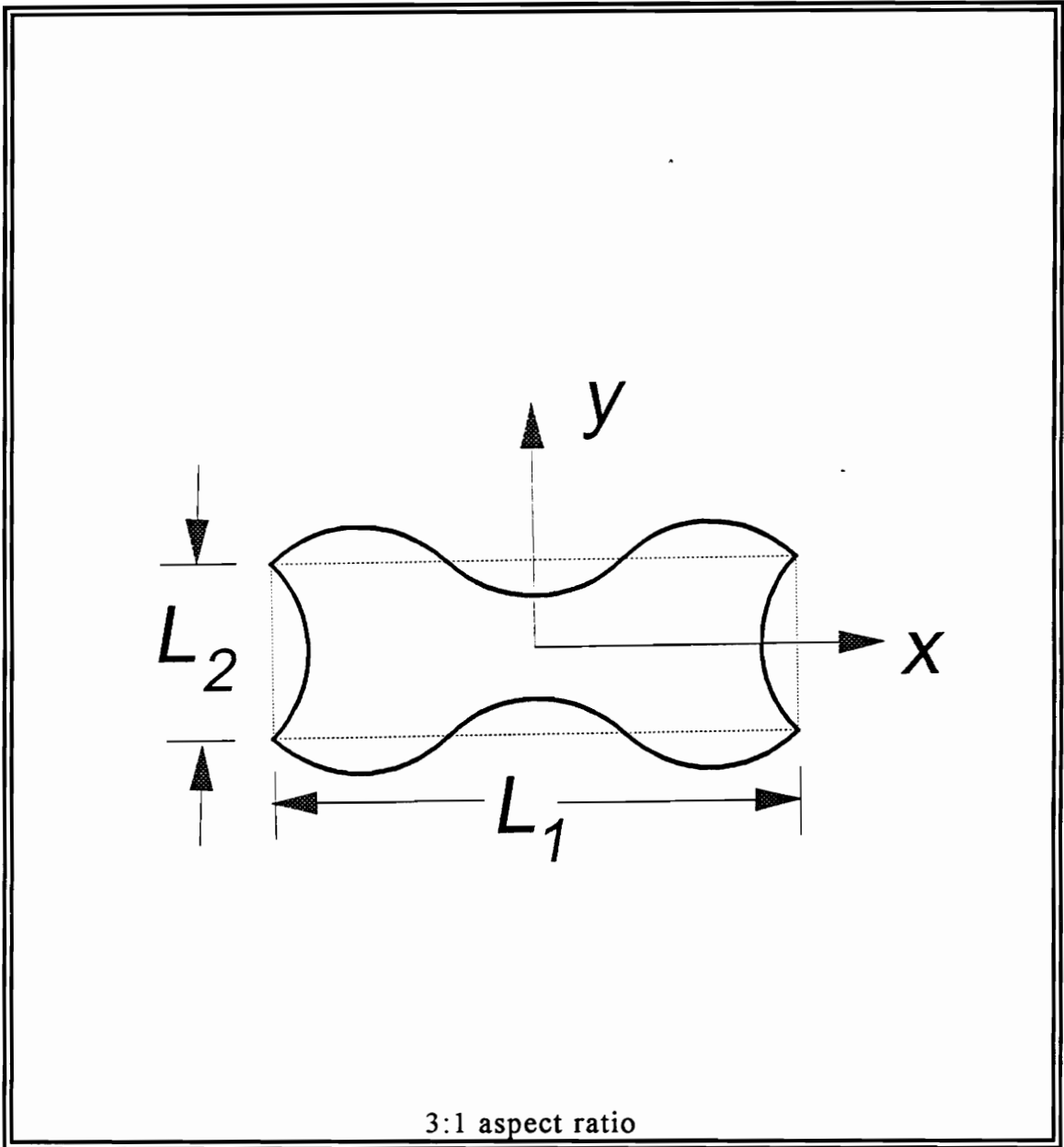


**Figure 19. Lamé mode of a rectangular plate, displacement field.**

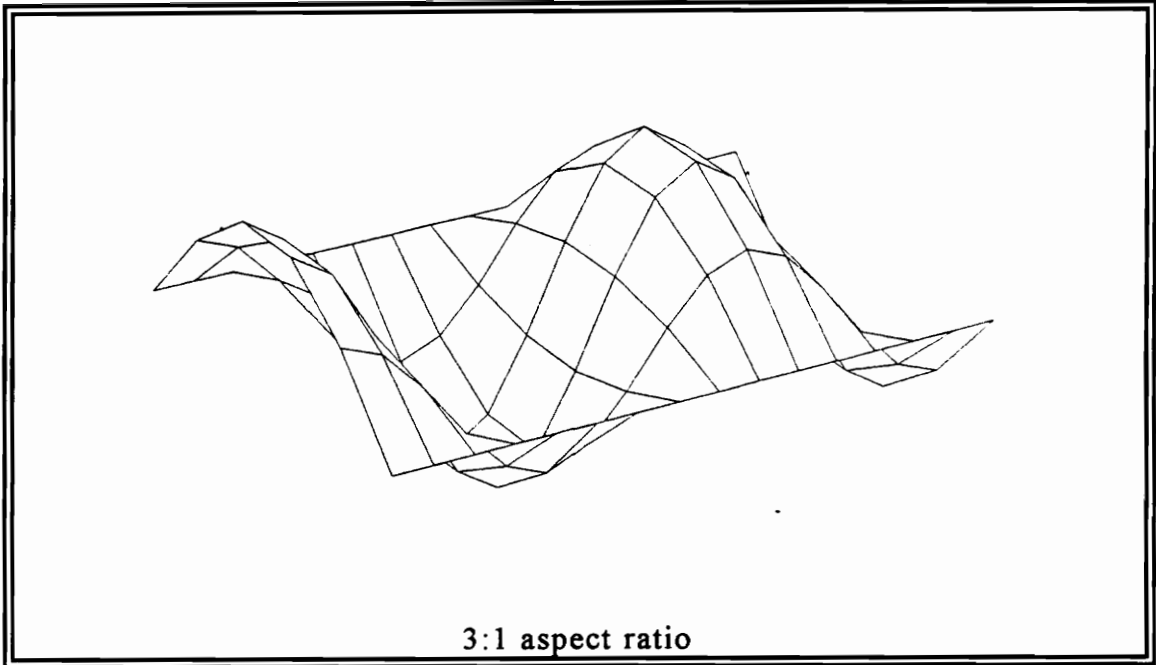


**Figure 20. Lamé mode of a rectangular plate, in-plane velocity  $V_x$ .**

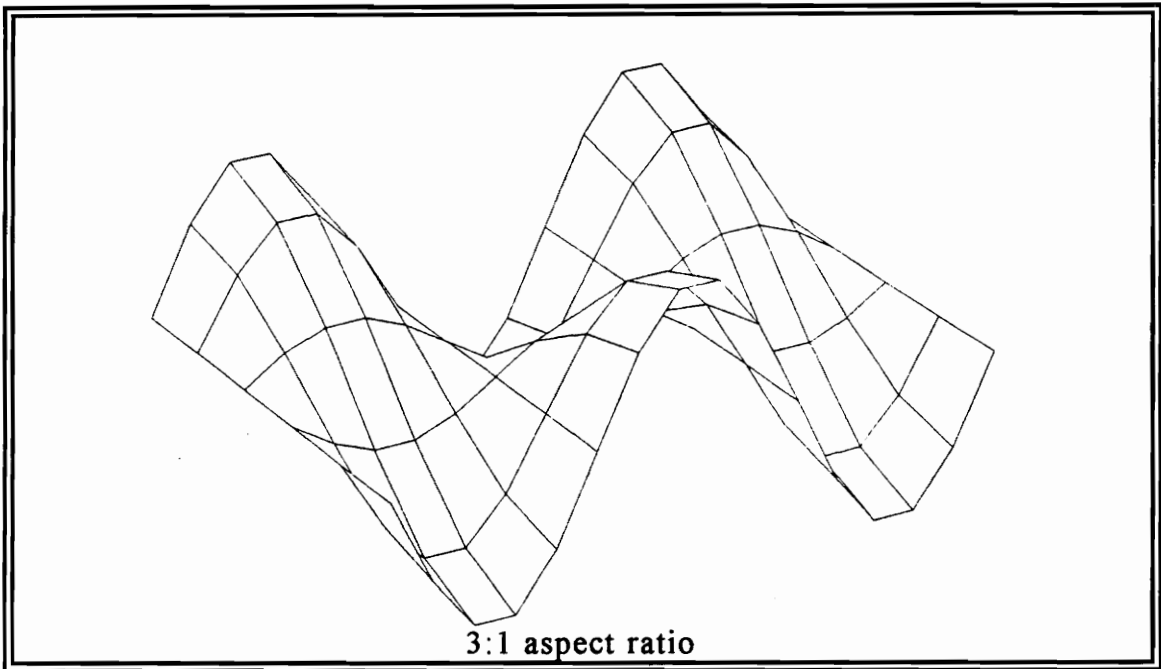


**Figure 21. Lamé mode of a rectangular plate, in-plane velocity  $V_y$ .**

For a rectangular-isotropic thin plate (3:1 aspect ratio) of known properties, the natural frequency of the Lamé mode is easily calculated by Eq. (4.13).

$$f_n = \frac{3\sqrt{E/\rho}}{2L_1\sqrt{1+\nu}} \quad (4.13)$$

For a structural-steel square plate:  $E = 206.8\text{GPa}$ ,  $\rho = 7820\text{kg/m}^3$ ,  $\nu = 0.29$ , and  $L_1 = 1.5\text{m}$  ( $L_1/L_2 = 3$ ). Using Eq. (4.13) results in  $f_n = 4527.7\text{Hz}$ . This result will be verified in later chapters by the use of numerical methods. In order to extract the angular velocity field from Eqs. (4.11 and 4.12) the  $\partial V_x/\partial y$  and  $\partial V_y/\partial x$  need to be calculated. Performing partial differentiation in this manner gives Eqs. (4.14 and 4.15). See Figs. 22 and 23.

$$\frac{\partial V_x}{\partial y} = -C_1 \frac{\pi}{L_2} \sin\left(\frac{3\pi x}{L_1}\right) \sin\left(\frac{\pi y}{L_2}\right) \quad (4.14)$$

$$\frac{\partial V_y}{\partial x} = 3C_1 \frac{\pi}{L_1} \sin\left(\frac{3\pi x}{L_1}\right) \sin\left(\frac{\pi y}{L_2}\right) \quad (4.15)$$

Subtracting Eq. (4.14) from Eq. (4.15) results in Eq. (4.16) which is an explicit closed-form solution for a Lamé-drilling velocity mode shape ( for a rectangular-thin plate, 3:1 aspect ratio, and free-free-free-free boundary conditions).

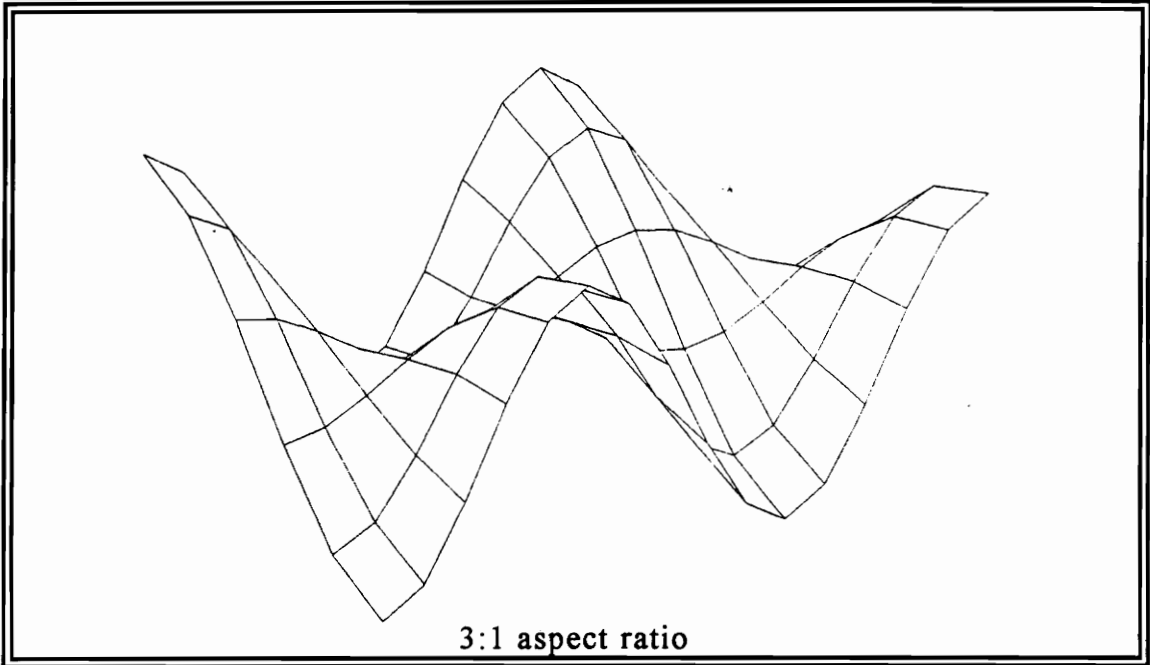


**Figure 22. Lamé mode of a rectangular plate,  $\partial V_y / \partial x$ .**

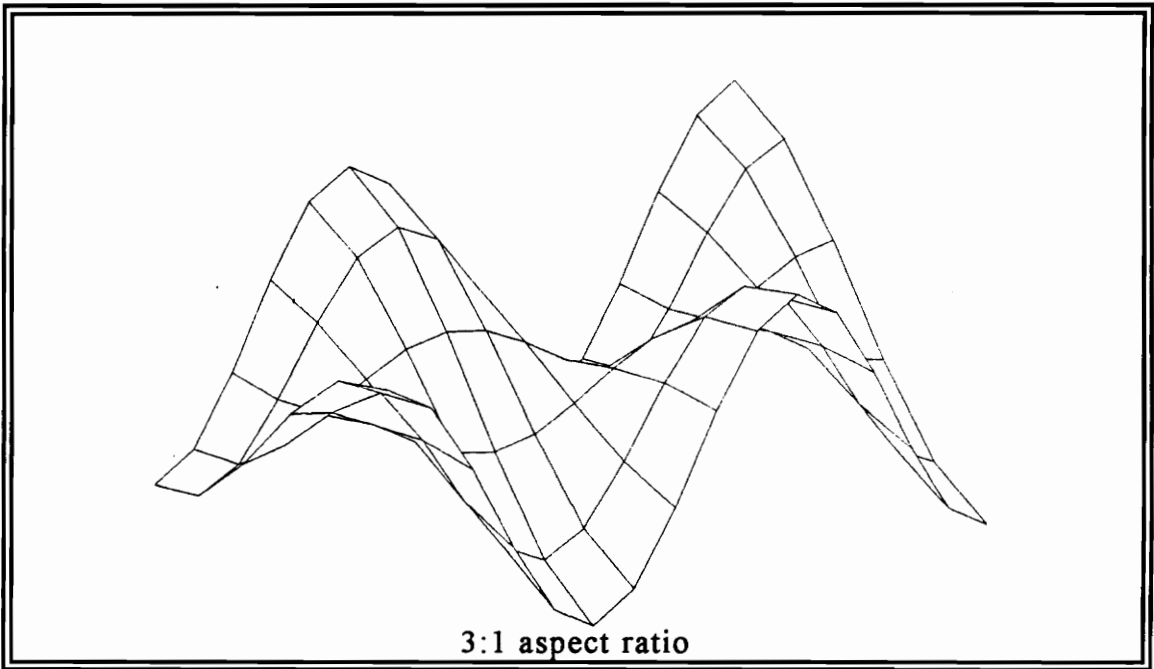


**Figure 23. Lamé mode of a rectangular plate,  $\partial V_x / \partial y$ .**

$$\dot{\theta}_z = \frac{\partial V_y}{\partial x} - \frac{\partial V_x}{\partial y} = C_2 \sin\left(\frac{3\pi x}{L_1}\right) \sin\left(\frac{\pi y}{L_2}\right) \quad (4.16)$$

where  $C_2 = C_1 \pi \left( \frac{3}{L_1} + \frac{1}{L_2} \right)$ ; and  $x, y$  are the Cartesian coordinates. For all analytical simulations of section 4.2 a  $6 \times 16$  spatial array of points is used. Finally, Fig. 24 is a simulation of the Lamé-drilling mode shape for a thin-rectangular plate (3:1 aspect ratio with free-free-free-free boundary conditions).

Please notice that like the square plate the maxima and minima of the rotational motion are located at the corners of the plate. In addition, maxima and minima are also located along each long side for  $1/3$  and  $2/3$  of side  $L_1$ .

All these analytical simulations of in-plane translational velocities and drilling-velocity mode shapes, can be used as a foundation for the numerical calculations of the next chapter. In chapter 5, drilling degrees of freedom are extracted numerically using MATLAB, and the results are compared to the theory of chapter 4.

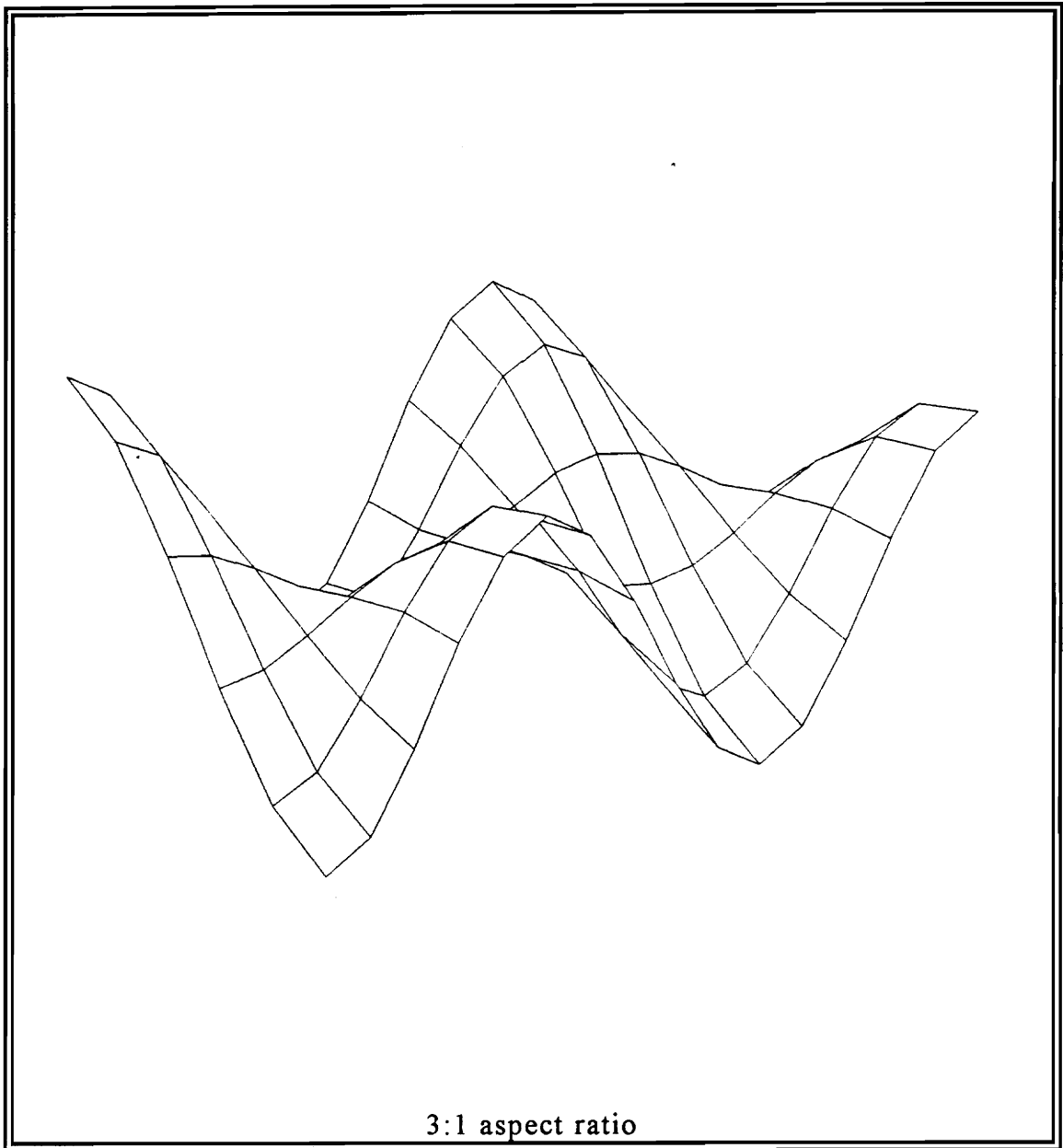


**Figure 24. Drilling-Lamé mode of a rectangular plate,  $\theta_z$ .**

# Chapter 5

## Numerical Simulations

In this chapter numerical methods are used for the calculation of in-plane translational velocities and the extraction of rotational degrees of freedom from a nodal-spatial array of translational degrees of freedom.

### *5.1 I-DEAS Finite Element Dynamic Code*

A finite element dynamic code in I-DEAS 4.1<sup>3</sup> is used for generation of in-plane velocities for a spatial array of nodes. This spatial array is a representation of an isotropic-thin rectangular plate with boundary conditions free-free-free-free. The aspect ratio of the rectangular plate is either 1:1 (square plate) or 3:1. For these two cases the Lamé-mode shape is present, and its explicit closed-form theoretical solution is given in chapter 4. Consequently, the theoretical results can be used as a reference for the numerical results.

---

<sup>3</sup> I-DEAS 4.1 is a registered trademark of SDRC University.

The first step in finite element analysis is to enter the properties of the model. The material properties of the plate are  $E = 206\text{GPa}$ ,  $\rho = 7820\text{kg/m}^3$ , and  $\nu = 0.29$  (structural steel). The dimensions of the square plate are  $L = 1.0\text{m}$  and  $t = 0.0254\text{m}$  ( $11 \times 11$  spatial array of nodes). The dimensions of the rectangular plate are  $L_1 = 1.5\text{m}$ ,  $L_2 = 0.5\text{m}$ , and  $t = 0.0254\text{m}$  ( $6 \times 16$  spatial array of nodes).

The element used for in-plane dynamic analysis in I-DEAS is thin-shell linear quadrilateral. Generally, the thin-shell linear quadrilateral has all six degrees of freedom active per point; however, the drilling degree of freedom is artificial [38]. Therefore, it cannot be calculated directly from most commercially distributed finite element codes. Some finite element codes under special formulation make use of the drilling degree of freedom, but they are complicated and difficult to implement [39,40,41]. In this case, in order to perform in-plane dynamic analysis only the in-plane translations  $x$  and  $y$  were activated. The rest degrees of freedom remained inactive [46].

Next, Guyan reduction is used for solving the equations. Ordinarily, the Guyan reduction is used as a mass condensation technique. Condensation reduces the number of degrees of freedom which reduces the computing time [47]. When properly used there is no significant loss in accuracy. I-DEAS 4.1 also utilizes simultaneous vector iterations (SVI solver) for dynamic analysis. The SVI solver is recommended for most dynamic cases; nevertheless, for in-plane dynamic analysis the SVI solver would not work. The only way to perform in-plane dynamic analysis using I-DEAS 4.1, is to use Guyan reduction without mass condensation.

Guyan reduction without mass condensation takes place when all degrees of freedom are master with no slave degrees of freedom present in the spatial array of nodes. That means 242 master degrees of freedom for the square plate and 192 master degrees of freedom for the rectangular plate (3:1 aspect ratio).

For better representation of the results, both consistent-mass and lumped-mass models are considered. The consistent-mass model is based on a mass-matrix formulation as described in [47,48]. The lumped-mass model replaces continuum configuration with discrete masses connected by massless elements which have the same elastic properties as the continuum configuration [48]. According to Knight [38], the consistent-mass solution overestimates the actual eigenvalue solution and the lumped-mass solution underestimates the actual eigenvalue solution. As a result, the actual eigenvalue solution is found between the two. In most cases, the consistent-mass model is more accurate; thus, more frequently used.

In Appendix-A, the first three in-plane mode shapes of a square plate (all specifications mentioned in the beginning of this section) are found for using consistent-mass model. Likewise, in Appendix-B, the first three in-plane mode shapes of a rectangular plate (all specifications also mentioned in the beginning of this section) are found using the consistent-mass model.

The accuracy of the results is dropping as the natural frequency of the mode shape becomes higher in value. In section 5.3.1 will be shown that up to the third in-plane eigenvector, the results are accurate. Hence, the square-plate Lamé mode can be found using finite elements in I-DEAS 4.1. This happens because the SS-1 mode shape, corresponding to the square-plate Lamé mode, is the third in-plane eigenvector appearing in the finite element solution. To the contrary, the SS-2 mode shape, corresponding to the rectangular-plate (3:1 aspect ratio) Lamé mode, is the ninth in-plane eigenvector to appear in the finite element solution and could not be adequately analyzed for the given number of degrees of freedom. Due to the special use of the Gyan reduction solver with all degrees of freedom specified as master and no slave degrees of freedom present, the I-DEAS software does not accept more than 250 master degrees of freedom used [46]. As a result, software limitations do not allow a sufficient increase in the number of degrees of freedom to get more accurate solutions.

Up to this point theoretical analysis was one way to generate the in-plane translational velocities  $V_x$  and  $V_y$  (Lamé eigenvectors only). The finite element method is an alternative way of performing the same operation. Of course, there is some loss in accuracy; but at least it provides accurate results for the first three in-plane mode shapes of the structure. This means that additional solutions of other eigenvectors different than the Lamé mode can be described successfully.

The simulation of the in-plane translational velocities  $V_x$  and  $V_y$  is of great importance because they are the input of the MATLAB code. The MATLAB code is used for the extraction of the drilling-angular velocities as explained next.

## 5.2 MATLAB Drilling-Velocity Extraction Code

Sun [16] performed angular velocity extraction using one-dimensional Discrete Fourier Transform-Inverse Discrete Fourier Transform (DFT-IDFT) technique. Using this process on MATLAB<sup>4</sup> he determines successfully  $\dot{\theta}_x$  and  $\dot{\theta}_y$  [49]. The same technique with few modifications can be used for the calculation of the drilling-angular velocity  $\dot{\theta}_z$ .

As mentioned in the previous section, the in-plane translational velocities  $V_x$  and  $V_y$  are loaded as the input. This is done in the form of two separate spatial arrays  $V_x$  and  $V_y$ . As shown in chapters 3 and 4, partial differentiation of the two arrays and then subtracting one array from the other determines the drilling-mode shape. This is true, but in reality this case is more complicated than it seems. Using experimental data means that both spatial arrays contain noise. Hence, velocity data smoothing is needed in addition to differentiation. The finite difference method seems to be a solution; however, Kochersberger [15] refers to the finite difference method as a noise amplifier. All the above reasons make the DFT-IDFT technique very suitable, because it acts as a lowpass spatial filter, and differentiation is relatively simple in the spatial frequency domain. Differentiation is attained by multiplying the spatial frequency data with the proper frequency-domain differentiation operator.

---

<sup>4</sup> MATLAB is a registered trademark of MathWorks, Inc.

In other words, for differentiation with respect to  $x$  multiply spatial frequency data with  $j\omega_x$  and for differentiation with respect to  $y$  multiply spatial frequency data with  $j\omega_y$ .

The major problem with using this technique is that it requires spatial periodic data to reduce leakage. In general, spatial data are not periodic in a real structure. The periodicity problem of the spatial data is solved and described in detail in [16]:

"One effective method for making sequence periodic is to connect its two end points with a straight line. The curve is then replotted on the original axes by using the velocity differences between the original curve and the connecting line. This "shears" the data sequence so that its end points lie on the  $x$  axis or a "DC" line defined by left end point. The waveform is then rotated through  $180^\circ$  counterclockwise about its right end point. This forms a new curve continuous in amplitude and slope at end points and middle. While this produces a periodic record, the cost is twice as much data to be processed."

In order for the code to work properly, the plate dimensions and the number of spectral lines must be specified. The only important dimensions for the MATLAB algorithm are the length and the width of the plate. Thickness does not enter the calculations (thin plate).

The number of spectral lines is also a very critical issue. Sun [16] uses a preliminary rule of thumb and suggests:

"...at least 2.5 basic spatial harmonics must be retained. In the double size spatial domain this would mean 5.0 times the basic spatial harmonics. ...there is a tradeoff here. The more spatial spectral lines that are retained the better the reconstruction where there is no noise in the data. However, the more retained spectral lines the greater chance that the noise will be reproduced in the reconstructed smoothed spatial shape."

Sun's rule of thumb works fine in this research; however, best results are obtained for half the number suggested by Sun. This could be the result of the fact that the arrays used in this research are very coarse (approximately one hundred points) compared to the experimental arrays used by Sun (thousands of points).

Appendix-C contains the MATLAB code used for numerical extraction of the drilling mode shapes. In order to validate the numerical procedures discussed in the last two sections, theory is going to be used as reference where possible.

## 5.3 Validation of Numerical Methods

When numerical methods like the I-DEAS and MATLAB code are used for solutions of the nature as specified earlier in this chapter, there is no way to know how accurate the results are. Nevertheless, the analytical solutions of chapter 4 provide the means for comparison and can be used as a reference.

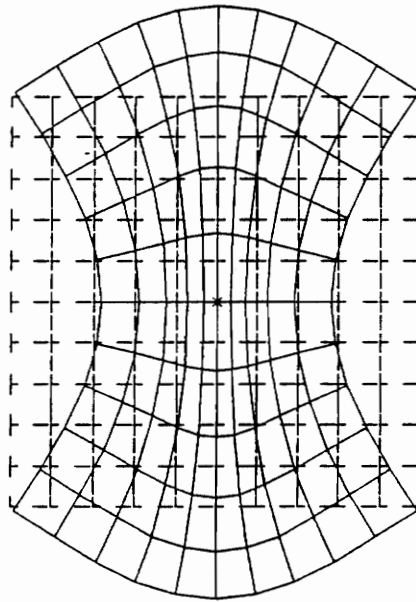
### 5.3.1 Theory vs. Finite Element Code

The Lamé in-plane mode shape of a square-thin plate (11×11 nodal-spatial array) with boundary conditions free-free-free-free, is calculated with I-DEAS 4.1 and shown in Fig. 25. Note that the corners of the plate are not stationary as the closed-form solution finds. In order to find out how close the finite element results are to theory, Table 1 is constructed. Table 1 shows the % error of in-plane velocity  $V_x$  as defined by Eq. (5.1). The matrix of the in-plane velocity  $V_y$  is equal to the negative of the inverse of  $V_x$  matrix, and as a result it does not need to be compared to the theory.

$$\%error = \frac{V_x^{theory} - V_x^{fe}}{V_x^{theory}} \times 100 \quad (5.1)$$

In Table 1 the symbol "UND" stands for undefined (division by zero). The maxima of the error occur around the perimeter of the plate. Within the plate the calculations seem to be very accurate.

IN-PLANE DYNAMIC ANALYSIS, SQUARE PLATE  
FREQ: 2276.8168  
MIN: 1.42E-08 MAX: 1.00E+00



Y  
L  
X

**Figure 25. Lamé mode of square plate by using I-DEAS 4.1.**

**Table 1. Validation of finite element code, %error of  $V_x$ .**

	1	2	3	4	5	6	7	8	9	10	11
1	UND	UND	UND	UND	UND	UND	UND	UND	UND	UND	UND
2	-8.6	-8.3	-8.2	-8.0	-7.8	0.0	7.8	8.0	8.2	8.3	8.6
3	-2.6	-2.3	-2.1	-2.0	-2.0	0.0	2.0	2.0	2.1	2.3	2.6
4	-0.9	-0.6	-0.4	-0.3	-0.2	0.0	0.2	0.3	0.4	0.6	0.9
5	-0.2	0.1	0.3	0.4	0.4	0.0	-0.4	-0.4	-0.3	-0.1	0.2
6	0.0	0.3	0.6	0.6	0.6	0.0	-0.6	-0.6	-0.6	-0.3	0.0
7	-0.2	0.1	0.3	0.4	0.4	0.0	-0.4	-0.4	-0.3	-0.1	0.2
8	-0.9	-0.6	-0.4	-0.3	-0.2	0.0	0.2	0.3	0.4	0.6	0.9
9	-2.6	-2.3	-2.1	-2.0	-2.0	0.0	2.0	2.0	2.1	2.3	2.6
10	-8.6	-8.3	-8.2	-8.0	-7.8	0.0	7.8	8.0	8.2	8.3	8.6
11	UND	UND	UND	UND	UND	UND	UND	UND	UND	UND	UND

Numbers from 1 to 11 are horizontal and vertical nodal positions.

### 5.3.2 Theory vs. MATLAB Code

Two  $16 \times 6$  arrays of discrete theoretically exact in-plane translational velocities  $V_x$  and  $V_y$  for the Lamé mode of a thin-rectangular plate (aspect ratio 3:1 with boundary conditions free-free-free-free), are now used as an input for the MATLAB code. The output is a numerically calculated drilling mode shape. This mode shape is compared to the theoretical one calculated in chapter 4.

Since the in-plane velocities are noiseless and smooth, the filtering of the DFT-IDFT process does not affect the results, and the drilling mode shape entirely agrees with the theory. In other words the error throughout the array is zero. The number of spectral lines along the long side of the plate is 3. The number of the spectral lines along the short side of the plate is 1. Other combinations also work. In general, for this MATLAB code the number of spectral lines along the two sides ( $ns_x$  and  $ns_y$ ) is controlled by Eq. (5.2).

For a  $(n,m)$  array of points,

$$ns_x < 2n-2 \quad \text{and} \quad ns_y < 2m-2 \quad (5.2)$$

The number of points along each side is doubled because the data length is doubled in order to make the data periodic. The two points subtracted represent the two end points. The partial derivative of  $V_y$  with respect to  $x$  and the partial derivative of  $V_x$  with respect to  $y$  are given in Figs. 26 and 27 respectively. The drilling-mode shape is shown in Fig. 28.

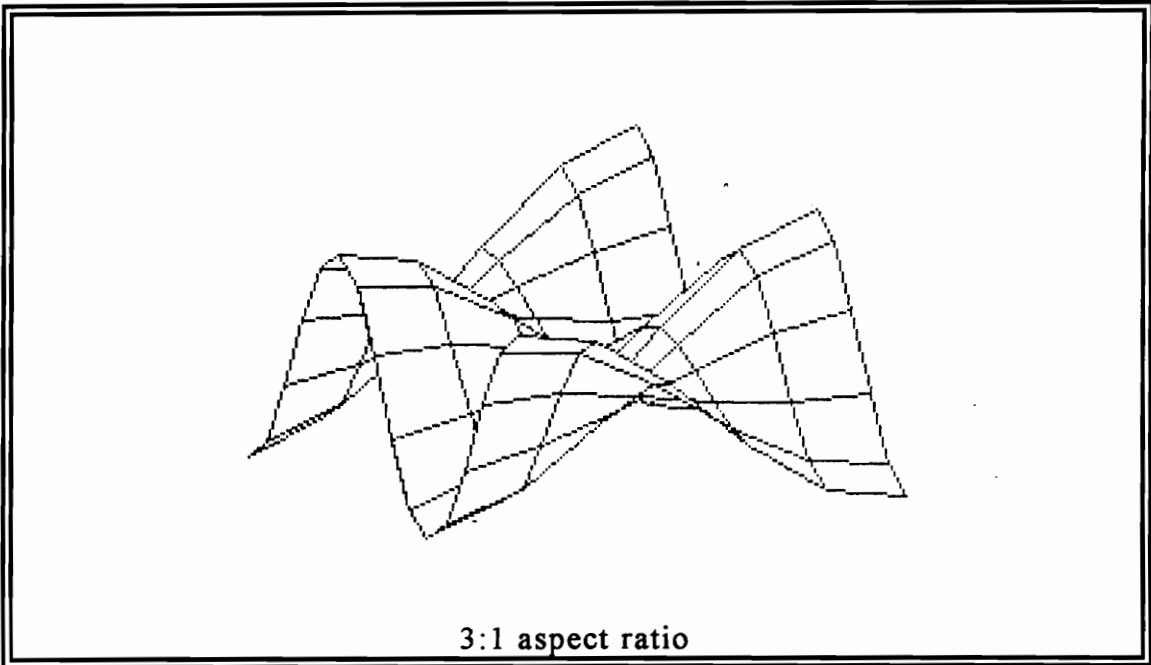


**Figure 26. MATLAB code,  $\partial V_y/\partial x$ .**

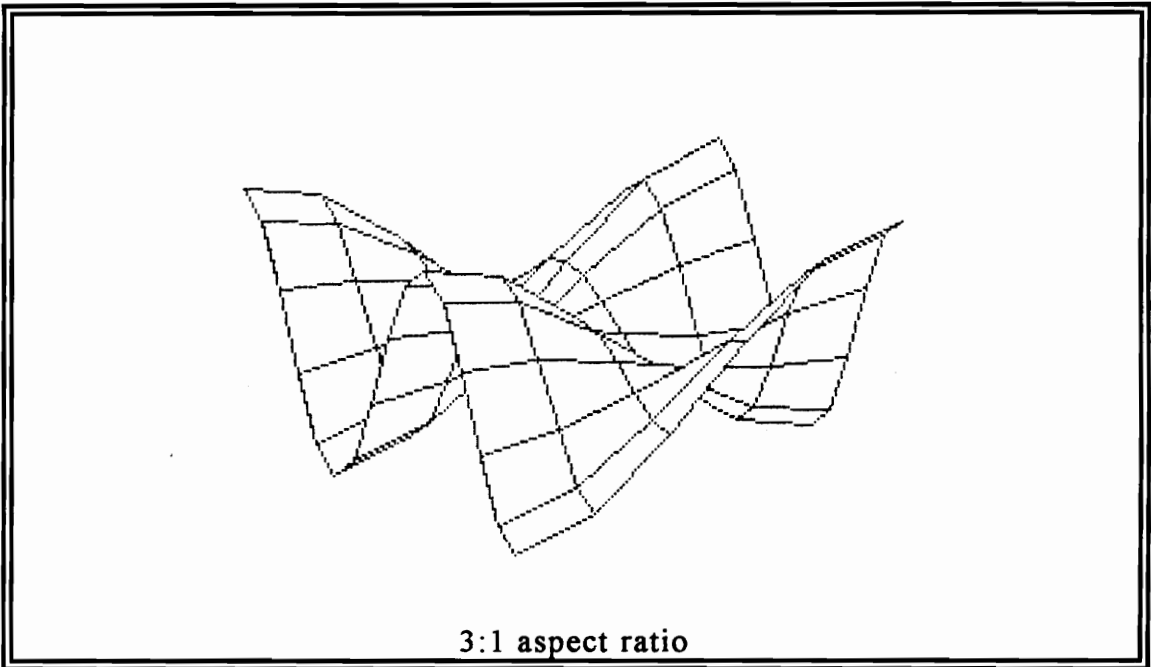


**Figure 27. MATLAB code,  $\partial V_x/\partial y$ .**

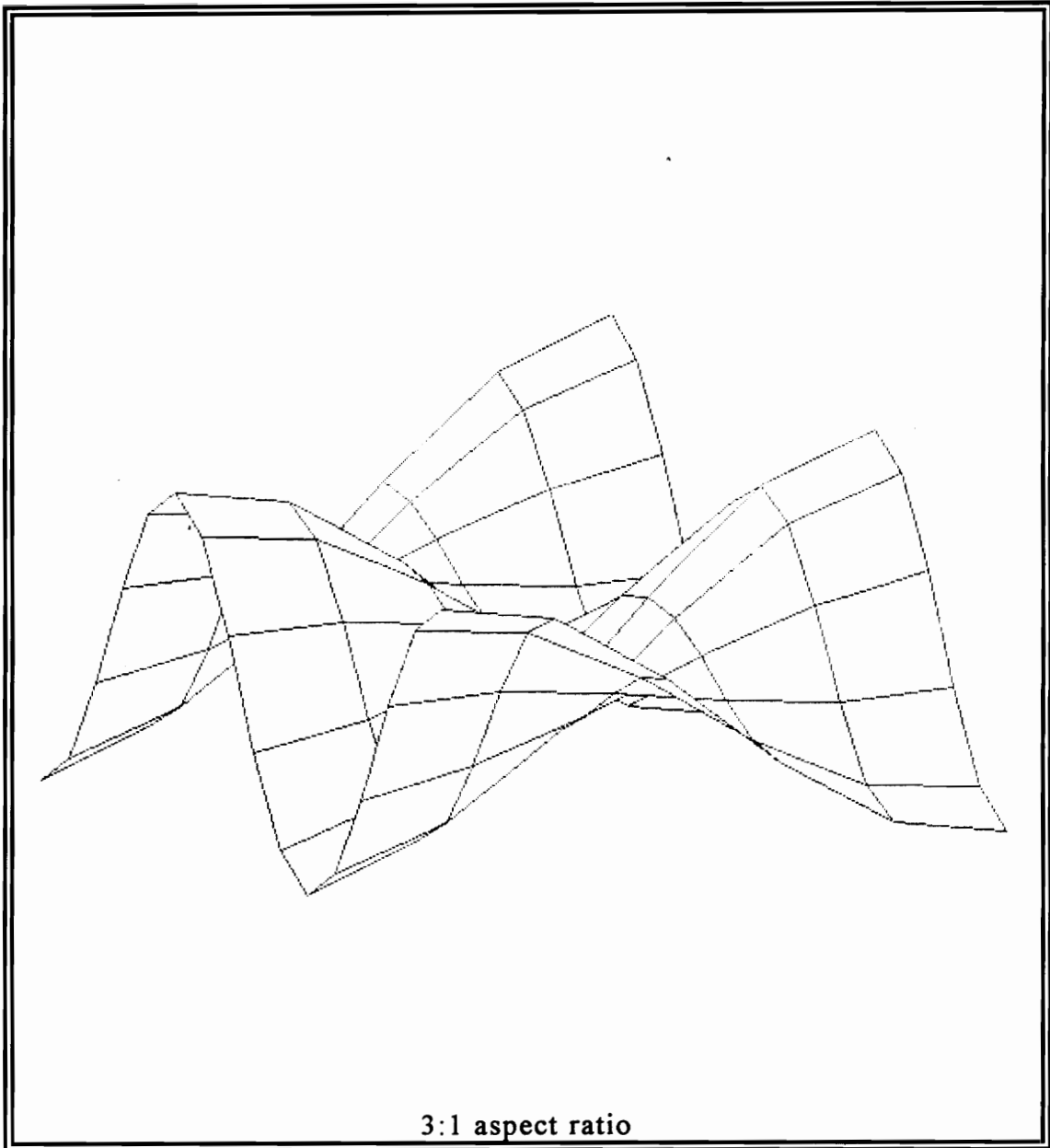


**Figure 28. MATLAB code, drilling-mode shape.**

### 5.3.3 Theory vs. Finite Element+MATLAB Code

In this section both numerical methods (finite element and MATLAB code) will be utilized in obtaining estimates of the drilling-mode shapes. First, the finite element method using I-DEAS 4.1 is used to acquire in-plane translational velocities using an  $11 \times 11$  equally spaced nodal array. Then, the MATLAB code filters, takes the partial derivatives and forms the proper differences of the partials to yield the drilling-angular velocities. The number of spectral lines along each side is 2.

The in-plane translational velocities simulated in I-DEAS are shown in Figs. 29 and 30. Next, using MATLAB the partial derivative of  $V_y$  with respect to  $x$  and the partial derivative of  $V_x$  with respect to  $y$  are calculated and given in Figs. 31 and 32. Finally, the drilling-mode shape is shown in Fig. 33.

Table 2 contains the %error of the drilling-mode shape ( $11 \times 11$  spatial-nodal array) of Fig. 33 with respect to the theory. The %error is defined in Eq. (5.3).

$$\%error = \frac{\dot{\theta}_z^{theory} - \dot{\theta}_z^{fe+MATLAB}}{\dot{\theta}_z^{theory}} \times 100 \quad (5.3)$$

It is interesting to observe in Table 2 that the %error of the drilling-mode shape has maxima less than 2%; moreover, in Table 1 the %error of the in-

plane velocities can reach values up to 9%. The last few sections validate the feasibility of both I-DEAS 4.1 or MATLAB code.

Based on comparisons with theory, these numerical methods provide accurate results in the absence of "noise" but are affected by the accuracy of the finite element estimate. The estimate may have non-random, non-noise like bias in the calculation of the eigenvectors. The errors shown in Table 2 should not be taken as measures of the effect of noise such as measurement noise. They are only a measurement of the finite element's biased eigenvector errors.

A view of Table 2 shows that there is an antisymmetric bias about the horizontal and vertical lines of symmetry of the plate. Thus, the effect of potential experimental noise must be investigated in the estimate of the drilling modes.

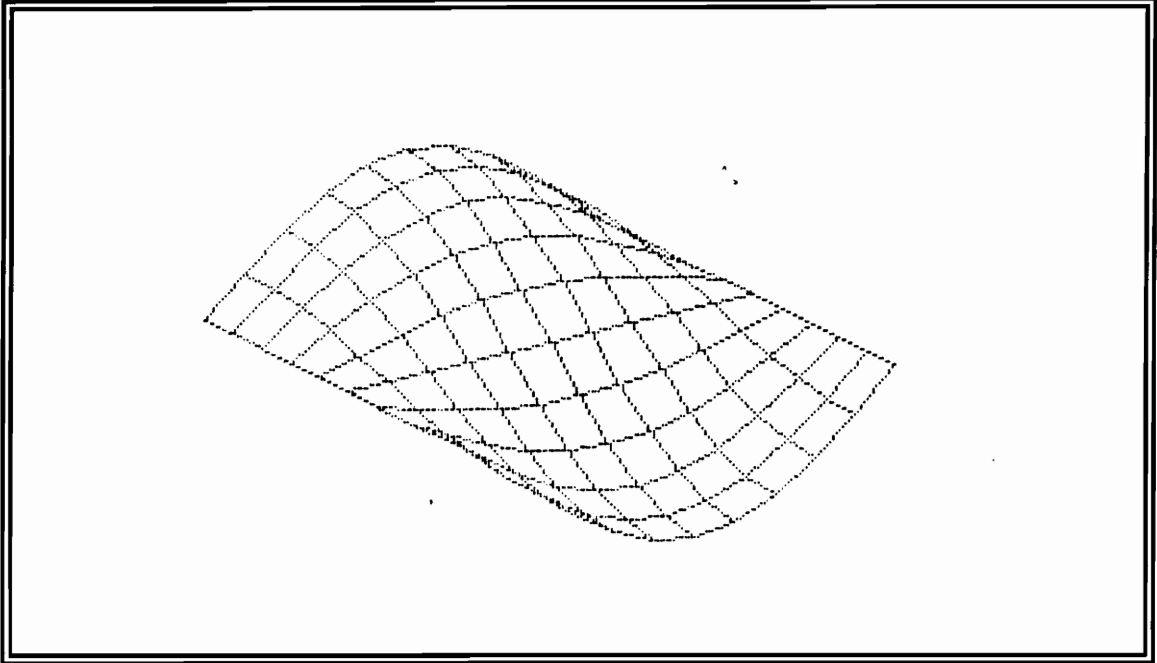


**Figure 29. Finite element code, in-plane translational velocity  $V_x$ .**

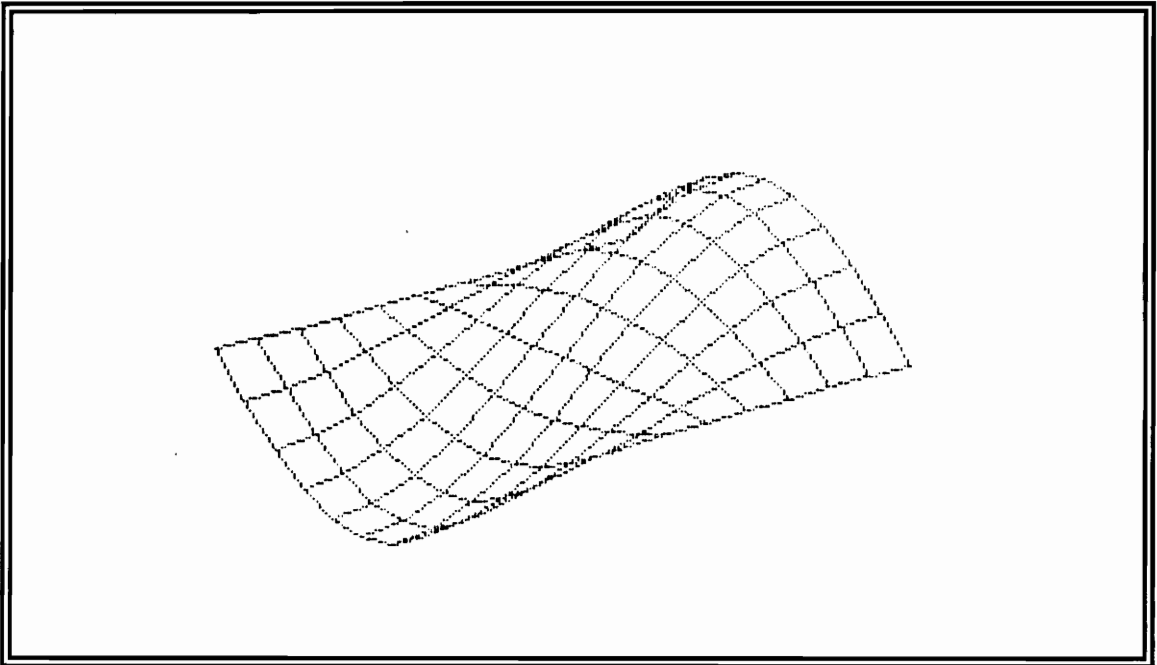


**Figure 30. Finite element code, in-plane translational velocity  $V_y$ .**

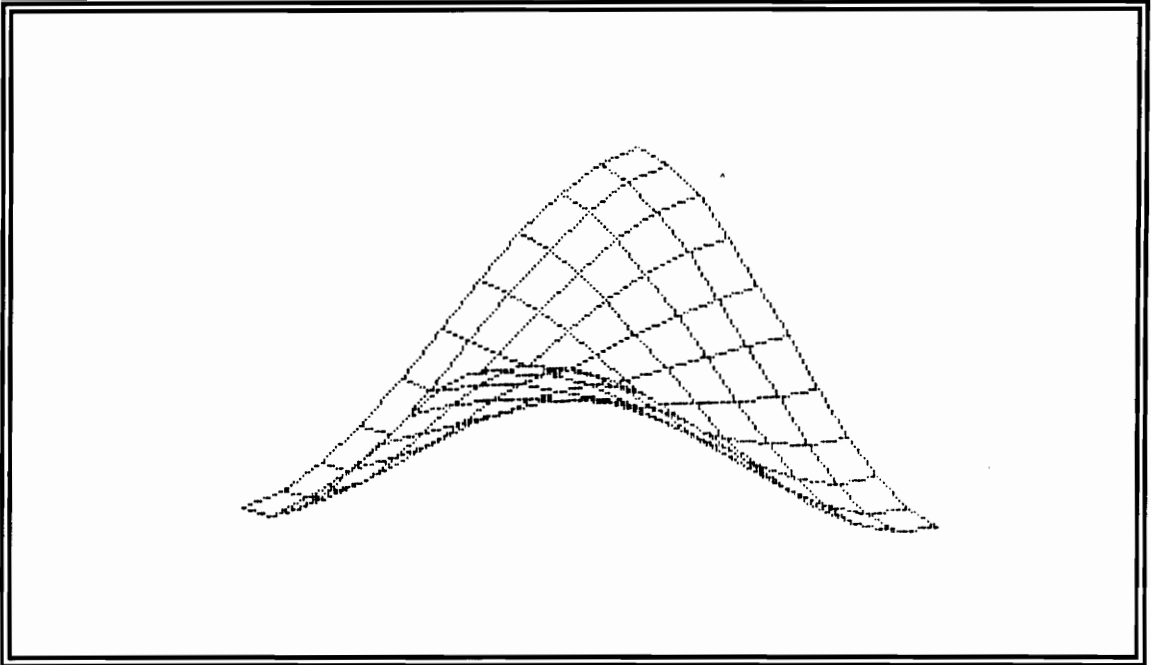


**Figure 31. Finite element+MATLAB code,  $\partial V_y/\partial x$ .**

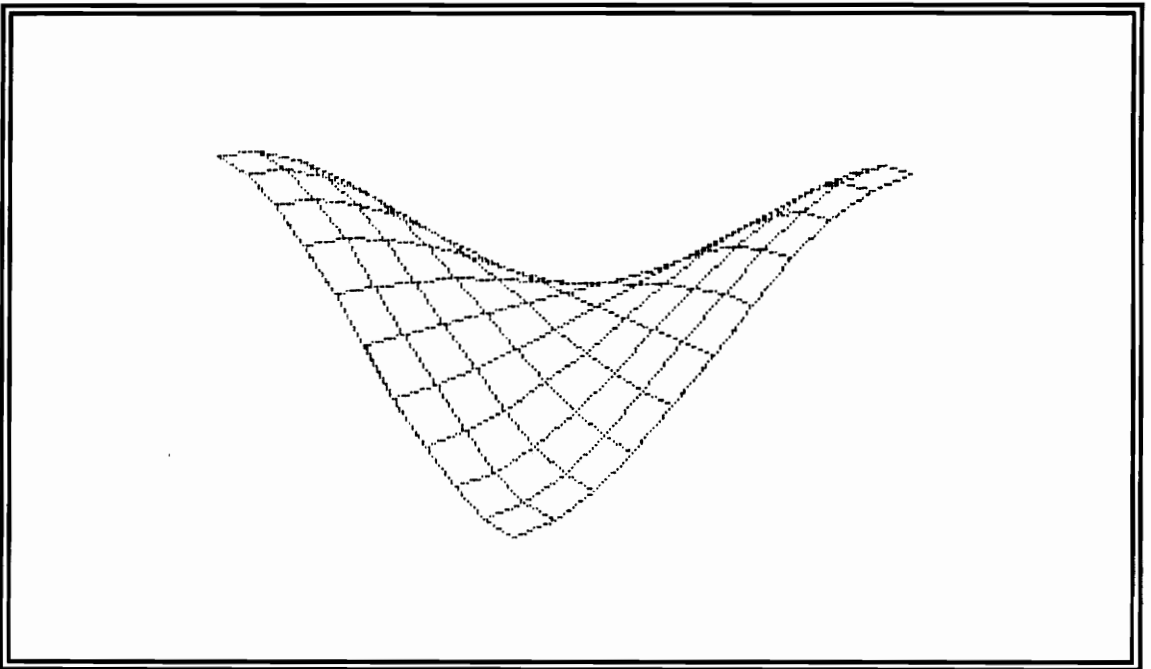


**Figure 32. Finite element+MATLAB code,  $\partial V_x/\partial y$ .**

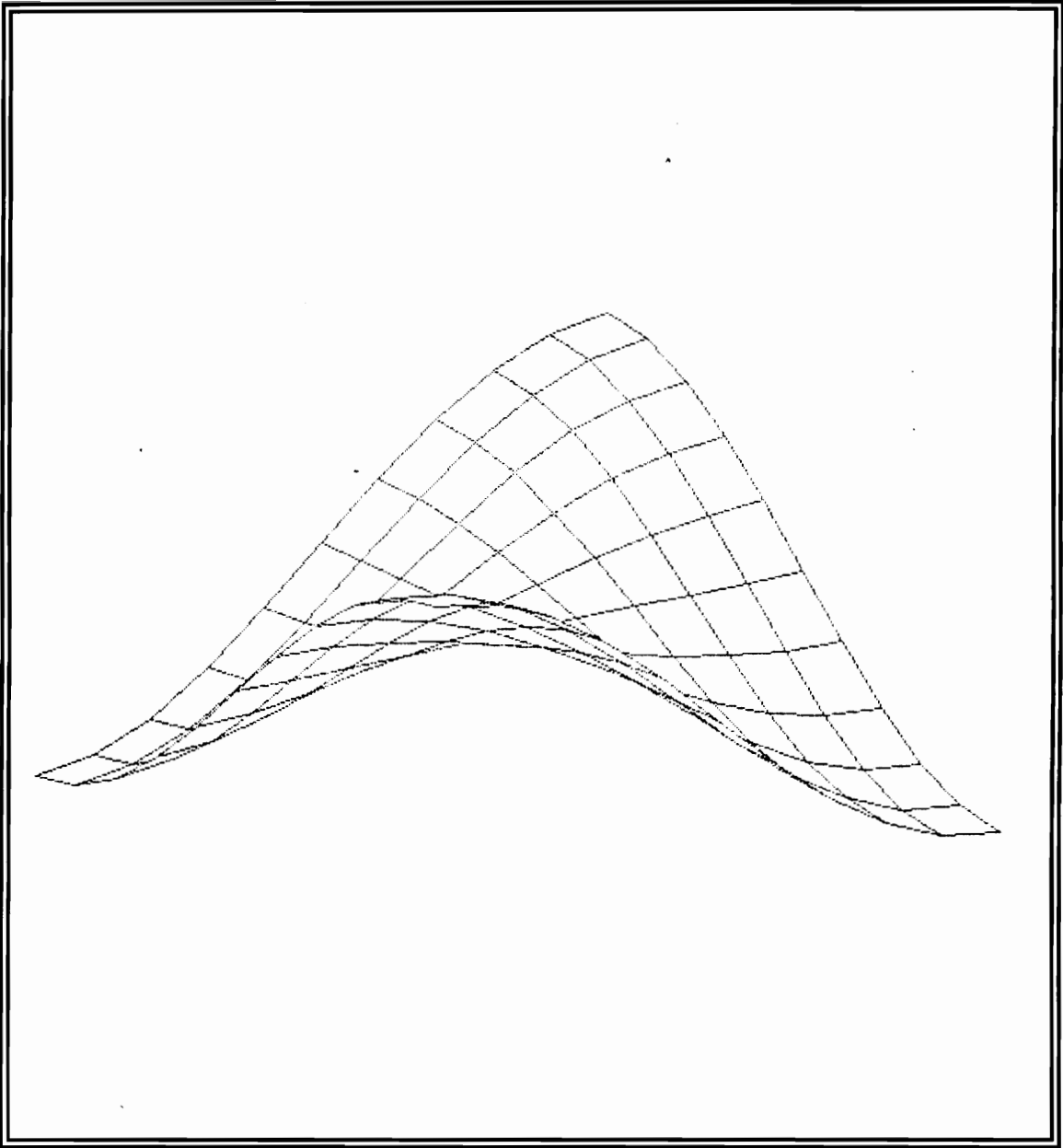


**Figure 33. Finite element+MATLAB code, drilling-mode shape.**

**Table 2. Finite element+MATLAB code, %error in  $\theta_z$ .**

	1	2	3	4	5	6	7	8	9	10	11
1	0.00	-0.08	-0.07	-0.07	-0.06	0.00	0.06	0.07	0.07	0.08	0.00
2	-0.08	-0.15	-0.16	-0.14	-0.14	0.00	0.14	0.14	0.16	0.15	0.08
3	-0.07	-0.16	-0.15	-0.15	-0.12	0.00	0.12	0.15	0.15	0.16	0.07
4	-0.07	-0.14	-0.15	-0.14	-0.11	0.00	0.11	0.14	0.15	0.14	0.07
5	-0.06	-0.14	-0.12	-0.11	-0.10	0.00	0.10	0.11	0.12	0.14	0.06
6	0.00	0.00	0.00	0.00	0.00	0.00	0.00	0.00	0.00	0.00	0.00
7	0.06	0.14	0.12	0.11	0.10	0.00	-0.10	-0.11	-0.12	-0.14	-0.06
8	0.07	0.14	0.15	0.14	0.11	0.00	-0.11	-0.14	-0.15	-0.14	-0.07
9	0.07	0.16	0.15	0.15	0.12	0.00	-0.12	-0.15	-0.15	-0.16	-0.07
10	0.08	0.15	0.16	0.14	0.14	0.00	-0.14	-0.14	-0.16	-0.15	-0.08
11	0.00	0.08	0.07	0.07	0.06	0.00	-0.06	-0.07	-0.07	-0.08	0.00

Numbers from 1 to 11 represent the horizontal and vertical nodal positions

### 5.3.4 Theory vs. MATLAB Code with Noise Content

As explained in previous sections, experimental data acquired from vibrations of real structures contain noise. In order to test the sensitivity of the MATLAB code to such noise, Gaussian noise is added (with a standard deviation 1% of the maximum translational in-plane velocity of the entire plate) to the theoretical in-plane translational velocities (16×6 nodal spatial array, thin-rectangular plate of aspect ratio 3:1, free-free-free-free). Since this investigation does not deal with real experimental data, noise is generated using the MATLAB random number generator. The random number generator generates noise with a normal distribution (mean = 0 and variance = 1). The noise addition is controlled from Eq. (5.4).

$$noise = 0.01 \times V_{\max} \times random\# \quad (5.4)$$

where *random#* stands for a random number from a Gaussian random number generator with zero mean and unity variance, and  $V_{\max}$  is the maximum velocity value of the array. Next, the MATLAB code is utilized, and the drilling-angular velocity mode shape is obtained as before by using 3 spectral lines along the long side of the plate and 1 spectral line along the short side of the plate. To examine the error distribution of the noise contaminated drilling mode, simple statistical techniques are applied. Wicks [50] suggests Monte-Carlo analysis of the data. This technique requires a sufficient number of samples ( $N > 30$ ).

In this case each sample is 16×6 nodal spatial array of drilling-angular velocities. Gathering many samples, provides statistical information that can be used to estimate  $\dot{\theta}_z$  for each point of the array. Since the actual value of  $\dot{\theta}_z$  is known from theory, error discussions are possible.

A Monte-Carlo analysis is used for  $N = 100$ . The in-plane translational velocities (contaminated with noise) of sample number 50 are shown in Figs. 34 and 35. The noise-contaminated drilling mode is given in Fig. 36. The mean of the samples  $\bar{\dot{\theta}}_z$  is calculated by Eq. (5.5). Table 3 shows the sample mean value of each point of the array computed from 100 independent observations. The random variable  $\dot{\theta}_{z,i}$  is being used as an estimator for the true mean value  $\mu_{\dot{\theta}_{z,i}}$ . When the number of samples approaches the infinity then the true mean value should be equal to the theoretically calculated value of drilling velocity at that point of the array. A table of the theoretically calculated values is presented at the end of this section.

$$\bar{\dot{\theta}}_z = \frac{\sum \dot{\theta}_{z,i}}{N} \quad (5.5)$$

The standard deviation of the samples is given in Eq. (5.6). Table 4 shows the standard deviation of each point of the array for 100 samples.

$$S_{\dot{\theta}_z} = \sqrt{\frac{\sum \dot{\theta}_{z,i}^2 - N\bar{\dot{\theta}}_z^2}{N-1}} \quad (5.6)$$

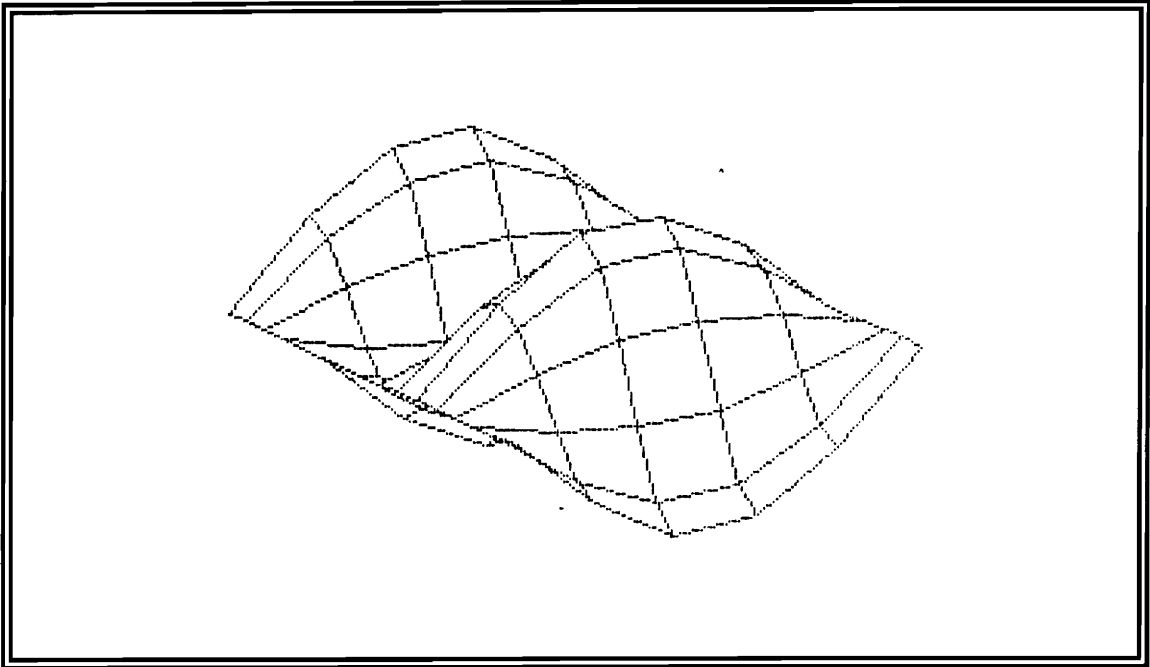


**Figure 34. Gaussean noise ( $\sigma = 1\%$  of  $V_{\max}$ ), in-plane velocity  $V_x$ .**

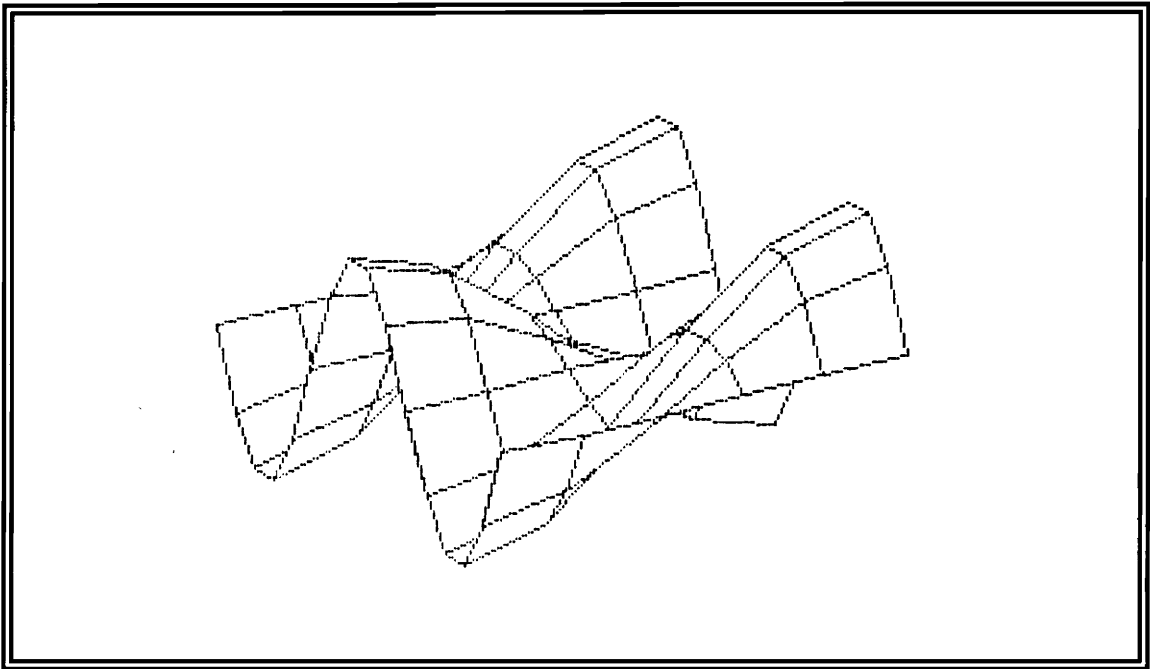


**Figure 35. Gaussean noise ( $\sigma = 1\%$  of  $V_{\max}$ ), in-plane velocity  $V_y$ .**

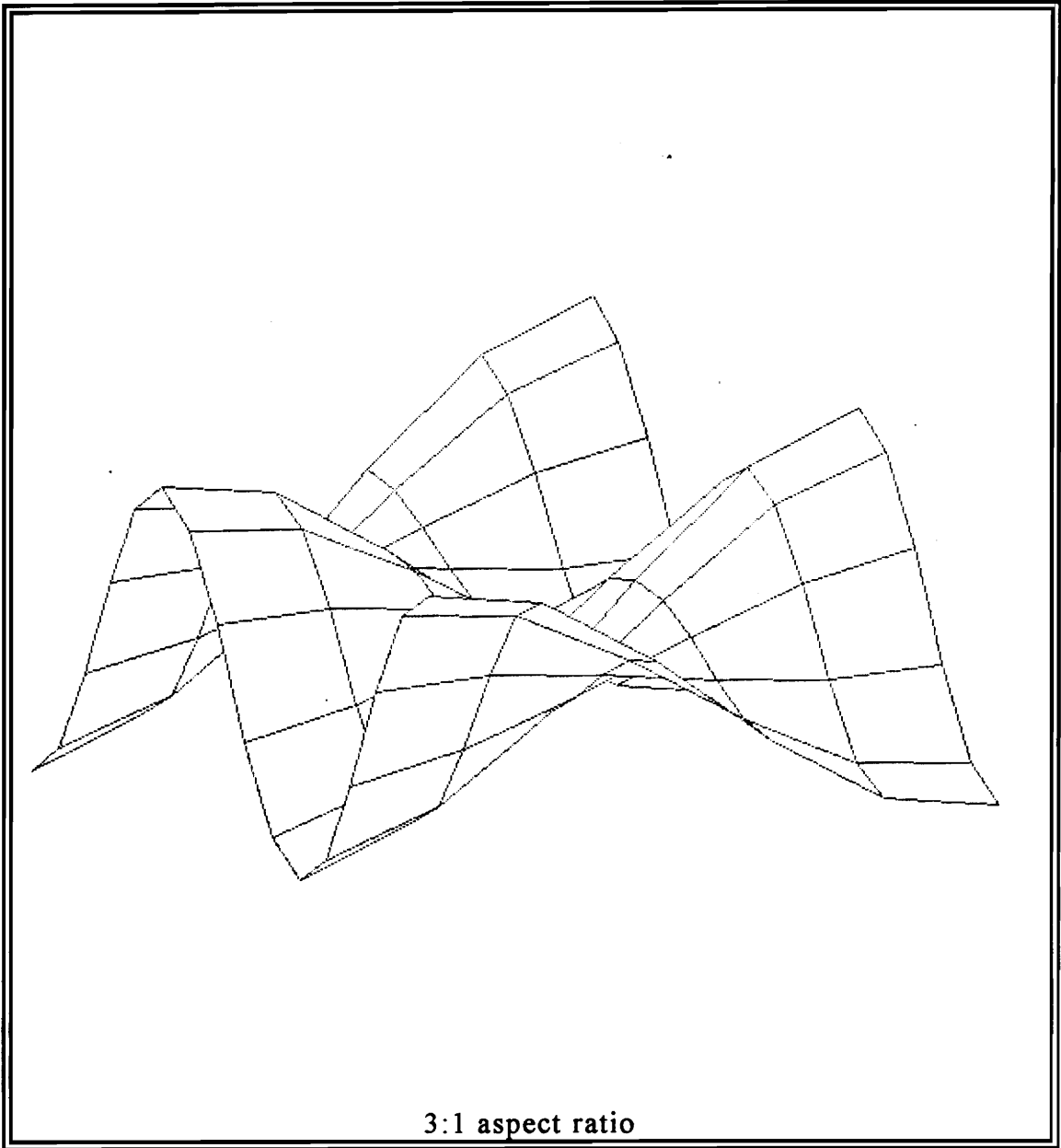


**Figure 36. Gaussean noise ( $\sigma = 1\%$  of  $V_{\max}$ ), drilling mode.**

**Table 3. Sample mean value of drilling-mode shape,  $N = 100$ .**

	1	2	3	4	5	6
1	-0.9999	-0.8085	-0.3086	0.3090	0.8087	0.9998
2	-0.8089	-0.6540	-0.2496	0.2500	0.6542	0.8088
3	-0.3096	-0.2503	-0.0954	0.0958	0.2505	0.3096
4	0.3090	0.2500	0.0956	-0.0954	-0.2499	-0.3090
5	0.8090	0.6543	0.2500	-0.2499	-0.6542	-0.8089
6	0.9997	0.8084	0.3088	-0.3088	-0.8084	-0.9996
7	0.8081	0.6534	0.2495	-0.2496	-0.6535	-0.8080
8	0.3096	0.2502	0.0955	-0.0956	-0.2503	-0.3095
9	-0.3095	-0.2505	-0.0958	0.0956	0.2503	0.3096
10	-0.8090	-0.6544	-0.2501	0.2499	0.6543	0.8090
11	-1.0000	-0.8088	-0.3091	0.3089	0.8087	0.9999
12	-0.8089	-0.6541	-0.2500	0.2498	0.6541	0.8088
13	-0.3098	-0.2505	-0.0958	0.0956	0.2505	0.3098
14	0.3087	0.2498	0.0954	-0.0956	-0.2498	-0.3088
15	0.8090	0.6544	0.2500	-0.2501	-0.6544	-0.8091
16	0.9998	0.8087	0.3089	-0.3091	-0.8087	-0.9999

Numbers from 1 to 6 represent the horizontal nodal positions.

Numbers from 1 to 16 represent the vertical nodal positions.

**Table 4. Sample standard deviation of drilling-mode shape,  $N=100$ .**

	1	2	3	4	5	6
1	0.0066	0.0057	0.0041	0.0042	0.0054	0.0067
2	0.0063	0.0055	0.0036	0.0038	0.0056	0.0056
3	0.0050	0.0044	0.0027	0.0027	0.0044	0.0050
4	0.0048	0.0042	0.0019	0.0019	0.0042	0.0051
5	0.0048	0.0041	0.0023	0.0020	0.0040	0.0048
6	0.0060	0.0049	0.0028	0.0027	0.0048	0.0057
7	0.0056	0.0048	0.0026	0.0028	0.0041	0.0052
8	0.0054	0.0046	0.0024	0.0023	0.0039	0.0051
9	0.0057	0.0050	0.0025	0.0022	0.0043	0.0057
10	0.0056	0.0048	0.0027	0.0025	0.0045	0.0058
11	0.0055	0.0047	0.0027	0.0028	0.0044	0.0051
12	0.0058	0.0047	0.0021	0.0024	0.0047	0.0058
13	0.0056	0.0044	0.0021	0.0020	0.0043	0.0054
14	0.0061	0.0046	0.0026	0.0028	0.0045	0.0060
15	0.0065	0.0060	0.0033	0.0039	0.0053	0.0068
16	0.0069	0.0058	0.0043	0.0042	0.0052	0.0066

Numbers from 1 to 6 represent the horizontal nodal positions.

Numbers from 1 to 16 represent the vertical nodal positions.

Using Eqs. (5.5 and 5.6), if  $\bar{\theta}_z$  and  $S_{\theta_z}$  are the mean and the standard deviation of a random sample (nodal-spatial array) from a normal population with unknown variance  $\sigma_{\theta_z}^2$ , a 95% confidence interval for the true average  $\mu_{\theta_z}$  can be found as shown in Eq. (5.7).

$$\bar{\theta}_z - \frac{1.96S_{\theta_z}}{\sqrt{N}} \leq \mu_{\theta_z} < \bar{\theta}_z + \frac{1.96S_{\theta_z}}{\sqrt{N}} \quad (5.7)$$

The upper and lower bounds of the interval are given in Table 5 and Table 6 respectively. Table 7 contains the actual values of the drilling-mode shape as calculated from the theory. It is easy to notice that the actual values are within the intervals for all points of the array. The Statistics successfully estimate the true value of the drilling-angular velocity for every point of the spatial array.

**Table 5. Upper bound of 95% confidence interval,  $N = 100$ .**

	1	2	3	4	5	6
1	-0.9986	-0.8074	-0.3078	0.3099	0.8098	1.0011
2	-0.8077	-0.6529	-0.2489	0.2508	0.6553	0.8099
3	-0.3086	-0.2494	-0.0949	0.0963	0.2513	0.3106
4	0.3100	0.2508	0.0960	-0.0950	-0.2490	-0.3080
5	0.8100	0.6551	0.2504	-0.2495	-0.6534	-0.8080
6	1.0009	0.8094	0.3093	-0.3083	-0.8075	-0.9985
7	0.8092	0.6544	0.2500	-0.2491	-0.6527	-0.8070
8	0.3107	0.2511	0.0959	-0.0952	-0.2496	-0.3085
9	-0.3084	-0.2495	-0.0953	0.0961	0.2512	0.3107
10	-0.8079	-0.6534	-0.2496	0.2504	0.6552	0.8101
11	-0.9989	-0.8079	-0.3085	0.3095	0.8095	1.0009
12	-0.8077	-0.6532	-0.2495	0.2503	0.6550	0.8099
13	-0.3087	-0.2497	-0.0954	0.0960	0.2513	0.3108
14	0.3099	0.2507	0.0959	-0.0950	-0.2489	-0.3076
15	0.8103	0.6556	0.2506	-0.2494	-0.6534	-0.8078
16	1.0011	0.8099	0.3098	-0.3083	-0.8077	-0.9986

Numbers from 1 to 6 represent the horizontal nodal positions.

Numbers from 1 to 16 represent the vertical nodal positions.

**Table 6. Lower bound of 95% confidence interval,  $N = 100$ .**

	1	2	3	4	5	6
1	-1.0012	-0.8096	-0.3094	0.3082	0.8077	0.9985
2	-0.8101	-0.6551	-0.2503	0.2493	0.6531	0.8077
3	-0.3106	-0.2512	-0.0959	0.0952	0.2496	0.3086
4	0.3081	0.2492	0.0953	-0.0958	-0.2507	-0.3100
5	0.8081	0.6535	0.2495	-0.2503	-0.6550	-0.8099
6	0.9986	0.8074	0.3082	-0.3093	-0.8094	-1.0007
7	0.8070	0.6525	0.2490	-0.2502	-0.6543	-0.8090
8	0.3085	0.2493	0.0950	-0.0961	-0.2511	-0.3105
9	-0.3106	-0.2514	-0.0963	0.0952	0.2495	0.3085
10	-0.8101	-0.6553	-0.2506	0.2495	0.6534	0.8079
11	-1.0011	-0.8097	-0.3096	0.3084	0.8078	0.9989
12	-0.8100	-0.6551	-0.2504	0.2494	0.6532	0.8076
13	-0.3110	-0.2514	-0.0962	0.0952	0.2497	0.3087
14	0.3075	0.2489	0.0949	-0.0961	-0.2507	-0.3100
15	0.8078	0.6533	0.2493	-0.2509	-0.6555	-0.8104
16	0.9985	0.8076	0.3081	-0.3099	-0.8097	-1.0011

Numbers from 1 to 6 represent the horizontal nodal positions.

Numbers from 1 to 16 represent the vertical nodal positions.

**Table 7. Actual values of drilling-mode shape.**

	1	2	3	4	5	6
1	-1.0000	-0.8090	-0.3090	0.3090	0.8090	1.0000
2	-0.8090	-0.6545	-0.2500	0.2500	0.6545	0.8090
3	-0.3090	-0.2500	-0.0955	0.0955	-0.2500	0.3090
4	0.3090	0.2500	0.0955	-0.0955	-0.2500	-0.3090
5	0.8090	0.6545	0.2500	-0.2500	-0.6545	-0.8090
6	1.0000	0.8090	0.3090	-0.3090	-0.8090	-1.0000
7	0.8090	0.6545	0.2500	-0.2500	-0.6545	-0.8090
8	0.3090	0.2500	0.0955	-0.0955	-0.2500	-0.3090
9	-0.3090	-0.2500	-0.0955	0.0955	0.2500	0.3090
10	-0.8090	-0.6545	-0.2500	0.2500	0.6545	0.8090
11	-1.0000	-0.8090	-0.3090	0.3090	0.8090	1.0000
12	-0.8090	-0.6545	-0.2500	0.2500	0.6545	0.8090
13	-0.3090	-0.2500	-0.0955	0.0955	0.2500	0.3090
14	0.3090	0.2500	0.0955	-0.0955	-0.2500	-0.3090
15	0.8090	0.6545	0.2500	-0.2500	-0.6545	-0.8090
16	1.0000	0.8090	0.3090	-0.3090	-0.8090	-1.0000

Numbers from 1 to 6 represent the horizontal nodal positions.

Numbers from 1 to 16 represent the vertical nodal positions.

# Chapter 6

## Applications

As shown in the previous chapter, a numerical method (MATLAB code) is used to extract drilling-angular velocities from a translational-velocity field. The sensitivity of MATLAB code to data containing noise is checked by comparing to theoretical closed-form solutions of the same in-plane mode shape (Lamé mode). Utilizing this code in addition to the MATLAB code written by Sun [16] results in a complete three-dimensional description of rotational velocities  $\dot{\theta}_x$ ,  $\dot{\theta}_y$ , and  $\dot{\theta}_z$ . Some possible applications of the MATLAB code are explored next.

### *6.1 Numerical Applications*

In sections of the previous chapter is shown that using the finite element method (I-DEAS 4.1) for simulation of in-plane velocities results in error up to 9%. It is also shown that using these velocities as an input for the MATLAB code results in calculation of drilling-angular velocities with error less than 2%. The errors do not contain any noise and they are a measurement of the finite element's biased eigenvector errors.

In some cases in-plane mode shapes other than the Lamé mode shape need to be considered. Provided the finite element code is accurate enough this can be accomplished easily. In I-DEAS 4.1 the calculation of in-plane mode shapes (with limitations explained in chapter 5) is reasonably accurate for the first three to five eigenvectors depending on the accuracy desired.

In Fig. 37 the first in-plane eigenvector using I-DEAS 4.1 is determined. This finite element analysis is performed for square-thin plate (11×11 nodal-spatial array) with boundary conditions free-free-free-free.

Figures 38 and 39 show the in-plane translational velocities  $V_x$  and  $V_y$  calculated in I-DEAS and used as input for the MATLAB code. Figures 40 and 41 show the partial derivatives of the above velocities with respect to  $y$  and  $x$  respectively. Finally, Fig. 42 shows the drilling-mode shape for the first in-plane mode of the square plate.

Observe the saddle shaped drilling-mode. The maxima and minima occur at the half-points of the four sides of the square plate as expected.

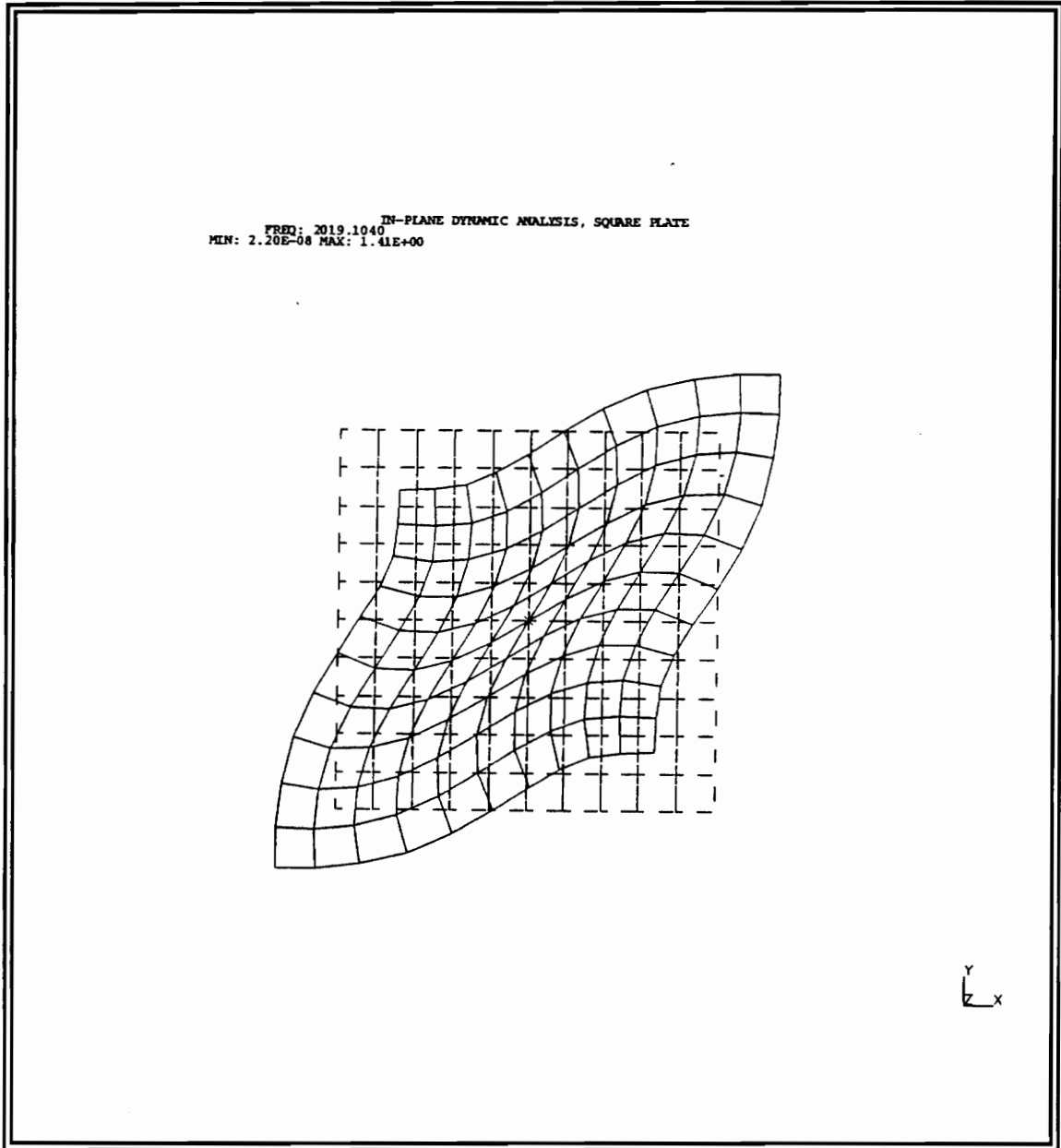


**Figure 37. First in-plane mode of a square plate using I-DEAS 4.1.**

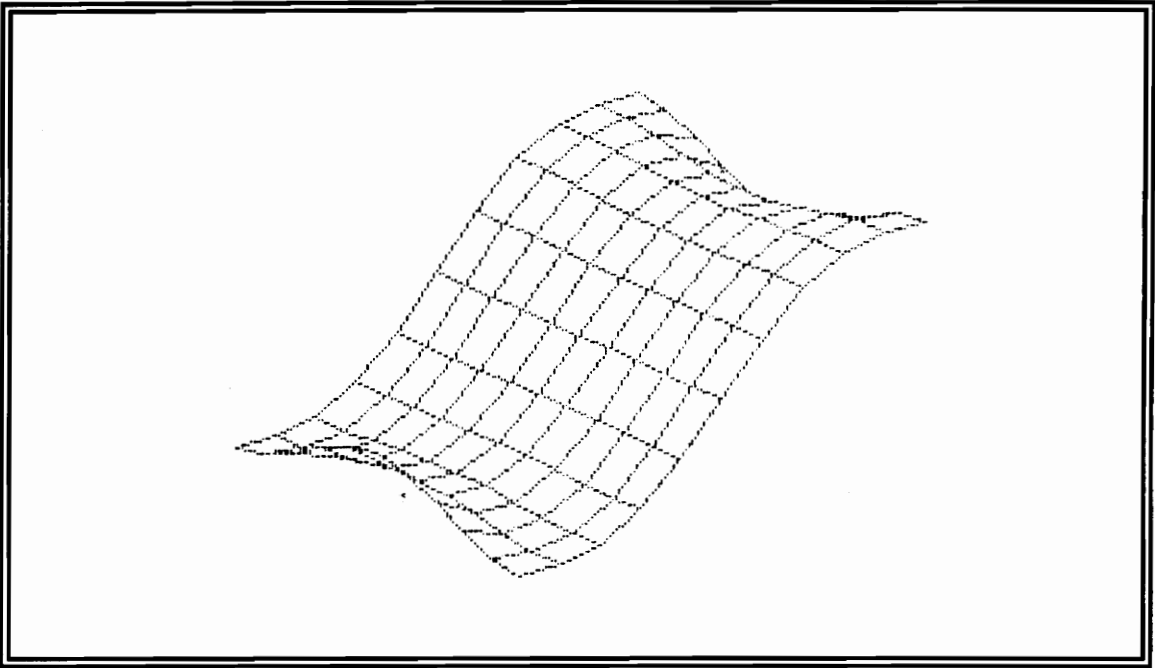


**Figure 38. First in-plane mode of a square plate,  $V_x$ .**

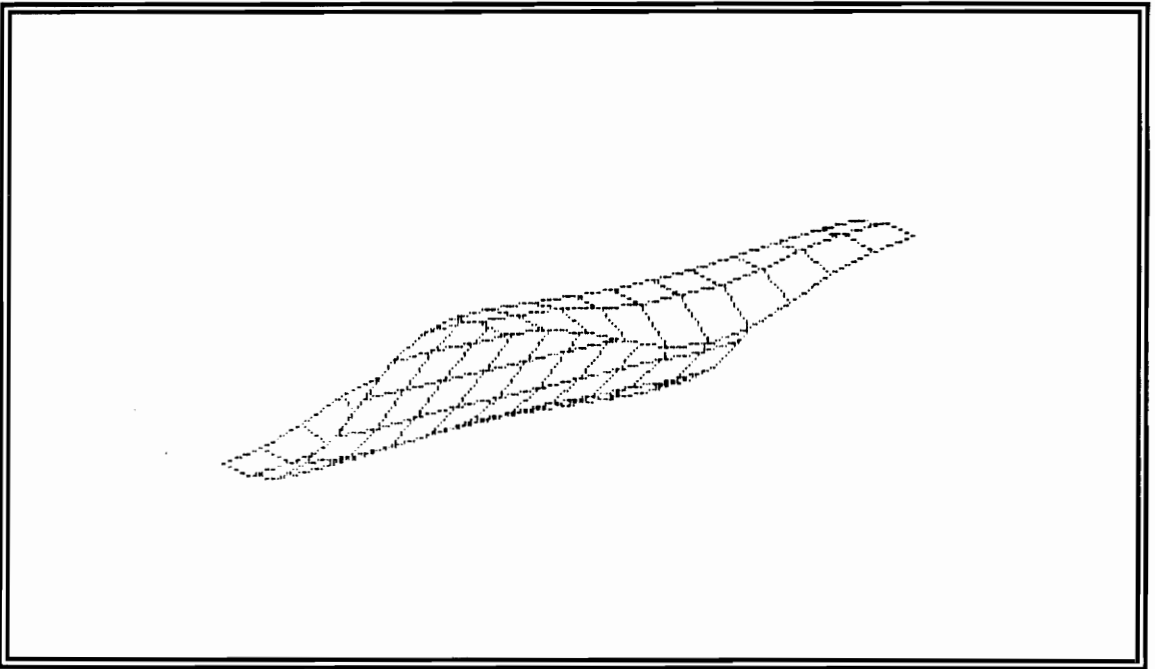


**Figure 39. First in-plane mode of a square plate,  $V_y$ .**

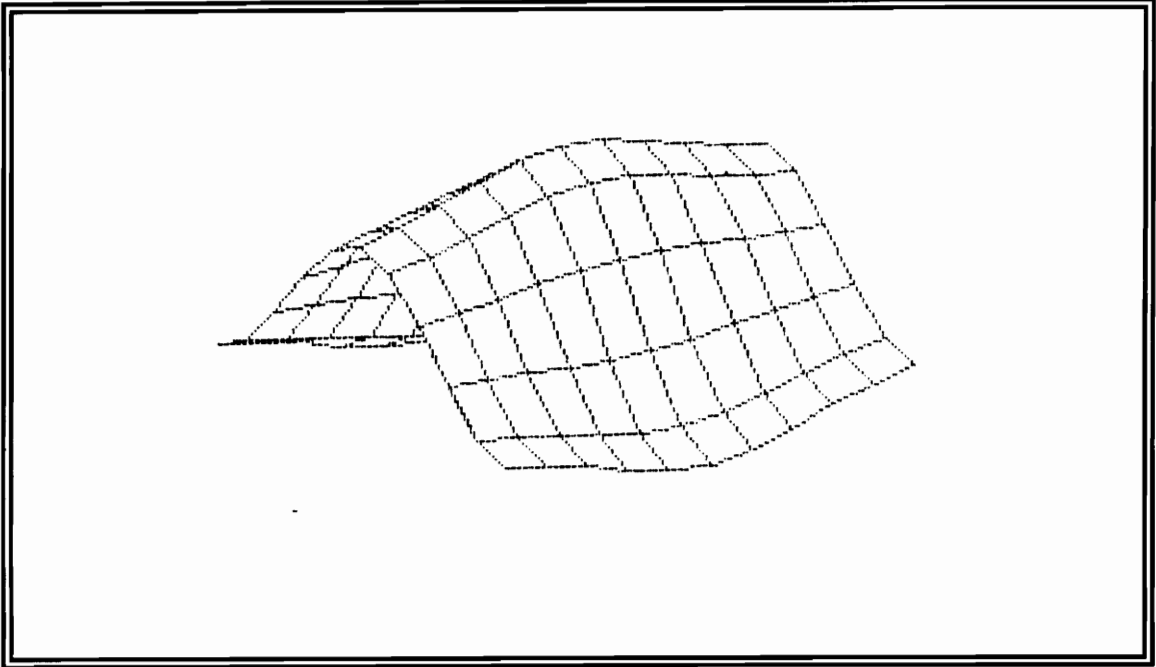


**Figure 40. First in-plane mode of a square plate,  $\partial V_x/\partial x$ .**

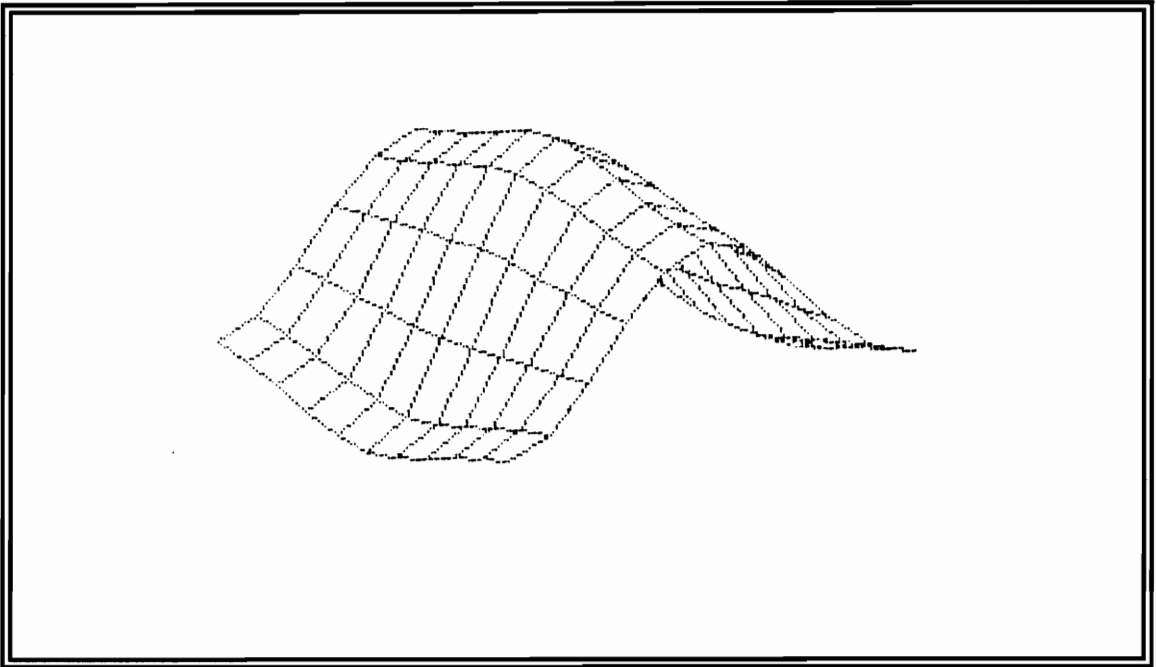


**Figure 41. First in-plane mode of a square plate,  $\partial V_x/\partial y$ .**

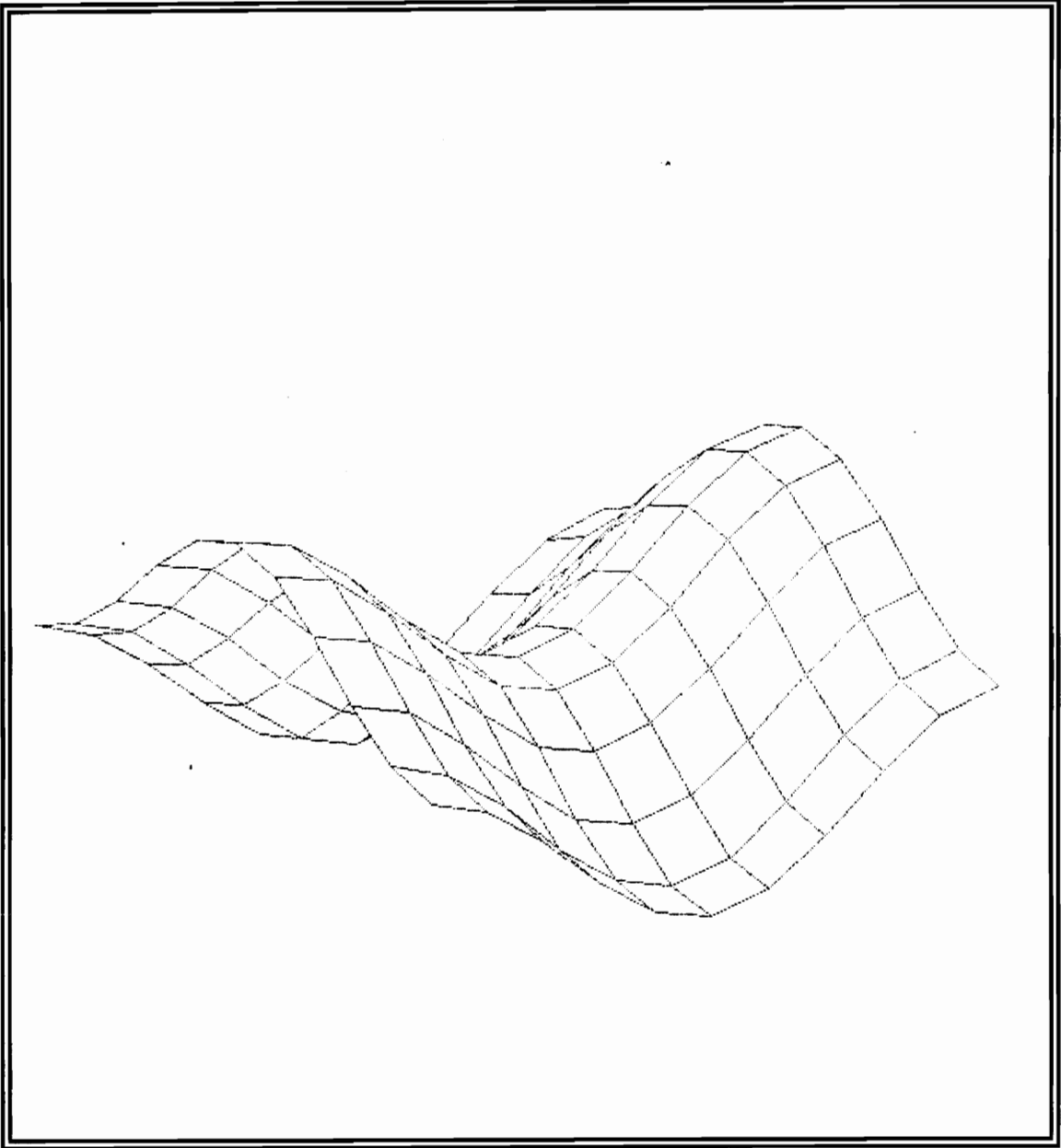


**Figure 42. First in-plane mode of a square plate,  $\theta_z$ .**

## ***6.2 Experimental Applications***

This research can be used as a theoretical foundation for drilling-mode extraction from three-dimensional velocity data using a one-dimensional laser-Doppler vibrometer. VPI sensor (see chapter 1) is a one-dimensional, laser-Doppler vibrometer which is used for velocity data acquisition of the line-of-sight structural motion. Utilizing experimental measurements taken in three independent positions (laser shots of a single point from different view angles) and the MATLAB codes written for angular-velocity extraction, all six degrees of freedom for a point of a structure can be acquired.

As explained in chapter 1, real-life vibrations of structures are always three dimensional. Utilizing this work and the findings of other researchers on the field along with laser vibrometry, three-dimensional vibration can be measured.

# Chapter 7

## Conclusions and Recommendations

The following statements conclude this work and can be used from other researchers as a source for further developments using laser vibrometry.

### *7.1 Conclusions*

This research is a theoretical study in extraction of drilling-angular velocities using a spatial-nodal array of translational velocities. Although much work has been done formulating the equations relating the angular to translational velocity field, and developing theoretical and numerical simulations of in-plane and drilling mode shapes, very little has been done using experimental real-life data. Hopefully, this thesis can be linked and carefully integrated with the work of other researchers in the area of three-dimensional vibrometry using lasers, to create the means of measuring three-dimensional vibrations of structures. The following statements are of great significance and importance for the continuation of this work:

- Theoretical closed-form solutions of in-plane translational velocities and drilling-angular velocities are used as a reference for the numerical calculations.
- All theoretical simulations are performed for the Lamé in-plane mode shape of rectangular plates (aspect ratio 1:1 or 3:1) because of its simple mathematical description.
- The finite element code using I-DEAS 4.1 is used as an alternative way to simulate in-plane translational velocities and it is accurate for a limited number of eigenvectors (first three to five in-plane modes).
- The MATLAB code used for the numerical extraction of drilling-angular velocities, requires that the in-plane translational velocities are already known and measured.
- The MATLAB code was originally designed for plates of known dimensions and negligible thickness. The aspect ratio of the rectangular plate is an input for the code.
- The number of spectral lines used is a variable but in the double-size spatial domain 2.5 to 5.0 times the basic spatial harmonics of each side is suggested.

- Real-life experimental data contain noise. Even though, low-pass filtering is performed during the DFT-IDFT procedure, additional filtering of the in-plane translational velocities may be required for best results. When large amounts of noise are contained in points close to the edge or the corner of the plate, it is important to filter this noise out before the DFT-IDFT process, so that it is not duplicated during the mirroring of the data length procedure.

As a conclusion, this thesis provides the means for theoretical determination of drilling-mode shapes using analytical and numerical techniques. The final section of this thesis is used for useful recommendations.

## ***7.2 Recommendations***

It is recommended that an experiment is carefully set up to acquire experimental data and validate the feasibility of the work presented in this thesis. Utilizing laser shots of a single point from different view angles by using a one-dimensional laser vibrometer like VPI sensor, the three-dimensional translational velocity field can be measured [18,19]. The extraction of the angular velocity field can be accomplished by using the MATLAB code presented in this thesis and the MATLAB code written by Sun [16]. Additional filtering of the experimental noise content is suggested prior the DFT-IDFT procedure. Using a "median" filter is an option worth examining; even though, a median filter does not work properly for the edges and corners of the rectangular plate. However, with some modifications median filtering could be applied for pre-smoothing of the velocity data.

Concluding, it is worth mentioning that even though this theoretical study is based on rectangular-thin plates of certain aspect ratio and free-free-free-free boundary conditions, it is envisioned that this thesis will be used as groundwork for three-dimensional laser vibrometry for structures of arbitrary shape and boundary conditions.

## References

1. Meriam, J. L., and Krage, L. G., *Engineering Mechanics: Volume 2 Dynamics*, 2nd ed., John Wiley and Sons, New York, NY, 1986, p. 469.
2. Drain, L. E., *The Laser Doppler Technique*, John Wiley and Sons, London, England, 1980, p. 224.
3. Halliwell, N. A., "The Laser-Doppler Measurement of Vibrating Surfaces: A Portable Instrument," *Journal of Sound and Vibration*, Vol. 62, No. 2, 1980, pp. 312-315.
4. Halliwell, N. A., Pickering, C. J. D., and Eastwood, P. G., "The Laser Torsional Vibrometer: A New Instrument," *Journal of Sound and Vibration*, Vol. 93, No. 4, 1984, pp. 588-592.
5. Halliwell, N. A., and Eastwood, P. G., "The Laser Torsional Vibrometer," *Journal of Sound and Vibration*, Vol. 101, 1985, pp. 446-449.
6. Pickering, C. J. D., Halliwell, N. A., and Wilmshurst, T. H., "The Laser Vibrometer: A Portable Instrument," *Journal of Sound and Vibration*, Vol. 107, No. 3, 1986, pp. 471-485.
7. Sriram, P., Craig, J. I., and Hanagud, S., "A Scanning Laser Doppler Vibrometer for Modal Testing," *The International Journal of Analytical and Experimental Modal Analysis*, Vol. 5, No. 3, 1990, pp. 155-167.
8. TSI Company Literature, "Laser Vibrometer: For Accurate, Non-Contact Vibration Measurements," TSI Inc., P.O. Box 64394, St. Paul, MN 55164.
9. Zonic Company Literature, "LAZON Automated Non-Contact Modal Testing," Zonic, Zonic A&D, Park 50 TechneCenter, Milford, OH 45150.

10. Cafeo, J. A., Rieker, J. R., "Application of a Three Degree of Freedom Laser Vibrometer for Experimental Modal Analysis," *Proceedings of the 9th International Modal Analysis Conference*, Society for Experimental Mechanics, Inc., Florence, Italy, 1991, pp. 1161-1167.
11. Cafeo, J. A., Trethewey M. W., and Sommer H. J., "Measurement and Application of Experimental Rotational Degrees of Freedom for Mode Shape Refinement," *The International Journal of Analytical and Experimental Modal Analysis*, Vol. 7, No. 4, 1992, pp. 255-269.
12. Ometron Limited, "VPI Sensor Operator's Manual," Ometron Ltd., Kelvin House, London, England SE26 5BX.
13. Mitchell, L. D., Kochersberger, K., and West, R. L., "Measurement of a One-Dimensional Mobility Using a Laser-Doppler Velocimeter," *Proceedings of the 1991 SEM Spring Conference on Experimental Mechanics*, June 1991, Milwaukee, WI, pp. 846-853.
14. Wicks, A. L., Kochersberger, K., and Mitchell, L. D., "Laser Structural Imaging," *Proceedings of the 2nd USAF/NASA Workshop on System Identification and Health Monitoring of Precision Space Structures*, March 1990, California Institute of Technology, Pasadena, CA, pp. 24-42.
15. Kochersberger, K., Mitchell, L. D., and Wicks, A. L., "Structural Angular Velocity Extraction Using DFT/IDFT Techniques," *Proceedings of the 9th International Modal Analysis Conference*, Vol. I, Florence, Italy, April 1991, pp. 657-663.
16. Sun, F. P., and Mitchell, L. D., "Two-Dimensional Velocity Data Smoothing and Structural Angular Velocity Extraction Using a DFT-IDFT Technique," *Proceedings of the 13th Biennial ASME Conference on Mechanical Vibration and Noise*, September 22-25, 1991, pp. 303-309.
17. Arruda, J. R. F., "Surface Smoothing and Partial Spatial Derivatives Computation Using a Regressive Discrete Fourier Series," Accepted for publication in *Mechanical Systems and Signal Processing*, Academic Press, Vol. 6, No. 3.

18. Donovan, Joseph B., "Three-Dimensional Vibrometry Via Three Positions of a One-Dimensional Laser Doppler Velocimeter." M.S. Thesis, Virginia Polytechnic Institute and State University, Blacksburg, VA, 1991.
19. Abel, Jeffrey J., "Three-Dimensional Velocity Extraction Using Laser Doppler Vibrometry." M.S. Thesis, Virginia Polytechnic Institute and State University, Blacksburg, VA, 1993.
20. Thomson, W. T., *Theory of Vibration with Applications*, 3rd ed., Prentice Hall, New Jersey, NY, 1988, p. 120.
21. Bendat, J. S. and Piersol, A. G., *Random Data: Analysis and Measurement Procedures*, John Wiley and Sons, New York, NY, 1986, p. 85.
22. Love, A. E. H., *Theory of Elasticity*, Dover Publications, New York, NY, 1944.
23. Timoshenko, S., *Vibration Problems in Engineering*, 2nd ed., D. Van Nostrand Company, Inc., New York, NY, 1937, p. 335.
24. Leissa, A. W., *Vibration of Plates*, NASA SP-160, U.S. Government Printing Office, Washington, D.C., pp. 41-159.
25. Leissa, A. W., Lee, J. K., and Wang, A. J., "Rotating Blade Vibration Analysis Using Shells," *Journal of Engineering for Power*, Vol. 104, April 1982, pp. 296-302.
26. Leissa, A. W., Lee, J. K., and Wang, A. J., "Vibrations of Twisted Rotating Blades," *The American Society of Mechanical Engineers*, June 1982, pp. 1-8.
27. Leissa, A. W., Lee, J. K., and Wang, A. J., "Vibrations of Doubly-Curved Shallow Shells," *Int. J. Solids Structures*, Vol. 19, No. 5, 1983, pp. 411-424.
28. Leissa, A. W., and Narita, Y., "Vibrations of Completely Free Shallow Shells of Rectangular Planform," *Journal of Sound and Vibration*, Vol. 96, No. 2, pp. 207-218.

29. Narita, Y., and Liessa, A. W., "Vibrations of Corner Point Supported Shallow Shells of Rectangular Planform," *Earthquake Engineering and Structural Dynamics*, Vol. 12, 1984, pp. 651-661.
30. Wauer, J., "In-Plane Vibrations of Rectangular Plates Under Inhomogeneous Static Edge Load," *European Journal of Mechanics and Solids*, Vol. 11, No. 1, 1992, pp. 91-106.
31. Kobayashi, Y., Yamada, G., and Honma, S., "In-Plane Vibration of Point-Supported Rectangular Plates," *Journal of Sound and Vibration*, Vol. 126, No. 3, 1988, pp. 545-549.
32. Lloyd, P., and Redwood, M., "Finite-Difference Method for the Investigation of the Vibrations of Solids and the Evaluation of the Equivalent-Circuit Characteristics of Piezoelectric Resonators," *The Journal of the Acoustical Society of America*, Vol. 39, No. 2, 1965, pp.347-361.
33. Lamé, M. G., *Leçons sur la théorie mathématique de l'élasticité des corps solides*, Gauthier-Villars, Paris, 1886, pp. 168-172.
34. Ekstein, H., and Schiffman, T., "Free Vibrations of Isotropic Cubes and Nearly Cubic Parallelepipeds," *Journal of Applied Physics*, Vol. 27, No. 4, 1956, pp. 405-412.
35. Mindlin, R. D., "Simple Modes of Vibration of Crystals," *Journal of Applied Physics*, Vol. 27, No. 12, 1956, pp. 1462-1466.
36. Kawai, T., and Yoshimura, N., "In-Plane Vibration Analysis by the Finite Element Method," (in Japanese), *Transactions of the Japan Society of Mechanical Engineers*, Vol. 36, 1970, pp. 723-730.
37. Fromme, J. A., and Leissa, A. W., "Free Vibration of the Rectangular Parallelepiped," *The Journal of the Acoustical Society of America*, Vol. 48, No. 1, 1970, pp. 290-298.
38. Knight, C. E., Personal Communication, Virginia Polytechnic Institute and State University, Randolph Hall, Room 114S, December 15, 1992, 5:00pm.
39. Hughes, T. J. R., and Brezzi, F., "On Drilling Degrees of Freedom," *Computer Methods in Applied Mechanics and Engineering*, Vol. 72, 1989, pp. 105-121.

40. Sze, K. Y., Wanji, C., and Cheung, Y. K., "An Efficient Quadrilateral Plane Element with Drilling Degrees of Freedom Using Orthogonal Stress Modes," *Computers & Structures*, Vol. 42, No. 5, 1992, pp. 695-705.
41. Handa, K. N., "Analysis of In-Plane Vibration of Shear Walls by a Finite Element Method," *Journal of Sound and Vibration*, Vol. 21, No. 2, 1972, pp. 169-180.
42. Schey, H. M., *Div Grad Curl and All That*, 2nd ed., W.W. Norton & Company, Inc., New York, NY, 1992, pp. 62-96.
43. Kreyszig, E., *Advanced Engineering Mathematics*, 6th ed., John Wiley & Sons, Inc., New York, NY, 1988, pp. 496-498.
44. Pierce, F. J., Personal Communication, Virginia Polytechnic Institute and State University, Randolph Hall, Room 124, April 28, 1993, 2:30pm.
45. Mitchell, L. D., Personal Communication, Virginia Polytechnic Institute and State University, Randolph Hall, Room 118A, April 30, 1993, 3:00pm.
46. SDRC University, Inc., *The I-DEAS Student Guide Level 4.1*, SDRC Software Products Marketing Division, Inc., 2000 Eastman Dr, Milford, OH 45150.
47. Cook, R. D., Malkus, D. S., and Plesha, M. E., *Concepts and Application of Finite Element Analysis*, 3rd ed., John Wiley & Sons, Inc., New York, NY, 1989, pp. 367-428.
48. Young, Kuao-John, "A Unified Approach to the Formulation of Non-Consistent Rod and Beam Mass Matrices for Improved Finite Element Modal Analysis." Ph.D. Dissertation, Virginia Polytechnic Institute and State University, Blacksburg, VA, 1990.
49. The MathWork, Inc., *PC-MATLAB*, The Mathworks, Inc., 21 Elliott Street, South Natick, MA 01760, 1989, pp. 3-50.
50. Wicks, A. L., Personal Communication, Virginia Polytechnic Institute and State University, Randolph Hall, Room 114U, March 5, 1993, 2:00pm.

# Appendix-A

## The First Three In-Plane Modes of a Square Plate

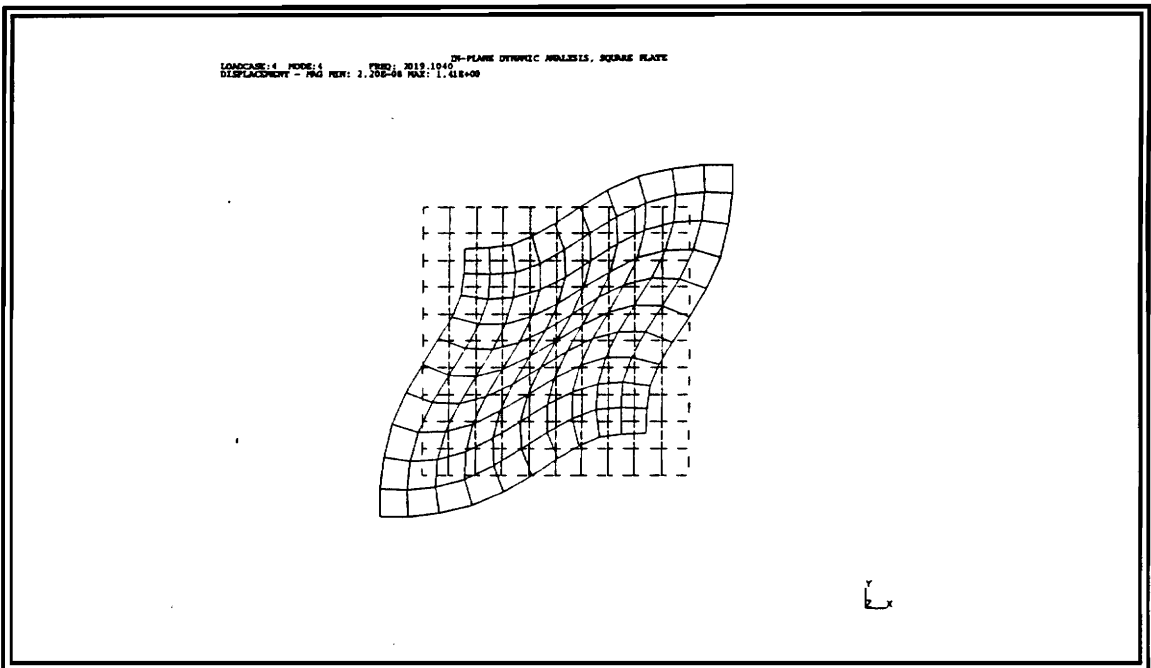


**Figure A1. Square plate, first in-plane eigenvector.**

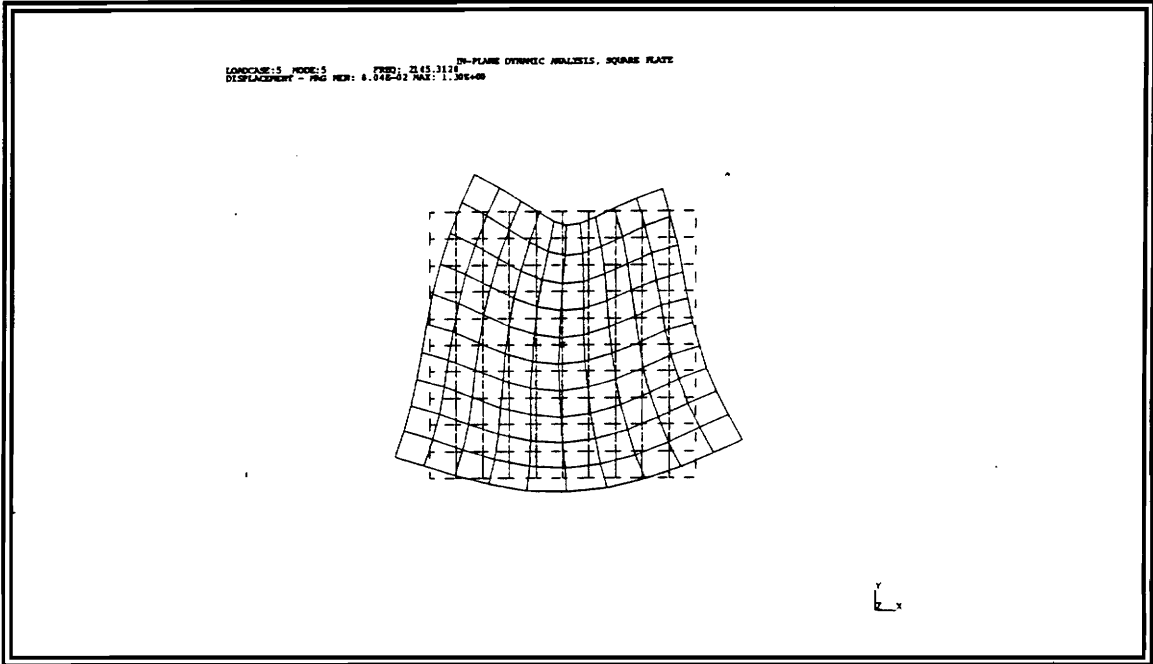


**Figure A2. Square plate, second in-plane eigenvector.**

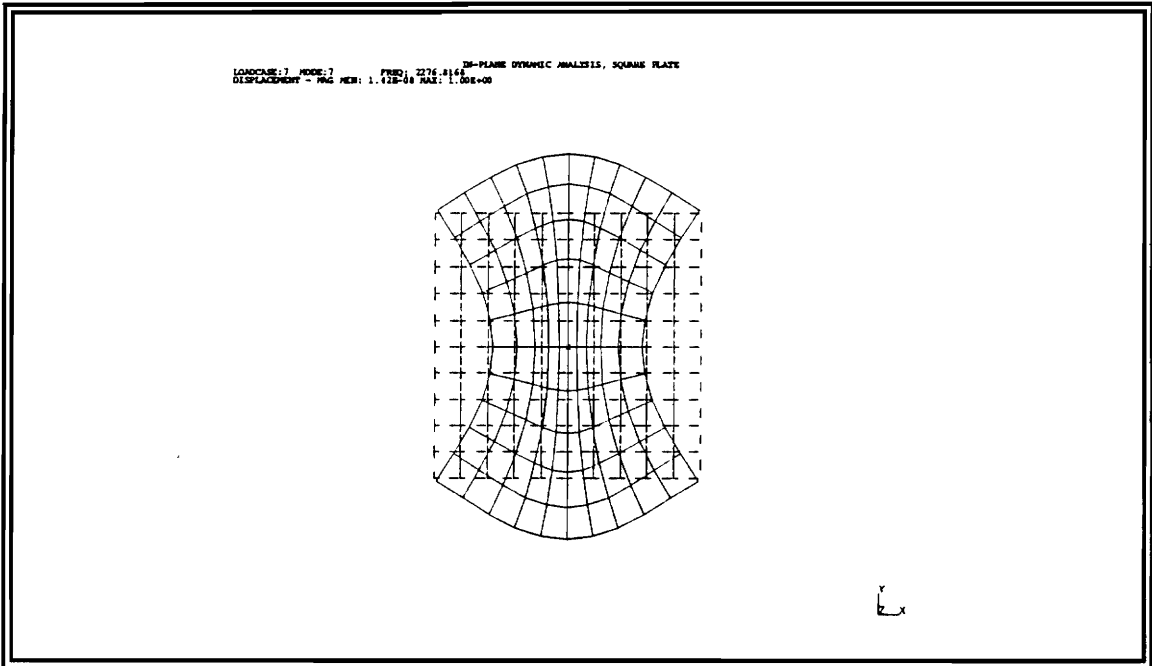


**Figure A3. Square plate, third in-plane eigenvector.**

# Appendix-B

## The First Three In-Plane Modes of a Rectangular Plate

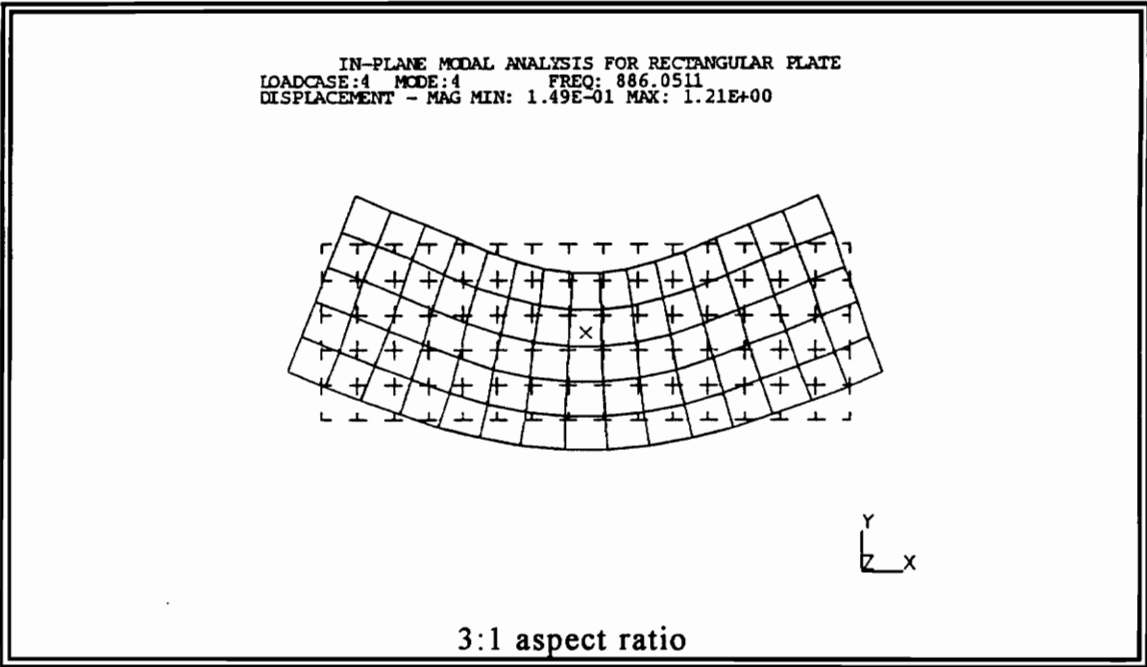
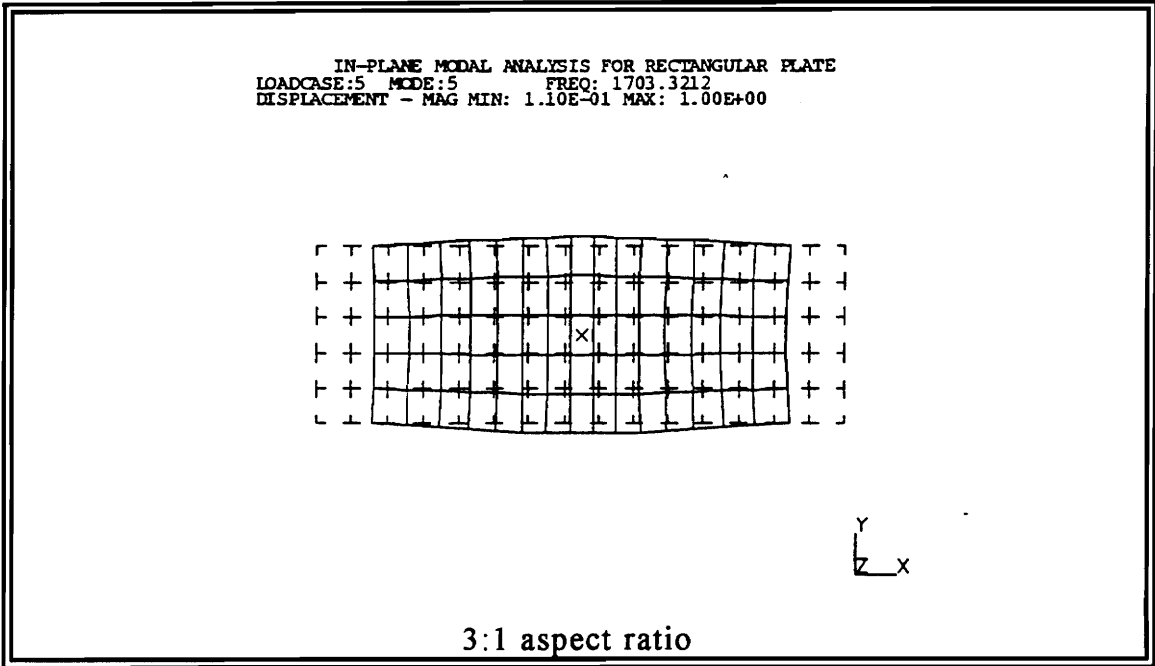
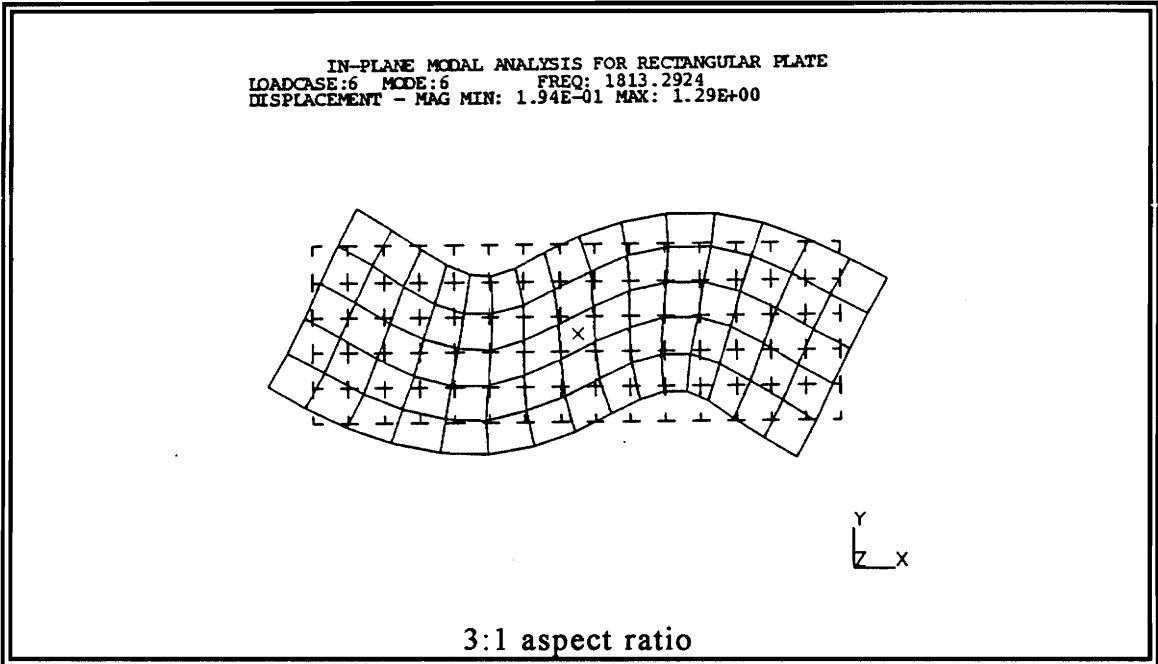


Figure B1. Rectangular plate, first in-plane eigenvector.



**Figure B2. Rectangular plate, second in-plane eigenvector.**



**Figure B3. Rectangular plate, third in-plane eigenvector.**

## Appendix-C

### MATLAB Code for Extraction of Drilling-Mode Shapes

```
% Please load data file and then assign zx=filex, zy=filey before executing
nsx=input('number of spectral lines ?');nsy=input('number of spectral lines ?');
xlink=input('xlink=?');ylink=input('ylink=?');
ms=[1,1,0.75];
vew=[-35,25];
subplot(221)
mesh(zx,vew,ms)
xlabel('x-axis in-plane velocity data')
mesh(zy,vew,ms)
xlabel('y-axis in-plane velocity data')
[n,m]=size(zy);
% calculation of spatial omega
omegax=2*pi/xlink;
omegay=2*pi/ylink;
% smoothing process
x=0:n-1;
z1=zy;
for ii=1:m;
    w=z1(:,ii); ii
    % rotate data record
    slop=(w(n)-w(1))/(x(n)-x(1));
    w(:)=w(:)-slop*x(:);
    % mirror and flip
```

```

w(n+1:2*n-2)=-w(n-1:-1:2)+2*w(n);
% fft-filtering-iff
w=fft(w);
w(nsx+2:2*n-2-nsx)=zeros(1,2*n-3-2*nsx);
w(1)=0;
% differentiation in frequency domain
for kk=1:nsx;
w(kk+1)=kk*i*omegax*w(kk+1);
w(2*n-1-kk)=-kk*i*omegax*w(2*n-1-kk);
end
w=ifft(w);
for kk=1:n;
z1(kk,ii)=w(kk);
end
end
mesh(z1,vew,ms)
xlabel('partial dVy/dx')
[n,m]=size(zx)
z2=zx';u=n;n=m;m=u;
x=0:n-1;
for ii=1:m;
w=z2(:,ii); ii
slop=(w(n)-w(1))/(x(n)-x(1));
w(:)=w(:)-slop*x(:);
w(n+1:2*n-2)=-w(n-1:-1:2)+2*w(n);

```

```

w=fft(w);
w(nsy+2:2*n-2-nsy)=zeros(1,2*n-3-2*nsy);
w(1)=0;
for kk=1:nsy;
w(kk+1)=kk*i*omegay*w(kk+1);
w(2*n-1-kk)=-kk*i*omegay*w(2*n-1-kk);
end
w=ifft(w);
for kk=1:n;
z2(kk,ii)=w(kk);
end
end
z2=z2';
mesh(z2,vew,ms)
xlabel('partial dVx/dy')
pause
% calculation of drilling mode
thetaz=z1-z2;
subplot
mesh(thetaz,vew,ms)
xlabel('z-axis angular velocity')
pause
tz=real(thetaz)
end

```

## Vita

George Stergios Galaitis was born in Veria, Macedonia, Greece. He studied in the 4th Lykeio of Veria. During this period he was the president of his class for four continuous years, and a local tennis champion. In 1986 he moved to U.S.A. and graduated from Lexington High School in Massachusetts. In 1991 he received his B.S. degree in Mechanical Engineering at University of Lowell in Massachusetts. During this period he was an active member of Tau Beta Pi and Pi Tau Sigma honor fraternities. In August of 1991 he moved to Blacksburg Virginia for graduate studies. During this period he was a graduate research assistant in Mechanical Engineering Department of Virginia Polytechnic Institute and State University, and the president of Hellenic Association for one year. He is expected to receive his Masters of Science in Mechanical Engineering in April of 1993.